Satellite Remote Sensing of Particulate Matter and Air Quality Assessment in the Western Cape, South Africa

by

YERDASHIN RAJENDRAN PADAYACHI

Submitted in fulfilment of the academic requirements of

Master of Science

in Environmental Science

School of Agriculture, Earth, and Environmental Sciences

College of Agriculture, Engineering and Science
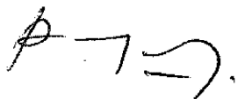
University of KwaZulu-Natal

Westville Campus

South Africa

February 2016

PREFACE

The research contained in this thesis was completed by the candidate while based in the Discipline of Environmental Sciences, School of Agricultural, Earth and Environmental Sciences of the College of Agriculture, Engineering and Science, University of KwaZulu- Natal, South Africa under the supervision of Dr Deshendran Moodley, Dr Tirusha Thambiran and Prof. Fethi Ahmed. The research was financially supported by the European Commission.

The contents of this work have not been submitted in any form to another university and, except where the work of others is acknowledged in the text, the results reported are due to investigations by the candidate.

Signed: Dr Deshendran Moodley

Date: 18 February 2016

DECLARATION 1: PLAGIARISM

I, Yerdashin Rajendran Padayachi, declare that:

     (i)   the research reported in this dissertation, except where otherwise indicated or acknowledged, is my original work;

     (ii)   this dissertation has not been submitted in full or in part for any degree or examination to any other university;

     (iii)   this dissertation does not contain other persons' data, pictures, graphs or other information, unless specifically acknowledged as being sourced from other persons;

     (iv)   this dissertation does not contain other persons' writing, unless specifically acknowledged as being sourced from other researchers. Where other written sources have been quoted, then:
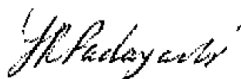
     a)   their words have been re-written but the general information attributed to them has been referenced;

     b)   where their exact words have been used, their writing has been placed inside quotation marks, and referenced;

     (v)   where I have used material for which publications followed, I have indicated in detail my role in the work;

     (vi)   this dissertation is primarily a collection of material, prepared by myself, published as journal articles or presented as a poster and oral presentations at conferences. In some cases, additional material has been included;

     (vii)   this dissertation does not contain text, graphics or tables copied and pasted from the Internet, unless specifically acknowledged, and the source being detailed in the dissertation and in the References sections.

Signed: Yerdashin Rajendran Padayachi

Date: 19 February 2016

ABSTRACT

Particulate Matter (PM) is a health risk, even at low ambient concentrations in the atmosphere. The analysis of ambient PM is important in air quality management in South Africa in order to suggest recommendations for pollution abatement. However the cost to monitor or to model surface concentrations are high. Satellite remote sensing retrievals of Aerosol Optical Depth (AOD) are cost effective and have been used in conjunction with surface measurements of PM concentrations for regional air quality studies. The aim of the study was to determine the extent to which AOD could be used as a proxy for air quality analysis of PM pollution in the Western Cape, South Africa. Surface concentrations of particles with diameter 10 μm or less (PM_{10}) measured at Air Quality Monitoring (AQM) stations in George and Malmesbury in 2011 were evaluated using temporal air quality analysis. The AOD were retrieved from the Moderate Resolution Imaging Spectroradiometer (MODIS) sensor onboard the Terra and Aqua satellites. Temporal trends of the AOD over Malmesbury and George AQM stations were determined and the extent of the AOD-PM_{10} relationship quantified through statistical correlation. Additionally meteorological parameters, including wind speed, temperature, rainfall and relative humidity measured at the AQM stations, were included in the study and their impact on AOD-PM_{10} trends was analysed. The annual AOD-PM_{10} correlations over Malmesbury in 2011 ranged between 0.24 and 0.36, while the correlations over George ranged between 0.24 and 0.34. A temporal mismatch was observed between seasonal PM_{10} concentrations and AOD at both sites. The AOD-PM_{10} relationship over Malmesbury and George were weak, suggesting that the AOD cannot easily be used as a proxy within the air quality analysis of PM_{10} concentrations measured at Malmesbury and George AQM stations. Specific meteorological conditions were found to be important confounding factors when observing AOD and PM_{10} trends. In spite of a few weaknesses in current satellite data products identified in this analysis, this study showed that improvements can be made to the use of satellite aerosol remote sensing as a proxy for ground level PM_{10} mass concentration by addressing the meteorological confounders of the AOD-PM_{10} relationship.

ACKNOWLEDGMENTS

TABLE OF CONTENTS

LIST OF FIGURES

LIST OF TABLES

LIST OF ABBREVIATIONS

AATSR	Advanced Along-Track Scanning Radiometer
ACE1	Aerosol Characterization Experiment 1
AEROINDOEX	AEROSOLS99 and INDian Ocean EXperiment
AERONET	Aerosol Robotic Network
AH	Absolute Humidity
AOD	Aerosol Optical Depth
$AOD_{aqua.db}$	AOD from the AQUA satellite retrieved using the deep blue algorithm
$AOD_{aqua.dt}$	AOD from the AQUA satellite retrieved using the dark target algorithm
AOD_{MODIS}	AOD retrieved using the MODIS sensor
AOD_{SEVIRI}	AOD retrieved using the SEVIRI sensor
$AOD_{terra.dt}$	AOD from the TERRA satellite retrieved using the dark target algorithm
AQM	Air Quality Monitoring
BLH	Boundary Layer Height
CALIOP	Cloud-Aerosol Lidar with Orthogonal Polarization
CALIPSO	CALIPSO
CCNC	Cloud Condensation Nuclei Particle Counter
CTM	Chemical Transport Modelling
DEA	Department of Environmental Affairs
DEADP	Department of Environmental Affairs and Development Planning
ERBS	Earth Radiation Budget Satellite
ESA	European Space Agency
EUMETSAT	European Organisation for the Exploitation of Meteorological Satellites
FLEXPART	FLEXible PARTicle
FMI	Finnish Meteorological Institute
GAWPFR	Global Atmosphere Watch Precision Filter Radiometer
HDF	Hierarchical Data Format
HERA	Hybrid Extinction Retrieval Algorithm
HYSPLIT	HYbrid Single-Particle Lagrangian Integrated Trajectory
LAADS	Level 1 and Atmospheric Archive and Distribution System
LPG	Liquid Petroleum Gas
LUT	Look Up Table
MERIS	MEdium Resolution Imaging Spectrometer
MFRSR	Multi-filter rotating shadowband radiometer
MLH	Mixing Layer Height
MISR	Multiangle Imaging Spectroradiometer
MODIS	Moderate Resolution Imaging Spectroradiometer
MPLNET	Micro Pulse Lidar Network
MSG	Meteosat Second Generation
NAAQS	National Ambient Air Quality Standard
NASA	National Aeronautics and Space Administration
NICAM	Nonhydrostatic ICosahedral Atmospheric Model
NMMB/BSC	Nonhydrostatic Multiscale Meteorological Model on the B grid / Barcelona Supercomputing Center
OMI	Ozone Monitoring Instrument
SAFARI	Southern African Fire-Atmosphere Research Initiative
PM	Particulate Matter

PM$_{2.5}$	Particles with diameters of 2,5 μm or less
PM$_{10}$	Respirable particles with diameters between 2.5 and 10 μm
POLDER	POLarization and Directionality of the Earth's Reflectances
RH	Relative Humidity
SAGE	Stratosphere Aerosol Gas Experiment
SeaWifs	Sea-Viewing Wide Field-of-View Sensor
SEVIRI	Spinning Enhanced Visible and Infrared Imager
SIBYL	The Selective Iterated BoundarY Locator
SPOT	Systeme Pour l'observation de la Terre
TEOM	Tapered Element Oscillating Microbalance
TSP	Total Suspended Particulates
TRACE A	Transport and Atmospheric Chemistry near the Equator-Atlantic
UTM	Universal Transverse Mercator
WHO	World Health Organisation
WMO	World Meteorological Organisation

CHAPTER 1: INTRODUCTION

1.1. Background

The majority of the global human population live within areas affected by poor air quality (Watson, 2014; Akimoto, 2003). One of the most widespread air quality pollutants is particulate matter (PM). PM are aerosols that adversely affect human health by exacerbating respiratory illness and contributing to lower lung function, increased morbidity related to respiratory and cardiovascular disease and greater mortality from cardiopulmonary diseases (Pope III *et al.* 1995).

PM is composed of sulphate, organic carbon, black carbon, mineral dust, nitrate and biomass burning particles. Biomass burning particles are a combination of inorganic particles (for example sulphate and nitrate), organic carbon and black carbon. PM concentrations are measured for two classes of respirable particles with diameters between 2.5 and 10 micrometres (μm) - PM_{10} - as well as fine PM which includes particles with diameters of 2,5 μm or less - $PM_{2.5}$ - [World Health Organization (WHO), 2006]. PM is emitted from both natural sources (examples soils and marine PM) and anthropogenic sources. PM sources includes fossil fuel, biofuel and biomass burning, biogenic emissions, agriculture practices (overgrazing, harvesting and ploughing) and industrial practices (cement production and transport). Secondary atmospheric processes in the atmosphere also form PM due to aqueous and gaseous phase chemical reactions and through vapour condensation (Forster *et al.* 2007). However, it is PM from anthropogenic sources mainly due to fossil fuel burning activities within industrial, residential, agricultural, transportation and business sectors which have resulted in deteriorated levels of air quality.

The disease burden associated with the inhalation of PM, from exposure to environmental sources and household sources has been shown to be substantial in the developing world (Cohen *et al.* 2005; Lim *et al.* 2012). Similar to other developing global regions in South America and Asia (Cohen, 2006; Schwela, 2012), motorised transportation and industrialization are driving greater contributions of pollutant sources to higher PM concentrations in Africa. Africa with its largely rural population (Jayne *et al.* 2012), consumption of mostly biomass fuels for domestic use (Lammel *et al.* 2013; Tanimowo, 2000) are particularly vulnerable due to the high PM concentrations emitted from domestic sources (Lim *et al.* 2012). Other biomass sources of PM include the seasonally natural or

purposeful burning of veld areas, for which Africa contributes substantially to regional and global air quality (Roberts *et al.* 2009; Lammel *et al.* 2013). African PM is sourced from a range of pollutant sources with implications for air quality at local, regional and at global scales.

In Africa, urbanisation is occurring at relatively faster pace when compared to other regions in the world with exception of Asia (United Nations, Department of Economic and Social Affairs, Population Division, 2014) and is affected by changes in population, transport, economic activity, settlement, movement of people and agriculture (Potts, 2012). These essential facets of development in turn are driving increases in PM concentrations (Schwela, 2012). There is a need to manage PM related air quality in Africa by determining the state of air quality, exposure to air quality risk in African regions and then formulating strategies to reduce adverse health impacts. The biggest challenge for understanding health impacts from PM_{10} exposure is that even the lowest PM_{10} concentration has a health impact (Cohen *et al.* 2004).

Information about temperature, wind direction and relative humidity (RH), population density, topography such as elevation and slope and land uses such as transport, settlement, industry and commercial are needed to better explain PM concentrations so as to inform the state of air quality (Jerret *et al.* 2005). All of these factors including PM concentrations exhibit spatio-temporal characteristics that are relevant to analysing exposure of populations and individuals to air quality risk. These factors can be spatially integrated to predict PM concentrations which can be achieved using geographical information systems. Such an approach is used in the development of early warnings systems which may be used to provide warnings to the public of future episodes of elevated PM concentrations in order to reduce adverse health effects (Grivas and Chaloulakou, 2005; Jerret *et al.* 2005).

The use of monitored PM data supplemented by meteorological data input into models to predict PM concentrations can be used to estimate the changes of PM concentrations over time and to analyse the effects of meteorological effects including temperature, RH, solar radiation, barometric pressure, rainfall, wind direction and wind speed on these changes. The satellite remotely sensed Aerosol Optical Depth (AOD) measure of PM in the atmosphere has been an input to these predictive models. The AOD is a measure of PM

concentration due to the prevention of light transmission due to PM radiative scattering and absorption effects (Kaufman *et al.* 2002).

The radiative and scattering effects of PM on the climate system increases the relevance of studying PM not just for human health but climate change. Understanding the role of PM in the climate system can benefit from satellite remote sensing which is able to retrieve aerosol optical and cloud properties over most of the earth's surface. In turn understanding the climate system interactions with PM for air quality studies can help in the development of models to predict PM concentrations.

The prediction of PM concentrations using a spatial prediction model requires that PM concentrations are represented spatially. There are a few approaches which have been used to achieve this including the interpolation of PM concentrations measured at different point locations (Pope and Wu, 2014) as well as chemical transport modelling (CTM) or dispersion modelling (Holmes and Morawska, 2006). Interpolation of PM data to map PM distributions depends upon a number of well distributed stations (for example Emili *et al.* 2010). The use of satellite remotely sensed AOD is the third approach which is advantageous as a spatial measure of PM concentration. The AOD data retrieved from the Moderate Resolution Imaging Spectroradiometer (MODIS) sensor (for example Wu *et al.* 2012), is used the most frequently in aerosol studies and are borne on two satellites, namely the AQUA and TERRA satellites (Gupta and Christopher, 2009). The AQUA and TERRA satellites are sunsynchronous polar orbiting satellites, with TERRA being launched in 1999 and AQUA being launched in 2002 (Tang *et al.* 2005). The MODIS sensor covers 36 spectral wavelengths from 400 nm to 1400 nm and has a swath of 2330 km. Both satellites were launched to monitor the environment with the TERRA satellite primarily monitoring the terrestrial environment and the AQUA satellite primarily monitoring the aquatic environment although both satellites actually measure many environmental variables on land, in the atmosphere and over freshwater and ocean environments (Parkinson, 2003). Studies initially used the satellite retrieved AOD to model $PM_{2.5}$ concentrations. One of the first studies was Wang and Christopher (2003) which estimated $PM_{2.5}$ from satellite retrieved MODIS AOD over Alabama, United States of America (USA) in 2002. Engel-Cox *et al.* (2004) correlated PM_{10} and $PM_{2.5}$ measurements measured in the eastern and mid-western regions of the United States in 2002 with MODIS AOD measurements over the region. Subsequently other studies have

estimated PM_{10} from AOD over Europe (for example Koelemeijer *et al.* 2006) and over Asia (for example Ku and Park, 2013).

1.2. PM Related Air Quality Studies in South Africa

South Africa is one of the few countries in Africa to combat the adverse health impacts of PM related air quality along with Zambia, Egypt, Ethiopia, Cameroon, Ghana and Senegal (Vahlsing and Smith, 2012). In South Africa, PM is regulated by National Ambient Air Quality Standards (NAAQS) within the National Environmental Management Act: Air Quality Act, 2004 (Act no 39 of 2004) by the South African Department of Environmental Affairs (SA DEA, 2009). Regulations include limits to ambient PM concentrations (DEA, 2009; DEA, 2012) and dust fall (DEA, 2013).

The concentrations of PM_{10} and $PM_{2.5}$ in ambient air are regulated in order to aim for better air quality to improve the health of the population. In South Africa, PM_{10} is the most frequently monitored PM type (DEA, 2015). The study of PM_{10} in South Africa has largely taken place in regions where the drivers of PM_{10} related air quality are in close proximity to vulnerable human populations. Studies have indicated negative PM_{10} related air quality impacts on health in many cities in South Africa (for example Naidoo *et al.* 2013; Wichmann and Kuku, 2012; Wichmann *et al.* 2009). At the regional level, within South Africa, a number of studies have characterised PM_{10} mostly over the north-eastern region (for example Laakso *et al.* 2012; Hirsikko *et al.* 2012; Vakkari *et al.* 2013).

PM_{10} air quality studies in South Africa have also included the AOD which can provide PM_{10} data over a larger spatial area than AQM stations (Sorek-Hamer *et al.* 2013). Studies which have analysed the use of AOD as a proxy for PM_{10} in South Africa and focussed upon PM in South African cities include Garland and Sivakumar, 2012 and Hersey *et al.* 2015). There is a scarcity of studies which explore the linkages between AOD and PM_{10} in South Africa and a scarcity of case studies which use MODIS AOD to do so.

Such case studies need to consider a complex array of air quality, meteorological and instrumentation information that include:
- The coefficients of PM_{10} concentration including the AOD and meteorology.

- The spatial resolution and coverage of the measurements.
- The temporal resolution and coverage of the measurements.
- The instruments and sensors used for measuring PM_{10} concentrations and the AOD.
- The different satellite platforms from which the satellite imagery were captured from.
- The algorithms that were used to retrieve the AOD from satellite imagery.

The assessment of ambient air quality monitored PM_{10} should further consider the severity of PM_{10} related air quality, the contributions of possible pollutant sources, the contributions of meteorological effects to the temporal trends of PM_{10} concentrations and the seasonal differences in PM_{10} concentrations and meteorology.

Air quality studies of PM_{10} are typically highly localised studies. PM_{10} data from continuous air quality monitoring (AQM) stations are operated by local and provincial South African government to monitor compliance to air quality legislation. The data from these AQM stations provide a longer record of PM_{10} data which is needed to track changes in PM_{10} concentrations over time. PM_{10} data are valuable to estimating health impacts and to quantify the change in health risk to the local population over time.

There is a need to study PM_{10} related air quality in all communities. However AQM stations cannot be set up in all communities as it is costly to establish and to maintain AQM stations (Mendez *et al.* 2011). The alternative is to use the AOD which is advantageous as a less costly spatial measure of PM_{10} which can provide PM_{10} data over a larger spatial area than AQM stations (Sorek-Hamer et al. 2013; Toth et al. 2014).

This study will contribute to the gaps in existing knowledge on the linkages between MODIS AOD and PM_{10} related air quality research in smaller towns of South Africa. As such, in this study, selected case studies from the Western Cape Province were included, in particular Malmesbury, a predominately agriculturally active town and George, a more urbanised town. Malmesbury is a periphery town with a Mediterranean climate located outside of the capital city of Cape Town. George is a major town with an oceanic climate distant from major cities, industrial centres and sprawling townships. As such the locations are unique and interesting case studies to study ambient air quality monitored - PM and

satellite retrieved AOD. To achieve this, PM_{10} concentrations and meteorology were characterised in George and Malmesbury. An assessment was undertaken to determine the extent of the correlation between satellite retrieved AOD and PM_{10} and the extent the AOD can be used in the analysis of PM_{10} concentrations in George and Malmesbury.

PM_{10} concentration air quality data and meteorological data were collected from the monthly AQM reports for the George and Malmesbury AQM stations. MODIS AOD data were collected from remotely sensed satellite data. GIS software was used as a tool to extract the satellite data for the points of interest, the AQM stations in George and Malmesbury. Databases with the air quality, meteorological and satellite data were compiled within spreadsheet software. The main analysis involved compiling collocated PM_{10} concentration, meteorological and AOD data and running correlation and regression statistical analysis using statistical software.

1.3. Aim and Objectives

The **aim** of the study was to determine the extent to which AOD could be used as a proxy for air quality analysis of PM_{10} pollution in the Western Cape, South Africa.

The **objectives** include:
1. To assess the acceptability of PM_{10} concentrations monitored in Malmesbury and George according to the WHO guidelines for PM_{10} in 2011.
2. To characterise the diurnal trends of PM_{10} associated ambient air quality and meteorology monitored in George and Malmesbury in 2011.
3. To characterise the monthly and seasonal trends of PM_{10} associated ambient air quality and meteorology monitored in George and Malmesbury in 2011 and to assess the correlations between the PM_{10} concentrations and the meteorology monitored in the two towns.
4. To characterise the satellite AOD over Malmesbury and George.
5. To assess the correlations between ambient air quality monitored PM_{10} and satellite AOD over Malmesbury and George.
6. To determine the effects of meteorology monitored in George and Malmesbury on the relationship between ambient air quality monitored PM_{10} and satellite AOD over Malmesbury and George.

1.4. Chapters Outline

The subsequent literature review chapter discusses the conceptual AOD-PM_{10} relationship, with the objective of the chapter to detail the multiple effects upon the assumptions and parameters of the relationship. Chapter 3 describes the case study area, the methodologies and methods used in the study. Chapter 4 presents the results of the statistical analysis of AOD, PM_{10} and meteorological data. The final chapter covers the discussion and conclusion of the research findings of the study.

CHAPTER 2: LITERATURE REVIEW

2.1 Aerosol Sources, Radiative Effects and Characteristics

2.1.1. Introduction

The roles of PM in the earth's climate system includes the radiative effects of PM within the atmosphere and the atmospheric component of the water cycle. The complexity of PM interactions with the earth's atmospheric and radiation system is due to the dynamic composition and concentration of PM at varying particle sizes within the atmosphere (Stevens, 2013).

This chapter discusses the types of PM and emission sources which are important to understanding the characteristics of PM air quality found in urban environments. Secondly the radiative forcing and radiative impacts of the different PM types is discussed in order to explain the importance of PM optical properties and the role of aerosols to the global climate system. Thirdly the effects of meteorology on aerosol transport and distribution is discussed as this is an important driver of PM ambient air quality in urban environments. An explanation is provided about how two important measures of PM in the atmosphere are related namely the AOD and the PM_{10} concentration. These measures have commonly been used within air quality studies of PM. This is then followed by a description about how the two important measures of PM are measured for air quality and PM studies. This chapter then goes on to explain the PM sources and radiative effects in South Africa in order to discuss the most common types of PM found in South Africa and the role PM has for South Africa's climate system. The role of synoptic weather systems in South Africa are highlighted as these systems are important for the large scale distribution of PM across the country. An explanation is then provided about how AOD and PM_{10} concentration have been measured in South Africa. Finally a summary is included to highlight the most important findings in the literature review.

2.1.2. Particulate Matter

PM sources that contribute to the radiative forcing effects include those from fuel combustion activities and anthropogenic land uses. The PM species directly emitted to the atmosphere include those containing biomass burning particulates, black carbon and mineral dust. Secondary atmospheric process including chemical reactions and vapour

condensation result in the formation of sulphate, nitrate and organic PM. (Haywood and Boucher, 2001; Forster *et al.* 2007).

In this section the following types of PM will be presented namely black carbon, mineral dust, sulphate, nitrate, organic and biogenic PM.

Black carbon PM is produced as a result of burning. Sources of black carbon include the burning of vegetative biomass, biofuels and carbon based fuel combustion due to partial combustion. Examples of these emission sources include coke production, petrochemical flaring, brick kilns, domestic biomass burning, agricultural, savannah and forest burning and off-road and road transport (Bond *et al.* 2013). Black carbon PM has a short atmospheric residence time for a limited number of days (Booth and Bellouin, 2015).

Anthropogenic mineral dust emissions are a result of land use practices and industrial practices. Mineral dust PM sources from human activities, includes those from farming activities such as the devegetation of land through the harvesting of crops and the overgrazing of cattle as well as the turning of fields for the planting of new crops and industrial emissions such as cement processing and production (Forster *et al.* 2007). The desertification impacts of climate change on vegetated land cover regions in water scarce regions around the globe, also increases the amount of dust PM to the atmosphere (Moulin and Chiapello, 2004). However desertification as a driver of dust sources may not be as dominant as meteorological and climate drivers, for example as in the case of dust storms affecting Asia (Zhang *et al.* 2003). Different particle sizes of dust PM can stay aloft in the atmosphere for a brief period of time (hours) or for longer (for years) (Huang *et al.* 2015). Mostly smaller particles can stay in the atmosphere for longer periods of time and be deposited further away from emission sources (Han and Zender, 2010).

Sulphate PM particles mainly are composed of particulates of sulphuric acid which acquire a pH of 0 when contacted with ammonia in its aqueous phase or in its partially solid phase. Reactions that result in the formation of sulphate occurs within liquid particles of cloud, due to sulphur dioxide and hydroxide reactions in their gaseous forms or via the condensation of sulphates upon already present sulphate particles (Penner *et al.* 2001). The sources of sulphates are largely from fuel combustion (about 72%), vegetation burning (about 2%), and emissions from phytoplankton (about 19%) and about 7% from volcanic eruptions (Forster *et al.* 2007). Sulphate PM particles have a relatively short residence time in the atmosphere spanning from a few days to a few weeks (Smith *et al.* 2010).

9

Linked to sulphate PM particles are nitrate PM particles. Nitrate PM particles are formed through secondary processes in the atmosphere when the pH of sulphate PM particles changes to neutral and also with the interaction of extra ammonia (Forster *et al.* 2007). Additionally nitrate PM particles are formed through a range of varied chemical reactions involving nitrogenous compounds including dinitrogen pentoxide, nitrate and nitric acid (Jacob, 2000). The PM particles have a short residence time of only a few days in the atmosphere (Bellouin *et al.* 2011).

Unlike nitrate PM particles which form through secondary atmospheric processes, organic PM particles form through primary and secondary processes. For example, secondary processes include the condensation of fossil fuel based gases such as natural gas and Liquid Petroleum Gas (LPG) with semi-low volatility from gas – particle phases changes (Hamilton *et al.* 2004). Primary emission sources of organic PM particles are those from conventional fuel burning such as fossil fuels and biomass fuel burning. The PM particles have a residence time in the troposphere which is a few days more than nitrate PM particles, however the PM particles are still short lived (Ellison *et al.* 1999).

Primary biogenic PM sources include direct emissions from vegetation, animals, bacteria, fungi and viruses. Biogenic PM particles are also formed from chemical reactions in the atmosphere with dimethyl sulphide from phytoplankton and volatile organic compounds emitted from vegetation, algae and fungi (Boucher, 2015). The PM particles become attached to substrates such as plant debris, cells and dust particles (Löndahl, 2014). The smaller biogenic PM particles are able to spend a longer time in the atmosphere particularly further up in the stratosphere (Löndahl, 2014). For example microbes can spend a few days or months in the atmosphere (Burrows *et al.* 2009).

2.1.3. Radiative Forcing of Particulate Matter

Primary and secondary emissions of PM, contribute to the direct and indirect radiative forcings on climate which constitute the two main groupings of the PM effects on the climate system. The effects of direct forcing account for impacts on the scattering and absorption of radiant energy affecting both long and short wavelengths. The PM indirect effect refers to the modifications to cloud nuclei by PM particles and the resultant change in the optical characteristics of clouds (Mahowald, 2011). The semi-direct effect refers to the modification of the earth energy budget by solar radiation absorbing PM particles and the modification to the static atmospheric stability of the atmosphere (Denman *et al.*

2007). The glaciation effect refers to the greater production of ice nuclei by PM particles with the resultant increased precipitation of ice (Lohman *et al.* 2007). The thermodynamic effect refers to the delay in the freezing of clouds due to the decrease in size of cloud droplets (Storelvmo *et al.* 2008).

These radiative effects of PM particles are determined from short term research campaigns, long term monitoring as well as modelling of the climate system. The use of long term monitoring data has provided a means to determine long term radiative effects at both the global and regional spatial levels. For long wave radiation to be impacted from direct radiative forcing, PM particle sizes must be large enough and numerous enough at higher atmospheric heights to sustain an effect (Forster *et al.* 2007).

The effects of PM particles on clouds and radiation are dependent upon the radiative properties of PM particles which are in turn affected by whether the PM particles are hydrophilic or hydrophobic, the age of the particle material, wet deposition and meteorological factors (Forster *et al.* 2007). Land cover contributes additionally to the net effect of PM radiative forcing as a PM source. Some PM types will not vary in the scattering effect on radiative forcing between different land cover types while other PM types will vary in their net effect on radiative forcing. For example PM particles composed of both scattering and absorption properties will have a scattering effect on radiative forcing over dark targets such as water bodies and dense vegetation and a absorption affect over bright surfaces such as polar areas and deserts (Haywood and Shine, 1995; Forster *et al.* 2007).

2.1.4. Radiative Impacts of PM particles

Black carbon plays a role in the warming of the troposphere and the upper cryosphere caused by the direct radiative forcing of the aerosol and role in snow melt (Bond *et al.* 2013). This in turn drives changes in precipitation, temperature and cloud systems. The largest concentrations of black carbon are found in Asia which affect the monsoon systems over the continent and can cause shifts in the Inter-Tropical Convergence Zone (Bond *et al.* 2013). Black carbon also has negative impacts for human health.

Dust PM particles have impacts on the climate system. For example, the radiative forcing from dust PM particles from North Africa may strengthen the easterly wave systems which occur over the Atlantic Ocean (Jones *et al.* 2004). Dust PM particles also have an impact

11

on circulation systems. For example, the region between mainland Eurasia and the adjacent oceans is affected by changes to the thermal system over the region due to modifications from dust PM particles, this in turn drives greater fluctuation of the Asian monsoon which in turn drives a decrease in the emissions of dust from its sources which caused the changes in the thermal system (Zhang *et al.* 2002). Dust PM particles have an impact on the vertical mixing of air within the atmospheric boundary layer through its radiative forcing effects which result in the decrease in the emission of dust PM particles to the atmosphere (Miller *et al.* 2004).

Dust PM particles have a role in nitrogen and sulphur cycles as a sink for pollutants such as sulphur dioxide and nitric acid (Dentener *et al.* 1996). Dust PM particles aid in the functioning of ecosystems. Dust PM particles are a supplemental source of nutrients to terrestrial ecosystems as well, for example the deposition of phosphorous over Hawaii from dust storms over the Asian continent (Chadwick *et al.* 1999) and the deposition of phosphorous over the Amazon from dust transported from Africa (Yu *et al*. 2015). One of the ways in which elemental iron is transported to the ocean is via atmospheric deposition of dust PM particles which have a role in the functioning of marine ecosystems (Jickells *et al.* 2005).

Sulphate PM particles can contribute to reductions in global warming and to changes in precipitation (Denman *et al.* 2007). It is likely that the contributions of sulphate PM to global cooling will be reduced due to plans to reduce sulphur dioxide emissions due to the negative impacts of the pollutant on humans, animals and ecosystems (Klimont *et al.* 2013). Sulphate PM particles are toxic to plants and therefore contribute to the carbon cycle, by damaging stomatal tissue and reducing photosynthesis in plants (Eliseev, 2015). Nitrate PM particles are expected to be considered as toxic air pollutants by 2030 (Bauer *et al.* 2007). Simulations of nitrate PM particles driving decreases in temperature and precipitation in China have been shown using the Regional Climate Chemistry Modelling System (Wang *et al.*2010).

Organic PM particles negatively impact human health and ecosystems as a pollutant, contributes to degraded visibility and contributes to global cooling by scattering radiation and increasing the cloud albedo (Mauderly and Chow, 2008). The PM particles contribute to ozone production (Sahan *et al.* 2008). Organic PM particles also play an important role in the global carbon cycle.

Due to the indirect effect of biogenic PM particles, the PM particles have a significant impact on precipitation (Boucher *et al.* 2013). Bacteria can contribute to chemical modifications to cloud chemistry when inside liquid droplets in clouds (Deguillaume *et al.* 2008). Bacterial biogenic aerosols can travel far from sources attached to dust PM particles which are important for the mobility of bacterial species (Burrows *et al.* 2009a).

2.2. Meteorological Effects on PM Transport and Distribution

Fluctuations in the trends of PM emissions and in the radiative effects of PM particles are partially driven by meteorological parameters particularly the boundary layer condition (for example Emili *et al.* 2011). Other meteorological parameters also include wind speed, temperature, rainfall, atmospheric stability conditions and soil water content (Trivedi *et al.* 2014). In this section, the effect of meteorological parameters on PM transport and distribution at the local spatial scale are explained.

2.2.1. Meteorological Parameters

At the regional spatial scale, synoptic weather systems contribute to the large scale distribution of PM particles across continents, countries and cities. These weather systems are mostly anticyclonic, with the rear of anticyclones contributing to PM pollution build up in the atmosphere. The occurrence of anticyclones may be seasonally variable. For example anticyclones occur throughout the year in the mid-western United States (Dharshana *et al.* 2010) but are more frequent in summer in Beijing, China (Matsui *et al.* 2009; Zhang *et al.* 2012). However in Hong Kong, China, the anticyclones occur during winter (Huang *et al.* 2009). Other weather systems to a lesser extent globally may contribute to high PM episodes. For example, In Dribugarh, India (Gogoi *et al.* 2008) and in the Klang Valley, Malaysia (Juneng *et al.* 2011), high PM episodes occurred before the passage of monsoon systems. Low pressure systems contributed to high PM episodes during spring in Greece (Kaskaoutis *et al.* 2008) and throughout the year except in winter in Bejing, China (Zhang *et al.* 2012).

At the local spatial scale, meteorological parameters including rainfall, wind speed, temperature and soil moisture can contribute to PM distribution and dispersion. This largely takes places within the atmospheric boundary layer where the most PM particles

are found. The height of the atmospheric boundary layer is controlled by atmospheric stability conditions.

The meteorological effects discussed below all take place within the atmosphere boundary layer. The atmospheric boundary layer is the closest layer to the surface within which most terrestrial life depends upon. The turbulent sub layer is situated above the lowermost laminar boundary sub layer (Emeis, 2010). Warmer temperatures, solid particulates and the momentum of air mix within the turbulent boundary layer which aids in the mixing of air making it important to the dispersion of pollutants from their source. During the daytime, warming of the surface directly aids the expansion of the turbulent layer. During the night, the turbulent layer contracts, as the surface cools down. As the mixing of the air occurs in this layer, this is also contributed by land sea breeze transport of air as well as from mountain plain winds (Emeis, 2010).

Turbulence is caused by both free and forced convection (Turns, 2006). Forced convention usually has greater importance within two meters of the surface and is affected by the shear and speed of the wind, as well as the roughness of the surface. Free convention occurs above forced convention, aiding in the transport of air which is composed of warmth, moisture and momentum under highly unstable atmospheric conditions. The resulting turbulent currents in the boundary layer which define different wind profiles are affected more by the roughness of the surface and by the stability condition (Tyson and Preston-Whyte, 2004 ; Turns, 2006).

Within the surface layer, the horizontal momentum flux increases and this is transferred to the upper air layers (Tyson and Preston-Whyte, 2004). The momentum flux is determined from the density of the air, the kinetic viscosity and the change of the wind with height. In the turbulent layer, the movement of air upwards retains the horizontal momentum but the speed at which the air rises is reduced. When the air motion is downwards, the overall speed of the wind increases, while the horizontal moment flux is conserved in the turbulent layer generating more aggressive winds than those in the upper layers. In the turbulent layer the momentum is determined from the density of the air, the viscosity of the wind motions and the change of the wind with height (Tyson and Preston-Whyte, 2004; Turns, 2006).

The change in the boundary layer is different at night and during the day (Stull, 2005). Surface cooling due to lower temperatures at night, means that a layer of cool air forms at the surface and a layer of warmer air is retained above this. A diffusion gradient flow of sensible heat forming an inversion occurs which results in movement of sensible heat downward. This is reversed during the day when heating of the surface due to increasing temperature results in a layer close to the surface with warmer air than the air above it. The inversion may be disrupted by gusty winds. A diffusion gradient flow of sensible heat occurs which results in movement of sensible heat upward, the disruption of the night inversion occurs gradually, once the turbulence generated is enough to overcome the inversion. The process is slow and gradual during the day due to the steady change in temperatures as the day progresses, applicable during the day when the inversion is reduced and at night when the inversion grows with height (Stull, 2005).

The flow of moisture in the boundary layer is similar to the flow of sensible heat (Tyson and Preston-Whyte, 2004). Water vapour from evapotranspiration increases during the day at the surface. Mixing of the air during the day, distributes the water vapour. As night time encroaches, stability conditions reduce the mixing in the atmosphere and the water vapour content in the boundary layer is determined by dew formation and the degree of turbulence (Tyson and Preston-Whyte, 2004).

Two boundary layer conditions are relevant to terrestrial surfaces. The first being the daytime boundary layer defined by convection. This convective boundary layer through instability conditions, under cloud free skies can reach up to 2-3 km at its peak (Garrat, 1992). The convective boundary is characterised by reduction of the PM concentration in the atmosphere at the top of the convective boundary layer, due to the occurrence of subsiding air masses forming an inversion layer (Garrat, 1992). Beyond the top of the convective boundary layer, the PM concentration eventually stabilises with altitude (Garrat, 1992). The second being the night time boundary layer defined by stability conditions. Over the ocean, surface heating is not possible due to the presence of water. The boundary marine layer is weaker and usually has a layer of clouds above it, with less mixing of the air (Tyson and Preston-Whyte, 2004).

The boundary layer is not typically cloud free in mid latitude regions (Stocker *et al*. 2001). The turbulent region is covered by a cloud layer, which in turn is covered by an inversion layer. Typical cloud features include stratus and stratocumulus clouds. Stratus clouds form

closer to the surface than stratocumulus clouds while stratocumulus clouds may form higher in the atmosphere and are structured by convective mixing (Stocker *et al*. 2001).

Urbanised settlements significantly impact on the properties of roughness, heat, thermal flux and moisture flux which directly affect the boundary layer (Oke, 1987). Urban materials provide services that modify energy flow into the natural environment. By covering the ground surface, water is not able to drain into soil surfaces and to aid in surface cooling. Human activities result in waste streams which eventually feed into the atmosphere and freshwater sources in the form of water and heat flow. Building arrangements and building shape confines thermal energy and air preventing flow into the atmosphere. The building materials used also can act as good insulators (Oke, 1987).

Urban areas give rise to the urbanised boundary layer which is directly related to the surface properties of the urban area and is related to the climate (Oke, 1987). Beneath the urbanised boundary layer at the intraurban scale, smaller scale climate processes are a characteristic below the roof level of buildings (Oke, 1987). At the urban scale, meteorological processes within the modified boundary layer aid in the transport of PM due to vertical mixing or conversely cap the pollutants beneath an inversion layer. At the regional and global spatial scale, large synoptic weather systems contribute towards the movement of PM particles across cities, towns and countries (Oke, 1987).

Rainfall plays a role in wet deposition of atmospheric PM particles thereby reducing the time spent by PM particles in the atmosphere. Increasing PM loadings in the atmosphere can also decrease the rate at which rainfall forms, increasing the time spent and the distance travelled by PM particles in the atmosphere. Associated with stratocumulus clouds over marine regions, are the occurrences of distributed cloud features which aid in the wet deposition of PM particles through weak rainfall (Sharon *et al.* 2006).

Through indirect effects of rainfall on plants via the opening and closing of the stomata organs, PM emissions from plants and trees are also affected. Rainfall aids in the formation of secondary PM particles. For example the PM size distribution is impacted by the oxidation of sulphur dioxide due to the interaction of water via precipitation (Denman *et al.* 2007).

With increasing soil water content, soil becomes more of a sink rather than a source of PM (Denman *et al.* 2007). Soil water content is important due to the indirect relationship with PM particles (Denman *et al.* 2007). A causal factor of high soil water content is low ambient temperature which reduces the loss of soil water due to evaporation. A higher amount of soil PM will be contributed to atmospheric PM due to the effect of lower soil water content. A causal factor of lower soil water content is high ambient temperature which increases the loss of soil water due to evaporation (Trivedi *et al.* 2014).

The quantity of primary PM emissions from a source is partly determined by the wind speeds at the surface. Wind speeds also effect secondary PM production via its precursor emissions from the source for example dimethyl sulphide emissions (Denman *et al.* 2007). The length of time PM particles spend in the atmosphere is determined by wind speeds and the deposition velocities of the PM particles (Denman *et al.* 2007).

Fluctuating temperatures contribute to changes in the PM chemical composition and the mass concentration (Im *et al.* 2012). Convective heating of air near the surface due to increases in temperature contribute to the vertical movement of PM in the atmosphere (Garrat, 1992). Temperature contributes to precipitation and cloud formation leading to the wet deposition of PM particles (Dawson *et al.* 2007). Temperature has a greater effect on the PM emissions from vegetation sources (Guenther *et al.* 1995). Gas to PM chemical reactions of secondary volatile organic carbon emissions are also affected by temperature (Kanakidou *et al.* 2005). Temperature within city environments contribute to the urban heat island effect when temperatures within urban areas are warmer than the surrounding rural areas. The urban characteristics of cities, including the covering of natural surfaces with impervious materials such as cement and asphalt and the anthropogenic heat emissions from buildings, people and traffic alter the surface energy and radiation budgets, increasing the temperatures within cities (Oke, 1982; Lowry and Lowry, 1989). The urban heat island is therefore an important driver of PM_{10} related air pollution within city environments.

2.3. PM and AOD Relationship

2.3.1. Introduction

PM_{10} concentration and the Aerosol Optical Depth (AOD) are two important measures of PM in the atmosphere. This section will discuss how these two measures are empirically related. This will be followed by a review of different case studies which have determined the AOD-PM_{10} relationship in Asia and in Europe. Finally a discussion on the effects of weather on the AOD- PM_{10} relationship will be discussed.

2.3.2. Empirical Relationship between PM and AOD

The PM and AOD relation from Koelemeijer *et al.* (2006) shown below in equations 1-5 is based upon 2 crucial assumptions. The first is that there is a uniform distribution of PM within the atmospheric column. The second is that the shape of the PM particles within the atmospheric column are spherical. This assumption was used due to the dependence of the optical characteristics of PM particles on the structure of the PM particles (Tsay *et al.* 1991).

PM concentration is mass per volume based - PM, measured after drying of the air samples. The drying of PM samples controls for the effect of water molecules on hygroscopic particles which can affect the mass concentration of the PM sample. For reproducibility of the measurement of mass concentration of PM particles, the samples are dried. The concentration per volume cubed is dependent upon the PM size distribution - $n(r)$ and the PM mass density - ρ (Koelemeijer *et al.* 2006). This is expressed as:

$$PM = \frac{4}{3}\pi\rho \int r^3 n(r)\mathrm{d}r$$

Equation 1

The AOD for an atmospheric column of certain height is affected by several parameters. The first is the size distribution assuming an ambient environment - $n_{amb}(r)$ with RH. Two important differences between the measurement of PM and the measurement of AOD are highlighted, one being the measurement of tropospheric particles without the effect of water on mass concentration included, whilst measuring the AOD aims to integrate the effect of water vapour into the determination of the AOD which is representative of both tropospheric and stratospheric aerosols. The second is the extinction efficiency, which is affected by the particle refractive index and size. The extinction efficiency is expressed

18

under environmental ambient conditions - $Q_{\text{ext,amb}}$ and under dry conditions - $Q_{ext,dry}$ (Koelemeijer *et al.* 2006). $f(RH)$ is the ratio between the two extinction efficiencies with the size distribution integrated into them. This is expressed as:

$$\text{AOT} = \pi \int_0^H \int_0^\infty Q_{\text{ext,amb}}(r) n_{amb}(r) r^2 \mathrm{d}r\, \mathrm{d}z$$

$$= \pi f(RH) \int_0^H \int_0^\infty Q_{ext,dry}(r) n_{amb}(r) r^2\, \mathrm{d}r \mathrm{d}z$$

Equation 2

As a function of RH, the extinction efficiency is expressed as a ratio between the extinction efficiency under ambient conditions and the extinction efficiency under dry conditions (Koelemeijer *et al.* 2006). By considering the extinction efficiency under ambient and fry conditions, the hygroscopic growth of particles due to water vapour in the atmosphere is considered. The extinction efficiency can therefore be expressed as:

$$\langle Q_{ext} \rangle = \frac{\int r^2\, Q_{ext}(r) n(r) \mathrm{d}r}{\int r^2\, n(r) \mathrm{d}r}$$

Equation 3

Also effecting the AOD –PM relationship is the particle effective radius - r_{eff} (Koelemeijer *et al.* 2006). The dispersion and distribution of particles in the atmosphere is dependent on particle size. The relation between PM and AOD assumes that particles are evenly distributed throughout the atmosphere and therefore have a homogenous particle size. The r_{eff} is expressed as:

$$r_{eff} = \frac{\int r^3(r) n(r) \mathrm{d}r}{\int r^2 n(r) \mathrm{d}r}$$

Equation 4

The AOD and PM relation (Koelemeijer *et al.* 2006) can be expressed as:

$$AOD = PMHf(RH) \frac{3\langle Q_{ext} \rangle}{4\rho r_{eff}}$$

Equation 5

Deviations from these assumptions do occur for the AOD-PM_{10} relationship, such as the increased variability in the distribution of PM particles in the atmospheric column and the

greater variability of the PM particle shape. In terms of only PM, the presence of water vapour in the air at the surface (the atmosphere from which measurements of PM occur) will also affect the AOD-PM_{10} relation. The PM size distribution and refractive index especially in humid atmospheres is affected by the additional water vapour content of the atmosphere, having the most impact on soluble aerosols (Tsay *et al.* 1991). The assumption of particle sphericity and the dry sampling of particulate mass, is contrasting due to the particles which are drier having less sphericity than moist particles (Tsay *et al.* 1991).

Uncertainties in satellite retrieval algorithms are directly related to the extent, the algorithms consider the properties of aerosols over a region so as to address the limitations of the empirical relationship between the AOD and PM. Algorithms should include region specific information about aerosol properties including aerosol type, refractive indices, hygroscopicity, density and size distribution (Hoffman and Christopher, 2009). Resolving the challenges within algorithms to simulate the "real" properties of aerosols has contributed to the diversity of satellite data available which measure aerosols. This will be discussed in section 2.4.2.

2.3.3. AOD and PM_{10} Correlations

The Mixing Layer Height (MLH) and the RH have been identified by the literature as being the main meteorological factors which affect the AOD-PM_{10} relationship. Most of the case studies which have determined the AOD-PM_{10} relationship considered the multiple meteorological effects including temperature, atmospheric pressure, wind speed and wind direction, MLH and the RH. Previous studies which have analysed the AOD and PM_{10} relationship have primarily been undertaken in Europe and in Asia with fewer studies for example Engel-Cox *et al.* (2004), undertaken in North America. Previous North American studies have largely modelled the AOD and $PM_{2.5}$ relationship because the correlations between AOD and $PM_{2.5}$ were found to be stronger in North America relative to the AOD and PM_{10} relationship (Hutchison *et al.* 2005; Gupta and Christopher, 2008; Li *et al.*, 2009). Vidot *et al.* (2007) determined that seasonality effects on the vertical distribution of the RH needed to be considered for the AOD-PM_{10} relationship. Zha *et al.* (2010) observed examples of pollution episodes when the AOD-PM_{10} relationship was strengthened over China due to meteorological conditions characterised by high

temperatures, a high RH accompanied by weakened pressure systems and wind speeds. For these pollution episodes, Zha *et al.* (2010) found that the contribution of local emission sources were the dominant sources of PM. Kumar *et al.* (2007) observed that the relationships between RH, sea level pressure and the wind direction also had an impact on the AOD-PM$_{10}$ relationship.

2.3.3.1. Case Studies in Asia

When comparing the AOD-PM$_{10}$ correlation over different AQM stations, a wide range of correlations were determined even when the meteorological conditions were typified to a common set of observations. Zeeshan and Oanh (2014) used a clustering technique to group values of meteorological variables including sea level pressure, wind direction, visibility, dry bulb temperature, dew point and cloud cover according to synoptic weather types (Table 1). Meteorological variables were integrated into the AOD-PM$_{10}$ relationship for Thailand for each synoptic type with correlations ranging from 0.3 to 0.6. Zha *et al.* (2010) used cluster analysis and the meteorological variables were used as grouping variables including RH, temperature, wind speed and atmospheric pressure for the seasonal AOD-PM$_{10}$ relationship for Nanjing China for the period 2004 to 2006. The use of the clustering method did not improve the AOD-PM$_{10}$ correlation which was 0.2- 0.7 before clustering was applied and 0.2 - 0.6 after clustering was applied.

Spatially or temporally averaging AOD and PM$_{10}$ observations achieved high AOD-PM$_{10}$ correlations. For example Wang *et al.* (2010) determined that the MLH and RH integrated AOD-PM$_{10}$ correlation over Beijing was weaker ($R^2 = 0.47$) when all observations were collated together. The AOD-PM$_{10}$ correlation was stronger ($R^2 = 0.66$) when all the observations either were averaged temporally (over a month) or spatially (for many stations). When Kumar *et al.* (2008) spatially averaged the PM$_{10}$ measurements for New Delhi, India to the spatial scale of the AOD measurements; the AOD-PM$_{10}$ correlation was good with an R^2 of 0.61 at the hourly temporal scale.

The correlations between meteorology and PM$_{10}$ may be higher than the correlations between AOD and PM$_{10}$. The correlations between PM$_{10}$ measured in Borneo, Indonesia in 2004 and the AOD were poor with R^2 values ranging between 0.2-0.4 (Mahmud *et al.* 2012). The correlation between PM$_{10}$ and its meteorological coefficients were greater and

indicated that meteorology had a substantial effect on the PM_{10} concentrations with R^2 values between 0.7 and 0.8. The poor correlations between AOD and PM_{10} indicated the presence of confounding factors.

The integration of only one meteorological was insufficient to improve the AOD-PM_{10} relationship over Beijing, China. Although Absolute Humidity (AH) was found to be a significant predictor of PM_{10}, the correlation between the AH calibrated AOD and the AH modified PM_{10} was low with an R of 0.22 (Wang *et al.* 2013). Using neural network modelling to integrate MLH, RH, temperature, wind speed, wind direction and the AOD to model PM_{10} concentrations, Wu *et al.* (2012) determined a wide range of correlations for different AQM stations in Beijing with R =0.09 - 0.66. An *et al.* (2007) determined a high R^2 of 0.8 for the hourly AOD-PM_{10} relationship for an air quality episode in Beijing in April 2005 by integrating the AOD with modelled meteorological parameters including the wind speed, wind direction, atmospheric pressure, temperature and the RH.

An *et al.* (2007) highlighted that the AOD-PM_{10} is correlated the best for a specific set of meteorological observations for a specific air quality episode. Other case studies in Asia, achieved AOD-PM_{10} that were highly correlated with correlations greater than 0.7. The bulk of the studies highlighted that despite the statistical modelling methods used, that it is typical for a region to have widely ranging AOD-PM_{10} correlations when the correlations are determined for each AQM station. However when the correlations for all stations are spatially or temporally averaged, the AOD-PM_{10} correlation is high. Additionally the case studies highlighted the importance of considering more than one meteorological variable within the AOD-PM_{10} relationship.

2.3.3.2. Case Studies in Europe

Koelemeijer *et al.* (2006) determined the MLH and RH integrated MODIS AOD-PM_{10} relationship over Europe for 2003, with an R range of 0.34-0.54 for hourly and daily AOD-PM_{10} correlations (Table 4). Using Sea-Viewing Wide Field-of-View Sensor (SeaWIfS) AOD, Vidot *et al.* (2007) determined the AOD-PM_{10} relationship over England, France and Belgium for the period 1999-2004 with an R^2 of about 0.4-0.61 after including the total precipitate water content, the wind speed, surface pressure and the RH. The correlations were dependent upon the type of validation used and better correlations were achieved when the satellite AOD was compared to *in situ* measured AOD.

Emili *et al.* (2010) determined greater AOD-PM$_{10}$ correlations over Switzerland with Spinning Enhanced Visible and Infrared Imager (SEVIRI) AOD with the AOD-PM$_{10}$ correlation ranging between 0.42 and 0.72 compared to the MODIS AOD correlations with PM$_{10}$ which ranged between 0.46 and 0.58. Nordio *et al.* (2013) determined the MODIS AOD-PM$_{10}$ relationship over Lombardy, Italy for the period 2000 - 2009 with an R^2 of about 0.8. The AOD data were included as an input to an integrated model which included major roads, PM$_{10}$ emissions, elevation, population density and meteorological parameters. A good correlation was also determined over Croatia, by Grguric *et al.* (2013) for the period 2008-2012 with the R ranging from 0.3 - 0.6 and was dependant on the type of statistical modelling used including multivariate linear regression and neural network modelling.

Studies which have determined the AOD-PM$_{10}$ correlation have been largely from Europe and from Asia. The studies that were discussed in this section, included meteorological effects to the AOD-PM$_{10}$ relationship, with the majority considering numerous meteorological effects including temperature, RH, air pressure, wind speed and wind direction variables. The two most important meteorological effects on the AOD-PM$_{10}$ relationship were the MLH and the RH. Comparisons between case studies were not possible in most cases due to the different geographic areas of interests used. However a few case studies have determined the AOD-PM$_{10}$ relationship for Beijing, China and the correlations increased when numerous meteorological effects were included for the AOD-PM$_{10}$ correlation. Location, satellite AOD validation, temporal and spatial averaging across a number of AQM stations and meteorological effects have a substantial effect on the AOD-PM$_{10}$ relationship.

2.3.4. Effects of Weather on the AOD-PM$_{10}$ Relationship

Different "scenarios" of PM vertical distribution affect the extent to which AOD can be used as a suitable proxy for PM$_{10}$ (Gupta and Christopher, 2009). The first example is the transport of PM aloft in the upper atmosphere, perhaps transported long distance or collected through vertical dispersion, the PM$_{10}$ concentration would not be representative of PM concentrations in the upper atmosphere with the AOD an unsuitable proxy for PM$_{10}$. The second example was if the boundary layer contains an inversion layer higher up in the atmosphere, the vertical dispersion of PM is then aided throughout the atmospheric

column. The PM concentrations would be low for this example and the AOD would not be a suitable proxy for PM_{10}. The last example was if the boundary layer contained an inversion layer near the surface then the vertical dispersion of PM would be constrained. For this example, the PM concentration would be high and the AOD would not be a suitable proxy for PM_{10}. Hence the AOD is less sensitive to PM loading at the surface (Gupta and Christopher, 2009) and may not be solely sufficient as a proxy for PM. There is need to consider the meteorological effects on the AOD-PM_{10} relationship.

Effects of the weather system on the AOD-PM_{10} relationship are substantial and the subsequent discussion focussed upon the studies which discussed the meteorological effects on the AOD-PM_{10} relationship. Only two meteorological parameters were identified in the discussion to individually impact substantially on the AOD-PM_{10} relationship namely the MLH and RH.

2.3.4.1. Mixing Layer Height

The MLH also known as the boundary layer height (BLH) has been used in case studies to further improve the AOD-PM_{10} relationship (for example Emili *et al.* 2011). The changes in the height of the boundary layer can contribute to changes in PM concentration at the surface and is indicative of the extent of vertical mixing of PM particles within the atmospheric boundary layer (Trivedi *et al.* 2014). For days when the MLH is low, and there is no inversion present, the use of the MLH complements the AOD-PM relationship as the aerosol loading would be closest to the surface (Estellés *et al.* 2012). In some cases, consideration of the MLH does not improve the AOD-PM relationship, for example Schaap *et al.* (2009) observed that the inclusion of MLH did not improve the AOD-PM relationship over Cabauw in the Netherlands. In most studies for example Emili *et al.* 2010, it was found that the inclusion of the MLH significantly improved the AOD-PM relationship.

The extent to which the AOD-PM_{10} relationship can benefit from the inclusion of MLH will vary for different locations and for different temporal periods. The MLH will vary for different locations due to the contribution of land cover features to the development of the boundary layer (Oke, 1987). MLH effects on the AOD-PM_{10} relationship will vary temporally due to the sampling period used, dependant on the prevailing seasonal meteorological conditions (Emili *et al.* 2010).

24

Emili *et al.* (2011) determined the AOD-PM$_{10}$ relationship over Italy and Switzerland with the inclusion of the MLH (Table 1). In Emili *et al.* (2010), it was found that the MLH had a greater effect on the correlation than the effect of RH. In Emili *et al.* (2011), the maximum MLH that is reached each day was incorporated into the algorithm used to estimate PM$_{10}$ concentration. It was observed in this study, that the use of the maximum MLH improved the AOD-PM$_{10}$ correlation over mountainous terrain due to the greater uplift of aerosol layers in the atmosphere over these areas compared to lower altitude terrain.

2.3.4.2. Relative Humidity

The RH is an indicator of water vapour content in the atmosphere. The extinction efficiency of aerosol particles increases under higher RH conditions, thereby increasing the AOD. PM represents the concentration for a dried parcel of air, and will remain unaffected by higher RH conditions (Koelemeijer *et al.* 2006). Aerosol particles will increase in size with the interaction of the particles with water vapour in the atmosphere and also due to the occurrence of secondary processes of PM formation (Grguric *et al.* 2013).

Kumar *et al.* (2008) found that the AOD-PM$_{2.5}$ relationship over New Delhi was more affected by the inclusion of RH than the AOD-PM$_{10}$ relationship. In Emili *et al.* (2010), the consideration of the vertical distribution of the RH for the AOD-PM$_{10}$ relationship was effective over some locations but not for others. In Guo *et al.* (2009), it was determined that the RH was not a dominant factor to influence the AOD-PM$_{10}$ relationship over China. The range of correlations between PM$_{10}$ and AOD over China were 0.35 - 0.62 before RH was included and the correlations were 0.36 - 0.63 after the RH was included. Kim *et al.* (2013) linked the peak AOD events over the central region of South Korea which occurred in May to the increase in RH and the occurrence of a stable atmosphere; however no meteorological analysis was done in the study. Since the RH was found in multiple studies to be a confounding factor affecting the AOD-PM$_{10}$ relationship, the RH should be accounted for when determining the AOD-PM$_{10}$ relationship.

Table 1: Studies which have investigated the AOD-PM$_{10}$ relationship (see appendix A for full table).

Reference	Time period	Location	Number of AQM stations	Correlation coefficients
Koelemeijer *et al.* (2006)	2003	Europe	> 100 AQM stations	R^2 = 0.17-0.54
An *et al.* (2007)	3-7 April 2005	Beijing, China	PM modelled	R^2 = 0.84
Vidot *et al.* (2007)	1999-2004	Europe (England, France and Belgium)	80 AQM stations	R^2 = 0.43
Kumar *et al.* (2008)	2000-2005	New Delhi, India	113 passive AQM sites, 1 AQM station	R = 0.61-0.64
Guo *et al.* (2009)	2007	China	11 AQM stations	R = 0.35-0.62
Emili *et al.* (2010)	2008	Switzerland	13 AQM stations	R = 0.46-0.72
Zha *et al.* (2010)	2004-2006	Nanjing, China	6 AQM stations	R^2 = 0.19-0.75
Emili *et al* (2011)	2008-2009	Italy and Switzerland	27 AQM stations	R = 0.50-0.51
Mahmud *et al.* (2012)	1 August 2004	Bornei, Indonesia	7 AQM stations	R = 0.17-0.36
Wu *et al.* (2012)	2007-2008	China	7 AQM stations	R = 0.12-0.66
Grguric *et al.* (2013)	2008-2012	Croatia	12 AQM stations	R = 0.28-0.6
Kim *et al.* (2013)	2009	Anmyon, Cheongwon and Ulleung, South Korea	3 AQM stations	R = 0.43-0.55

Table 1: continued.

Reference	Time period	Location	Number of AQM stations	Correlation coefficients
Nordio *et al.* (2013)	2000-2009	Lombardy, Italy		R = 0.787
Wang *et al.* (2013)	2006	Beijing, China	35 AQM stations	R = 0.22
Zeeshan and Oanh (2014)	Dry season 2000-2010	Thailand	22 AQM stations	R = 0.27-0.58

2.4. Measurement of Aerosols for Air Quality and Aerosol Studies

This section will briefly discuss the different air quality samplers used to measure PM_{10} concentration. This will then be followed by a discussion on aerosol monitoring using *in situ* monitors and satellite remote sensing.

2.4.1. Ground Level Measurements of PM

In situ measurements of PM_{10} concentration for air quality studies are localised using various types of air quality samplers. Measurements of PM loading are also localised, however the collective data collection and analysis from international PM measurement stations has facilitated the study of PM loadings and climatology at a global level.

High volume samplers have been used in some studies, which use size specific filters to capture PM_{10} particles, which are then later removed and then weighed in order to determine the particulate concentration in $\mu g/m^3$. For example Agarwal *et al.* (2013) determined the health effect of agricultural biomass burning in Patiala city, India over the period 2007 - 2010 and monitored PM_{10} using high volume samplers with glass fibre filters. Alghamdi *et al.* (2014) also used high volume samplers to collect PM_{10} samples on glass fibre filters in order to determine the micro organismal composition of the aerosol particles over Jeddah, Saudi Arabia, in 2012 and 2013 with measurements taken every 24 hours. Ana *et al.* (2013) used high volume samplers to collect PM_{10} samples, in Ibadan, Nigeria to determine the indoor air pollution impact of burning of wood used as cooking fuel.

Impactor samplers have been used in some studies which collect particulates at different size distributions for the same parcel of air that is pumped through the inlet pipe. For example Giorio *et al.* (2014) used a cascade impactor with Teflon fibre filters samplers to collect PM_{10} samples in Padova, Italy in 2006 and 2007 with a sampling timeframe of 24 hours. Laser photometry instruments such as the dustrack aerosol monitor which provide real time measurements of particulate mass have been used in some studies. Beh *et al.* (2013) used the dustrack aerosol monitor to collect measurements of PM_{10} concentration in Penang, Malaysia in 2012. One of the five instruments used by Heal *et al.* 2000 was the dustrack monitor which was used to take measurements of PM_{10} in England, U.K. in 1997 and 1998.

Optical particle counters have also been used in some studies to take measurements of particulates. In addition to the use of impactor samplers, Giorio *et al.* (2014) used optical particle counters which provided continuous real time measurements of PM_{10} concentrations. Hu *et al.* (2006) used the measurements of PM_{10} concentration from duel scattering angle optical particle counters in conjunction with LIDAR retrievals to aid in the determination of PM_{10} vertical profiles over Beijing, China.

Tapered Element Oscillating Microbalance (TEOM) measurements which measure PM concentrations from dried air samples, have been used in some studies to take measurements of particulates. Krieger *et al.* (2007) took TEOM measurements of PM_{10} and PM_1 concurrently in Zurich, Switzerland in 2005 and 2006 which were validated with measurements using high volume samplers. Wang *et al.* (2011) took TEOM measurements in Wuhan, China in 2009 and compared the PM_{10} measurements to *in situ* AOD measurements. TEOM instruments are used extensively in air quality monitoring sites in Europe and the United States (Marcazzan *et al.* 2001).

Low volume samplers have been used in some studies to take measurements of particulates. For example Ragosta *et al.* (2007) used a low volume sequential sampler with cellulose fibre filters to collect PM_{10} samples in Tito Scalo, Italy in 2001, which were then later removed and then weighed in order to determine the particulate concentration in $\mu g/m^3$ and further analysis was carried out to determine the individual heavy metal concentrations found in the PM_{10} samples collected. Chaloulakou *et al.* (2003) also used low volume samplers with glass Teflon fibre filters in Athens, Greece to obtain PM_{10}

measurements in 1999 and in 2000. For Ragosta *et al.* (2007) and Chaloulakou *et al.* (2003), an electronic microbalance was used to determine the concentrations of the PM_{10} collected on the fibre filters.

The measurement of PM on the ground largely employed gravimetric methods for passive sampling and used TEOM extensively for long term measurements at AQM stations internationally. The measurements of aerosol properties on the ground including measurements of the AOD largely employed photometric technology such as sun photometers for both passive sampling and long term sampling.

Globally spread networks of *in situ* PM monitors consist of the Aerosol Robotic Network (AERONET) and the Micro Pulse Lidar Network (MPLNET). The AERONET is a global network of spectral radiometers that has been used in global regional and local studies of PM properties (Holben *et al.* 1998). The Cimel sun photometer was the most common instrument used in AERONET, with measurements made at wavelengths at 440 nm, 670 nm, 870 nm and 1020 nm and the main measurement retrieved from the measurements is the AOD. The MPLNET is a network of lidar systems established globally since 2000 to monitor the vertical distribution of PM properties including the AOD (Welton *et al.* 2001). The Multi-filter Rotating Shadowband Radiometer (MFRSR) network is a global collection of PM measurements mostly located in the United States but with stations also found in other regions of the world (Alexandrov *et al.* 2002). The MFRSR instruments monitor PM particles at wavelengths between 415 nm, 500 nm, 615 nm, 670 nm, 870 nm, and 940 nm. The World Meteorological Organisation's (WMO's) Global Atmosphere Watch Precision Filter Radiometer (GAWPFR) network also measure the AOD for specific wavelengths including 368 nm, 412 nm, 500 nm, and 862 nm (Kim *et al.* 2008).

The key descriptors that are measured by the instruments used in the global monitoring networks as well as observed from satellite imagery to quantify the direct effect are included in Figure 1. The aerosol optical parameters are a measure of the total atmospheric column, which change according to the RH conditions and wavelength, from which the measurements are retrieved from. Temporally variable parameters include aerosol loading and the spatial distribution of aerosols (Haywood and Boucher, 2001; Forster *et al.* 2007). The long term data collected from these networks have been the main sources of aerosol data which have been used with, satellite observations of aerosol properties and climate

simulations in order to model the global aerosol climatology (Holben *et al.* 1998; Welton *et al.* 2001).
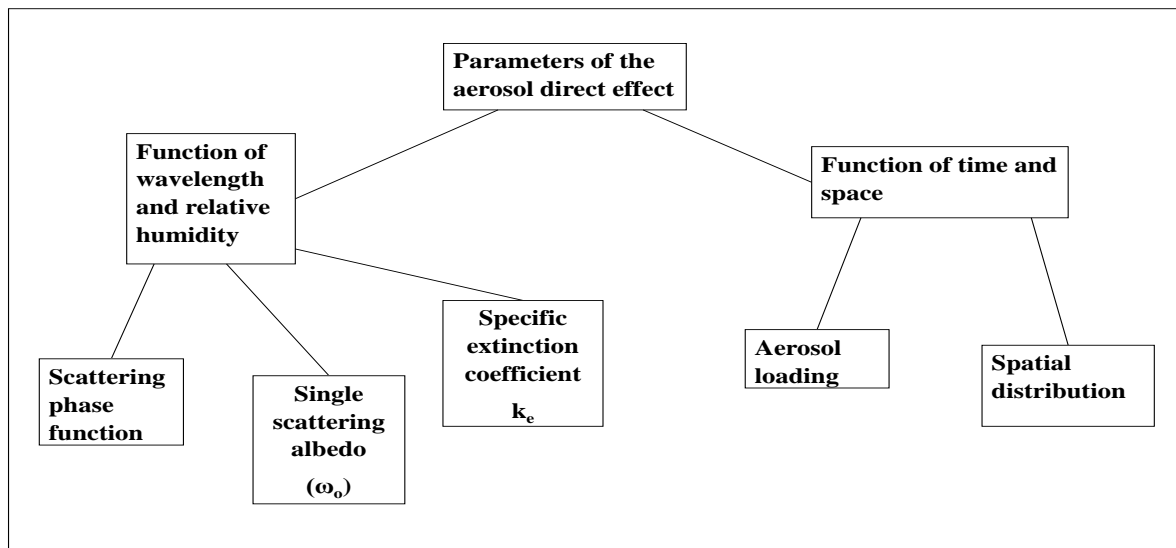
Figure 1: Factors which affect the aerosol direct effect (Source: Forster *et al.* 2007).

For example, by using AOD retrieved from satellite borne sensors and simulations of smoke emissions using the Community Atmosphere Model, it was possible to simulate the long term effects of smoke emissions to the climate system. The effects of the smoke emissions were found to contribute to increasing temperature, increasing AOD, decreasing radiation at the surface and modifications to the precipitation patterns (Tosca *et al.* 2013). Grythe *et al.* (2014) used the FLEXible PARTicle (FLEXPART) lagrangian dispersion model to simulate the meteorological contributions to sea spray aerosol production. Dai *et al.* (2014) modelled aerosol properties including single scattering albedo, AOD and the angstrom exponent using the Nonhydrostatic ICosahedral Atmospheric Model (NICAM) with validation using *in situ* measurements from the AERONET.

When new modelling components were determined for the Nonhydrostatic Multiscale Meteorological Model on the B grid / Barcelona Supercomputing Center (NMMB/BSC) chemical transport modelling, supplementary data were needed to model and assess the simulation of sea salt aerosols. (Spada *et al.* 2014). AOD data were retrieved from *in situ* measurements from sun photometers from AERONET. Data on the concentration of sea salt aerosols were obtained from the ocean aerosol network operated by the University of Miami which monitors the concentration of various aerosol species. Data were collected from two ship campaigns to study aerosol properties including the AEROSOLS99 and INDian Ocean EXperiment (AEROINDOEX) and the Aerosol Characterization

Experiment 1 (ACE1) (Spada *et al.* 2013). These case study examples indicate the extent to which climate modelling, *in situ* monitoring and satellite observation have aided the determination of radiative effects of aerosol emissions at the global scale.

2.4.2. Satellite Measurements of PM

Remotely sensed AOD retrievals have been sourced from a broad range of satellites. These satellites have been provided by space agencies including the National Aeronautics and Space Administration (NASA), European Space Agency (ESA) and the European Organisation for the Exploitation of Meteorological Satellites (EUMETSAT). In this section the satellites, sensors used to provide AOD retrievals will be discussed.

Kaskaoutis *et al.* 2010 retrieved AOD over Athens from MEdium Resolution Imaging Spectrometer (MERIS) imagery which is a sensor on board the Envisat satellite. Wu *et al.* (2012) used MODIS AOD retrieved over China provided from AQUA and TERRA satellites. Emili *et al.* (2010) retrieved AOD from the SEVIRI sensor on board the Meteosat Second Generation satellite (MSG) over Switzerland. Liu *et al.* (2002) retrieved AOD over Taiwan from Systeme Pour l'observation de la Terre (SPOT) imagery. Ahn *et al.* (2014) assessed AOD retrievals globally from the Ozone Monitoring Instrument (OMI) on board the AURA satellite. Vidot *et al.* (2007) retrieved AOD over Europe from the SeaWiFS sensor on board the OrbView-2 satellite. Sivakumar *et al.* (2009) compared in-situ AOD to AOD data from the Stratosphere Aerosol Gas Experiment (SAGE) II on-board the Earth Radiation Budget Satellite (ERBS) satellite. These past studies have indicated the many sources of AOD data from satellites which have populated the research field to the present.

Bréon *et al.* (2011) assessed AOD retrievals from different satellite sources over Africa, Europe and the Middle East by comparison of the satellite retrievals against sun photometer retrievals of AOD. In Bréon *et al.* (2011), MERIS retrievals of AOD were poorly correlated with *in situ* retrievals from sun photometer measurements. The MERIS Reduced resolution geophysical product—Level 2 data including the AOD is publicly available from the ESA (Santer and Ramon, 2011). The AOD product is at 443 nm, with a horizontal resolution of 1.2 km by 1.2 km and a revisit time of about three days varying for different latitudes (Santer and Ramon, 2011). In addition the measurements of AOD by MERIS were higher than the measurements by the sun photometers. Bocci *et al.* (2009)

had similar findings, with MERIS measurements of AOD tending to have larger AOD values for smaller AOD's measured by sun photometers in France. A comparison of MERIS AODs to PM_{10} over Germany in 2005 and 2006 by Rohen *et al.* (2011) were generally good, however MERIS retrievals of AOD were more uncertain over areas with greater PM_{10} loading in the atmosphere compared to loadings of smaller aerosols in the atmosphere. MERIS AOD was available through ESA as a level 2 product (Santer and Ramon, 2011).

SEVIRI AOD retrievals over North Africa were correlated with AERONET sunphotometers with correlations ranging from 0.52 to 0.73 (Banks and Bridley, 2013). The SEVIRI AOD and angström exponent product at 550 nm is publicly available from LSCE/ICARE at 550 nm, with a horizontal spatial resolution of 3 km by 3 km for an almost daily retrieved product (Jolivet *et al.* 2008). Over Switzerland, Emili *et al.* (2010) obtained correlations of more than 0.9 over Ispra, however over Laegeren the correlation decreased to 0.5 and over Davos, the correlation deceased further to 0.4. At the regional scale, correlations between *in situ* AOD and satellite AOD for SEVIRI were about 0.9 for the entire Central Europe region (Pop *et al.* 2007). Over Africa, the Middle East and Europe, correlations between SEVIRI AOD and sun photometer AOD were about 0.63 (Bréon *et al.* 2011). However, SEVIRI AOD data are not officially made available through EUMETSAT and access to SEVIRI data is limited (Bréon *et al.* 2011).

Sayer *et al.* (2012) found that SeaWiFS data were suitable for quantitative use, by comparison of global satellite AOD retrievals to AERONET retrievals. The SeaWiFS Deep Blue AOD and angstrom exponent product is freely available through NASA and has a horizontal spatial resolution of 13.5 km by 13.5 km. The product is available at 550 nm and the satellite has an almost daily revisit time (Hsu *et al.* 2012). The correlation between SeaWiFS AOD and AERONET AOD was 0.86 using the best quality data. Hsu *et al.* (2012) similarly found good correlations between SeaWiFS AOD and AERONET AOD by comparing the AOD at a global level. The data for SeaWiFS is available through NASA with a long term quantity of aerosol data spanning 20 years.

Imagery from higher spatial resolution satellites such as SPOT and Landsat have currently not been used for global retrievals of AOD. Soulakellis *et al.* 2004 used imagery from SPOT-1, SPOT-2 and SPOT-4 to retrieve AOD over Brescia in Italy for four days in 1997 and 1998. Liu *et al.* (2002) used SPOT imagery to map AOD over Chung-Li in Taiwan for

six days in 1998. Hadjimitsis and Clayton (2009) used Landsat TM imagery for the estimation of AOD over Heathrow airport in the UK and over Paphos airport in Cypress for five different case study days. These studies have been applied only at the local scale and for a limited number of days.

The Multiangle Imaging Spectroradiometer (MISR) level 2 aerosol product has a horizontal resolution of 17.6 km by 17.6 km, and is publicly available through NASA. The product has an almost daily temporal frequency and is available at the 446 nm, 558 nm, 672 nm and 866 nm wavelengths. Globally MISR AOD retrievals over terrestrial surfaces compared to MODIS retrievals over terrestrial surfaces, have a 70% correlation. The differences were attributed to the constraints of the MISR AOD retrieval algorithm, for example such as the assumptions made for the MISR AOD retrieval and in the algorithm processing applied for AOD retrievals (Khan *et al.* 2009). For example over India, densely vegetated regions were more important for the retrieval of MODIS AOD than for the retrieval of MISR AOD (Prasad and Singh, 2007).

The Cloud-Aerosol Lidar Infrared Pathfinder Satellite Observations (CALIPSO) Lidar level 2, 5 km by 5 km aerosol data retrieved using the Cloud-Aerosol Lidar with Orthogonal Polarization (CALIOP) sensor on board the CALIPSO satellite was publicly available from NASA. The AOD product is available at 1064 nm and 532 nm wavelengths (Winker *et al.* 2009). For all aerosol types at the global scale, correlations between CALIPSO AOD and AERONET were R = 0.429. Although the correlation between CALIPSO AOD and AERONET AOD was weak, CALIPSO is advantageous in observing the vertical distribution of aerosols at a location, during nocturnal periods, in the vicinity of clouds and for land surfaces with high reflectance (Kittaka *et al.* 2011).

The MODIS sensor on board the AQUA and TERRA satellites is the source of the MODIS aerosol product level 2. This AOD is provided freely at 470 nm, 550 nm, 660 nm and 2130 nm wavelengths at a horizontal spatial resolution of 10 km by 10 km (Remer *et al.* 2005). Various studies have found good correlations between MODIS AOD and AERONET. Over Hong Kong, Wong *et al.* (2013) found that MODIS AOD correlated well with AERONET retrievals (R = 0.947). Over Thailand, Zeeshan and Oanh (2014) found that the MODIS-AERONET correlation was good ($R^2 = 0.81$). Emili *et al.* (2010) found varied correlations (R=0.67 - 0.93) over three sites in Europe (Ispra, Laegeren and Davos). Remer *et al.* (2008) found good global correlations between MODIS terrestrial AOD and

AERONET terrestrial AOD (R = 0.908 - 0.926). Similarly Levy *et al.* (2010) found good correlations between MODIS terrestrial AOD and AERONET AOD (R = 0.88). Bréon *et al.* (2011) found that MODIS offered the best estimates of cumulative AOD when compared to POLarization and Directionality of the Earth's Reflectances (POLDER) AOD, MERIS AOD, SEVIRI AOD and CALIOP AOD with an R = 0.86 when compared to AERONET retrievals and that the recovery of good quality data were more than 50%.

The Level 2 Aerosol Product from the OMI sensor on board the AURA satellite is publicly available through NASA at wavelengths 342.5 nm, 367 nm, 388 nm, 406 nm, 425.5 nm, 442 nm, 463 nm, 477 nm and 483.5 nm. The horizontal spatial resolution of the OMI AOD product is 24 km by 13 km with an almost daily temporal frequency. Over Europe, Ali *et al.* (2011) found that OMI multi-wavelength retrievals were better correlated to AERONET measurements than the OMI near UV aerosol retrievals. Over Hong Kong, Wong *et al.* (2013) found that the correlation of OMI AOD with AERONET was 0.589 compared to the correlation between MODIS AOD and AERONET which was 0.947. Over Western Europe, Curier *et al.* (2008) found that OMI and MODIS were fairly well correlated (R = 0.66). AOD estimates from OMI over the ocean were better than the AOD estimates over land (Curier *et al.* 2008). The studies discussed compared different OMI aerosol products with each other, compared OMI AOD retrievals with other satellite AOD retrievals and compared OMI AOD with AERONET AOD measurements.

The Advanced Along-Track Scanning Radiometer (AATSR) AOD product retrieved from the AATSR sensor on-board the Envisat satellite is publicly available from the Finnish Meteorological Institute (FMI). The horizontal spatial resolution of the product is 10 km by 10 km, with a temporal frequency of about three days and available at the 555 nm, 659 nm and 1610 nm wavelengths. AATR retrievals over Africa according to Sogacheva *et al.* (2010) correlated well with AERONET ground measurements of AOD. Sogacheva *et al.* (2010) also observed that AASTR retrievals of AOD were generally larger than the retrievals from AERONET. However one of the constraints of the AATSR AOD retrievals was that, they were unsatisfactory over land cover classes with high reflectance (Kolmonen *et al.* 2013). Kokhanovsky *et al.* (2009) observed that over a well vegetated area over Germany, AATSR retrievals of AOD compared well with MISR and MODIS AOD retrievals.

Comparison of the AOD retrieved by satellites to the AOD from *in situ* measurements indicated varying correlations based upon the satellite AOD product and the geographical area of interest. In most cases, the correlations were good; however exceptions were present, such as the poor correlation of MERIS AOD with *in situ* AOD over areas of Africa, Middle East and Europe. Additionally MERIS AOD does not retrieve AOD at the 550 nm wavelength. AATSR AOD product is good but the area of interest must have low reflectance due to being well vegetated for retrievals to have good correlations with *in situ* AOD. AOD products with high spatial resolution from Landsat and SPOT are not readily available and input data requirements for satellite AOD retrieval are intensive. SEVIRI AOD, SeaWiFS AOD, MODIS AOD, MISR AOD, CALIOP AOD and OMI AOD were found to be good sources of data which were freely available to use. Lidar measurements of aerosol distribution have been used to resolve the vertical distribution of aerosols in the atmosphere above a location and contributed to improving the correlations between satellite and in situ measured AOD (Sivakumar *et al.* 2010). In the next part of this section, the satellite retrieval algorithms used to retrieve aerosol information from satellite images are discussed.

The main algorithm used to retrieve AOD data from imagery captured by the MODIS sensor was the algorithm for remote sensing of tropospheric aerosol over dark targets from MODIS (Remer *et al.* 2005). The algorithm used the wavelengths from 470 nm, 660 nm and 2130 nm, to retrieve AOD over densely vegetated surfaces over land and a Look Up Table (LUT) approach was used to find the best fit estimation for the optical depth estimation based on different aerosol models (Remer *et al.* 2005).

The enhanced deep blue aerosol retrieval algorithm (Hsu *et al.* 2013), has also been used on imagery from the MODIS sensor but also used for imagery captured by SeaWiFS. The algorithm uses more channels in the retrieval of AOD than the algorithm for remote sensing of tropospheric aerosol over dark targets from MODIS (Hsu *et al.* 2013 and Remer *et al.* 2005), namely at 412 nm, 470 nm, 650 nm, 860 nm, 1240 nm and 2110 nm. AOD is retrieved over high reflectance surfaces such as desert areas and urban areas, with surface reflectivity characterised seasonally dealing with bidirectional reflectivity and vegetation effects, then a LUT approach is used to find the best fit estimation for the optical depth estimation based on different aerosol models (Hsu *et al.* 2013).

The MERIS ESA standard aerosol product over land algorithm is used for the retrieval of the level 2 aerosol product from the MERIS sensor (Santer *et al.* 1999). The wavelength channels used in the retrieval include 443 nm, 665 nm and 865 nm. The retrieval of AOD occurs over dense dark vegetated surfaces and a LUT approach is used to find the best fit estimation for the optical depth estimation based on different aerosol models (Santer *et al.* 1999).

The current operational algorithm for the Meteosat SEVIRI aerosol product is the MSG SEVIRI AOT retrieval algorithm (Bernard *et al.* 2011). The wavelength channels used in the retrieval of AOD are at the 800 nm and 1600 nm bands. Retrievals of AOD were based upon the use of AOD retrievals from clear sky minimum reflectance pixels in an image as a reference and for the use of an LUT approach to find the best fit estimation for the optical depth estimation based on different aerosol models (Bernard *et al.* 2011).

The MISR retrievals of AOD over terrestrial surfaces make use of the heterogeneous land algorithm (Diner *et al.* 2008). The wavelength channels used in the retrieval of AOD are at the 446 nm, 558 nm, 672 nm and 866 nm bands. The advantage of the algorithm is that AOD retrievals are retrieved over different terrestrial surface types including surfaces with high reflectance (Diner *et al.* 2008). The retrievals are achieved through the comparison of modelled reflectance as a result of aerosol models of varied composition to satellite measured TOA reflectance. The aerosol retrieval at the 558 nm wavelength band was used as a reference when fitting optical depths based on reflectance comparisons (Diner *et al.* 2008).

The CALIOP retrievals of AOD over terrestrial surfaces makes use of the Hybrid Extinction Retrieval Algorithm (HERA) (Young *et al.* 2008). The wavelength channels used in the retrieval of AOD are at the 1064 nm and 532 nm bands. The algorithm was made up of several subset algorithms. The Selective Iterated BoundarY Locator (SIBYL) algorithm classifies features in images as types of cloud or aerosols and initiates the retrieval of optical depth at the 532 nm wavelength. HERA continues this by completing the profiling and retrievals at both 532 nm and 1064 nm. (Young *et al.* 2008).

The OMI retrievals of AOD over terrestrial surfaces make use of the multi-wavelength algorithm (Stein-Zweers *et al.* 2011). The wavelength channels used in the retrieval of AOD, are the 331-500 nm bands. The retrievals are achieved through the comparison of

measured reflective compared to modelled reflectance and the use of an LUT approach to retrieve the best fit AOD according to different aerosol models (Stein-Zweers *et al.* 2011).

The AATSR retrievals of AOD over terrestrial surfaces make use of the dual view algorithm (Veefkind and de Leeuw, 1998). The wavelength channels used in the retrieval of AOD are namely the 555 nm, 659 nm, 865 nm, and 1600 nm wavelength bands. The observed surface reflectance is computed as a function of the nadir and forward view surface reflectance that change due to wavelength and surface geometry. The best fit modelled reflectance based on the aerosol models compared to the retrieved reflectance is used to estimate the AOD (Veefkind and de Leeuw, 1998).

Different retrieval algorithms have been used to retrieve AOD from satellites. Some of the algorithms retrieve AOD from fewer wavelengths such as the algorithms which retrieve AOD over dark targets, while other algorithms retrieve AOD from numerous wavelengths such as the deep blue algorithm and the dual view algorithm. AOD retrieved using numerous wavelengths have the advantage that good retrievals can be made over a number of different surface types.

2.5. Aerosol Sources and Radiative Effects in South Africa

In this section the prevailing PM emission sources in South Africa are discussed. This is followed by a brief discussion on the radiative effects of dominant PM emissions in the country.

Various sizes of particles make up the PM loading over South Africa. Over the Western and Eastern Cape, coarse particles (greater than 2.5 µm) are prevalent in summer months while finer particles (less than 2.5 µm) are dominant for the rest of the year (Tesfaye *et al.* 2011). The Western Cape and Eastern Cape regions are more affected by PM particles transported from marine regions, biomass burning sources, industrial and urban aerosol sources (Tesfaye *et al.* 2011). Over Cape Town, Gwaze *et al.* (2007) found a dominance of finer particles in the winter months. Piketh *et al.* (1999) found that particulate samples collected at Brandt se Baai in the Western Cape were mainly from marine sources and a significant proportion from industrial sources in the summer months. In winter months, the samples at Brandt se Baai were mainly from marine sources but significant proportions of the samples were from industrial and dust wind-blown dust sources. Over the Northern

Cape, Free State and KwaZulu-Natal provinces, coarse particles are dominant in the summer while finer particles were dominant in other seasons (Tesfaye *et al.* 2011). Over the North West, Gauteng, Mpumalanga and Limpopo provinces, the summer months are dominated by a mixture of coarse and finer particles with finer particles dominant in other months of the year (Tesfaye *et al.* 2011). The North West, Gauteng, Mpumalanga and Limpopo provinces have the largest aerosol loading than the rest of South Africa.

Biomass burning activities are the dominant source of PM particles in the region during the July-October months (Tesfaye *et al.* 2014) for much of the South African region particularly Mpumalanga, KwaZulu-Natal and Limpopo provinces. PM loading over the Southern Africa region, peak in September and October months due to biomass burning (Queface *et al.* 2011) with lower aerosol loading occurring from December to May. The provinces of South Africa are not equally affected by PM emissions, with Limpopo, Gauteng, Mpumalanga and the North West Province experiencing the most and the provinces Western Cape, Free State, Northern Cape and KwaZulu-Natal experiencing the least PM emissions (Tesfaye *et al.* 2011)

Direct radiative effects as a result of biomass burning PM emissions occur over the South African region (Tesfaye *et al.* 2014). Biomass burning PM effects on the climate system contribute to modifications of the ambient PM loading in areas a greater distance away from burning sources. In addition changes in cloud cover are also linked to the PM semi direct effects on the climate system over the region, while direct radiative forcing effects plays a lesser role. Changes to wind speeds over the region were also observed due to both the PM semi direct and PM direct radiative effects which also modified the atmospheric boundary layer conditions over the affected regions (Tesfaye *et al.* 2014).

Besides biomass burning PM, wind-blown dust PM also contributes substantially to the PM loading over South Africa (Piketh *et al.* 1999). Wind-blown dust PM effects on the regional climate system primarily affect the Northern Cape Province (Tesfaye *et al.* 2015). At a regional to local spatial, wind-blown dust from mines, such as the may have climate effects particularly over the high veld region Through changes in cloud cover as result of the direct and semi direct effects of wind-blown dust PM, temperature and sensible heat climate conditions are reduced. In addition to cloud cover changes, wind-blown dust PM contributes to changes in the amount of cloud water droplets thereby contributing to the hydrological cycle in the Northern Cape Province.

2.6. Synoptic Weather Systems in South Africa

In this section, the prevailing synoptic weather systems in South Africa are discussed. The effects of the large scale weather systems on local meteorology are also discussed. The conduciveness of meteorological systems for pollution build up is highlighted. Finally the role of mesoscale weather systems in transport air masses regionally are discussed.

In South Africa, subtropical anticyclones are characteristic of the regional atmospheric circulation (Freiman and Piketh, 2003). These are associated with pleasant weather conditions. The anti-cyclonic system has considerable spread vertically in the atmosphere with its greatest focus over the north east of South Africa. The interior of South Africa especially the high veld are affected by anticyclonic systems in particular the winter months in June-August. Summer occurrences of anticyclonic systems over South Africa do occur over December–February months. When anticyclones occur in summer, they are accompanied, in addition to the warm temperatures in the interior by warmer days of fluctuating temperatures around coastal areas (Freiman and Piketh, 2003; Tyson and Preston-Whyte, 2004).

The typical anticyclonic system is accompanied by winds with no convergence closest to earth's surface, inversion layers, subsiding masses of cool dense air, minimal rainfall and almost approaching cloud free skies. The contribution of the Hadley cell and the circulation of air caused by the variable winds at the surface and the merging winds in the upper atmosphere contributes to the downward flowing subsiding air masses which break through the 500 hPa stable layer, into the atmosphere below (Tyson and Preston-Whyte, 2004).

The anticyclonic system is one of the most dominant circulation types occurring in South Africa (Cosijin and Tyson, 1996). The frequency of the system which is almost always associated with minimal rainfall besides establishing a stable atmosphere closer to the surface, also establishes stable layers at multiple levels in the atmosphere. Nearer coastal regions the stable layer of note generally is the 850 hPa layer. At higher elevations of the interior, the stable levels include 300 hPa, 500 hPa and 700 hPa. These stable layers in the atmosphere especially the 500 hPa don't cover just Southern Africa and are not just typical for anticyclonic systems but also occur on other days with minimal rainfall. These stable

layers are responsible for the distribution of aerosols in the atmosphere over Southern Africa (Cosijin and Tyson, 1996).

Less frequent than anticyclonic synoptic systems, are low pressure systems such as coastal lows (Reason and Jury, 1990). Topography plays a major role in the flow of the coastal low system in South Africa due to the interior plateau region, the great escarpment and the coastal lowlands. The coastal low system begins its flow from the west coast of South Africa, hugging the coastal low lying areas. The system is contained by the great escarpment and an inversion layer. Prefrontal air flow is warm and post frontal air is cooler. The coastal low is a system for which heavy rainfall may not occur as is the case for a cold front; instead mist or very weak rainfall may occur. Atmospheric air flow occurring with a coastal low does not extend vertically high into the atmosphere staying below about 850 hPa (Reason and Jury, 1990; Tyson and Preston-Whyte, 2004).

Linked to coastal lows and to cold fronts, berg winds are caused by warm air blowing towards the sea just before a front passes which may also have warm air blowing towards the sea from the interior plateau region. The direction and strength of the air flow is enough to blow aerosol dust out towards the sea (Tyson and Preston-Whyte, 2004). Jury *et al.* (1990) found that berg winds contributed to brown haze episodes in winter over Cape Town.

When the low pressure system over Southern Africa is interrupted by the ocean centred high pressure systems, this forms the easterly waves and lows that drives rainfall over the interior and contributes to the dry conditions of the western coast (Tyson and Preston-Whyte, 2004). The easterly waves form between the Intertropical Convergence Zone (ITCZ) and the high pressure systems. The east of Southern Africa has a low pressure system which is strengthened by the South Indian High Pressure System and towards the west, divergence of air masses occurs due to the presence of the South Atlantic Pressure System and the weakening of the low pressure system. The divergent conditions cause greater subsidence over the western region of Southern Africa and drier conditions over this area. Subsidence favours stable conditions and temperature inversions closer to the surface (Tyson and Preston-Whyte, 2004).

Easterly waves are prevalent closer to the surface at 850 hPa and 700 hPa where they are stronger at the 500 hPa layer, the waves are weaker as the vertical distance above these

layers increases (Tyson and Preston-Whyte, 2004). The convergent conditions at the surface and the eastern half of the region favouring rainfall is further enhanced by the divergent conditions in the upper atmosphere. Likewise to the western region of Southern Africa, the divergent conditions at the surface which favours drier periods are enhanced by convergent conditions in the upper atmosphere (Tyson and Preston-Whyte, 2004).

The easterly wave is different to the easterly low in that the convergent conditions that form in the lower atmosphere occur eastwards of the peak region of the low pressure system, enhanced by vertical flow of air upwards in the upper atmosphere past the 500 hPa layer. Convergent conditions with an easterly low occur eastwards of the low pressure system and the divergent conditions occur at much lower pressure levels in the upper atmosphere (Tyson and Preston-Whyte, 2004).

Westerly waves form from the incursions of low pressure systems that typically are located at mid latitudes at the juncture of the Polar and Ferrel cells (Tyson and Preston-Whyte, 2004). These low pressure systems move with the seasonal shift in the position of the sun. When these systems are located over Southern Africa, they move along the coast beginning from the western coast of Southern Africa moving up to the eastern coast but never reaching as far up as KwaZulu-Natal. At greater pressure levels nearer the surface, convergent conditions in the low pressure system occur pointed in the south west direction. At lower pressure levels in the upper atmosphere, from 500 hPa and lower, the low pressure system occurs pointed in the eastern direction. Westerly waves are different because only the upper segment of the mid latitude belt modify the Southern African climate. The most amount of rainfall occurs in the south western Cape. The climate system occurs mostly between October and April (Tyson and Preston-Whyte, 2004).

Cut of lows are independent low pressure systems that are displaced from the mid latitudinal westerly waves (Molekwa, 2013). Therefore the amount of rainfall that occurs due to these systems are of greater quantity than the rainfall events due to the cold fronts of the westerly waves. Upper atmospheric divergence occurs at lower pressure levels than the 500 hPa layer. This enhances the convergent conditions at surface pressure levels. Cut of low systems most frequently occur in March, April, May, September, October and November (Tyson and Preston-Whyte, 2004; Molekwa, 2013).

Also linked to the westerly waves are the ridging anticyclones that occur in October, November, December, March, April and May (Tyson and Preston-Whyte, 2004). The linkages occur in the upper atmosphere at about 500 hPa, with rainfall in the south eastern regions and clear stable conditions in the south west. Over the western regions, the stable conditions are accompanied by subsiding air masses which trap warmed air closer to the surface due to inversion conditions. The incursion of a high pressure system during the summer season transports moist air from the Indian Ocean into the eastern region of Southern Africa. Topography plays a greater role in the formation of clouds and the resultant rainfall that occurs over the eastern areas of Southern Africa (Tyson and Preston-Whyte, 2004).

Westerly waves which occur in the upper atmosphere westwards of South Africa accompanied with a low pressure system at the surface over the western coastal region of South Africa aids in the occurrence of precipitation over the western regions of South Africa (Tyson and Preston-Whyte, 2004). Frequently coupled with other synoptic systems including cut off lows and westerly waves, cold frontal systems, approach South Africa from the southerly and south westerly directions. The conditions produced in front of the approaching cold air masses are conducive to pollution build up characterised by subsiding air masses with low level atmospheric divergence, with cloud free skies and air masses moving largely in a northerly direction. At the back of the frontal system, the opposite occurs, the movement of air is largely in a southerly direction with uplifting air masses, convergence and cloudy skies conducive to the clean-up of pollutants in the atmosphere (Tyson and Preston-Whyte, 2004).

Also contributing to pollutant transport is the mesoscale transport of aerosols which are related to the winds that are generated between mountains and the lower lying areas near them (Tyson and Preston-Whyte, 2004). Even without altitudinal gradients, the flow of air masses can occur under inversion conditions which when strengthened by surface cooling, will also intensify the resultant winds. There are wind types that carry pollution from high altitude areas including katabatic winds and mountain breezes. When capped by inversion layers due to surface cooling particularly at night, these winds carry pollution downslope transported at great distances to lower lying areas. While mountain breezes occur at night, valley breezes occur during the day due to the uplift of warming air. If the stability conditions of the atmosphere are sufficient to prevent substantial upward dispersion of air to the upper atmosphere, the valley breeze is able to transport pollutants great distances to

higher lying areas. Without the inversion conditions present, pollutants are able to rapidly disperse upward to the upper atmosphere (Tyson and Preston-Whyte, 2004). Of importance is that the transport of air masses at the synoptic scale in South Africa is dominated by eastward movement of air towards the eastern regions of South Africa.

Synoptic systems in South Africa including subtropical anticyclones, ridging anticyclones, coastal lows, berg winds, westerly waves, westerly lows, easterly waves, easterly lows and cut of lows play a major role in the circulation of air in the region as well the circulation of aerosols in the region. The international studies have found that high PM episodes are dominated by high pressure systems in the Northern Hemisphere for which will differ seasonally from region to region in terms of frequency, scale of geographic impact and intensity. Likewise low PM episodes are associated more with low pressure systems in the northern hemisphere. Some studies have linked high PM episodes with greater AODs and low PM episodes with lower AODs. For these studies, AOD was a useful indicator of aerosol loading in the atmosphere at the regional scale. Similarly for South Africa, high PM events are associated with anticyclonic systems and prefrontal conditions of approaching frontal systems due to subsiding air masses. Low PM events are associated with post frontal conditions of passing low pressure systems which disperse PM through greater uplift of air masses.

2.7. Measurement of Aerosols for South African Air Quality and Aerosol Studies

A variety of instruments are employed in South Africa for the measurement of PM_{10}. Gravimetric measurements are used most frequently in passive sampling field studies with the advantage of this method being the collection of PM_{10} samples for laboratory analysis of aerosol chemistry. Notably TEOM instruments are used for continuous monitoring of PM_{10} and are used within air quality monitoring networks. Photometric methods to measure PM_{10} were also frequently employed in South Africa. Both photometric and gravimetric methods have been employed in the study of aerosol properties in South Africa. Satellite remote sensing has also been employed in the study of aerosol climatology in South Africa. This section will discuss firstly previous case studies of PM_{10} measurements in South Africa, secondly how aerosols have been measured in the country and lastly the use of satellite remote sensing in Southern Africa.

Worobiec *et al.* (2011) used the Grimm "filter-check" submicron aerosol spectrometer which similarly to the dustrack aerosol monitor used laser photometry to indirectly measure PM_{10} concentration in real time. Measurements of PM_{10} were made in Bethlehem in 2001. Venter *et al.* (2012) took measurements of PM_{10} in Marikana from 2008 to 2010. Venter *et al.* (2012) used a Model 5030 SHARP monitor, which takes real time measurements of PM_{10} concentration which were used in the study to conduct an overall air quality assessment of the area. The Model 5030 SHARP monitor is a hybrid instrument which used both photometry and beta attenuation to measure PM_{10} concentrations (Hyvärinen *et al.* 2011).

Van Zyl *et al.* (2014) also measured PM_{10} in Marikana in 2008 and 2009 in order to determine trace metal concentrations collected from PM_{10} samples. Minivol portable air samplers with Teflon filters which measure concentrations of PM_{10} gravimetrically were used. Minivol portable air samplers were also used by Chow *et al.* (2007). Niyobuhungiro and von Blottnitz (2013) also used Minivol samplers with quartz filters for measurements of PM_{10} in Cape Town.

One of the types of instruments used to measure PM_{10} by Reddy *et al.* (2012) was the TEOM samplers. Measurements of PM_{10} were taken in Durban in 2004 and 2005. Prior to the use of the SHARP beta attenuation sampler by Venter *et al.* (2012), a TEOM was used to measure PM_{10}. Kgabi *et al.* (2007) measured PM_{10} in Rustenberg in 2004 and 2005. A TEOM sampler was used in Kgabi *et al.* (2007) and PM_{10} samples were collected on Teflon filters to determine the elemental composition of the PM_{10} samples. Engelbrecht *et al.* (2001) measured PM_{10} in Qalabotjha in 1997. TEOM samplers were used by Engelbrecht *et al.* (2001) and an integrated sampling setup was also used which was equipped with either Teflon or quartz fibre filters. The samples collected by Engelbrecht *et al.* (2001) using the integrated setup were analysed further for elemental composition. TEOM instruments were employed by Tshwane Metropolitan Municipality to monitor PM_{10} continuously throughout the municipality for 2009 for which Wright *et al.* (2011) used the TEOM measurements to determine health impacts due to poor air quality in the municipality.

Moja *et al.* (2013) measured PM_{10} in Vanderbijlpark in 2009. Moja *et al.* (2013) used e-samplers which were hybrid samplers which employed both photometry and gravimetric based measurements for PM_{10} measurements. Moja *et al.* (2013) used the PM_{10} samples

44

collected to determine the composition and concentrations of the metallic particle components. Kaonga *et al.* (2011) measured PM_{10} in Rustenberg in 2008. A cascade impactor sampler with Teflon filters was used to measure PM_{10} but the elemental composition of the samples were not determined by Kaonga *et al.* (2011).

Wright *et al.* (2011) measured PM_{10} in KwaGuqa using a Turnkey Optical Particle Analysis System. The Turnkey Optical Particle Analysis System used by Wright *et al.* (2011) was a fixed station monitor which could measure PM_{10} and other PM measurements concurrently and continuously. The PM monitor used in Wright *et al.* (2011) also used filter based gravimetric methods, and the PM samples collected were analysed further for manganese and lead concentrations.

The research of PM properties at the regional and local scale in South Africa has been largely dependent on *in situ* measurements of PM properties using both gravimetric and photometric technologies. The first major sampling campaign took place in 1992 for the Southern African Fire-Atmosphere Research Initiative (SAFARI 92). Research studies were conducted in the Kruger National Park in South Africa as well as some locations in Zambia and Swaziland. The research campaign determined that biomass burning emissions contributed substantially to the PM loading over the region (Lindesay *et al.* 1996). For the SAFARI-92 campaign, Maenhaut *et al.* (1996) sampled aerosols at three sites in and around the Kruger National Park using stacked filter unit samplers to measure fine and coarse distributed PM, black carbon aerosols and various PM chemical species including phosphorous, potassium, zinc and manganese aerosol components.

As part of the Transport and Atmospheric Chemistry near the Equator-Atlantic (TRACE A) experiment, measurements of PM particles were taken on board an aircraft flying over the South Atlantic Region covering areas over the South American and Southern African region in September and October 1992. Measurements of the PM size distribution were obtained using a Passive Cavity Aerosol Spectrometer Probe (Anderson *et al.* 1996).

A study by Piketh *et al.* (1999) included the use of stacked filter unit samplers which were collected from five locations in Southern Africa including Etosha National Park, Palmer, Victoria Falls, Skukuza and Ben MacDhui. Streaker PM Samplers were also used at 5 sites including Elandsfontein, Misty Mountain, Kruger National Park, Brandt se Baai and Ben

MacDhui. PM composition was determined from streaker samples taken from Ben MacDhui (Piketh *et al.* 1999a).

For the Ben Macdhui High Altitude Trace Gas and Aerosol Transport Experiment (Piketh *et al.* 1999b), various PM measurements were made at Ben Macdhui. Streaker sampling units were used to measure PM for both coarse and fine mode particles. Stacked filter unit samplers and single stacked unit samplers were used to gravimetrically measure PM. High volume samplers were used to measure the Total Suspended Particulates (TSP). Aerosol samples collected were used in chromatography analysis to determine the composition of ionic PM species in the samples and further investigations were done using x-ray diffraction to determine the source composition of the PM particles sampled (Piketh *et al.* 1999b).

AOD was measured at the Sutherland site of the South African Astronomical Observatory for the period 1998-1999. A MFRSR instrument was used to measure the temporal AOD variations during the day. Nocturnal measurements of the AOD were retrieved from telescope measurements at the observatory of the stellar system which had been retrieved since 1974 (Formenti *et al.* 2002).

Terblanche *et al.* (2000) measured PM particles using instruments and aeroplane surveys. The PM samplers used, included the active sampling aerosol spectrometer probe and the forward scattering spectrometer probe. The active sampling aerosol spectrometer probe was used to measure PM concentration and PM size distribution parameters with the size range being between 0.12 and 3.12 µm. The forward scattering spectrometer probe was used to measure the size distribution and concentration of cloud droplet particles with the size range being between 2 and 32 µm. Cloud concentration nuclei number concentration was measured using a Cloud Condensation Nuclei Particle Counter (CCNC) 100A (Terblanche *et al.* 2000).

Over Durban, various studies have been conducted which have retrieved vertical profiles of the PM loading using in-situ lidar technology (Kuppen, 1996; Kuppen, 1999; Moorgawa; *et al.* 2007; Diab *et al.* 2003 and Bencherif *et al.* 2003). Studies such as Moorgawa *et al.* (2007), Diab *et al.* (2003) and Bencherif *et al.* (2003) have used PM profiles, measured using the Rayleigh Mie Lidar which operated from the site of the

University of Natal and used retrievals made in 1997 and 1999. The use of the LIDAR system was limited to cloud free days.

A Raman LIDAR was used to retrieve PM vertical profiles at 532 nm over the Atlantic Ocean near South Africa (Kanitz *et al.* 2013). The Raman LIDAR was hosted on a ship which was used for the OCEANET project. The LIDAR was operated for three ship cruises between South Africa, South America and Europe (Kanitz *et al.* 2013).

Abel *et al.* (2003) measured the properties of the PM from agricultural burning sources in the Southern African region in Otavi in Namibia. The measurements were taken during the SAFARI 2000 campaign. The aerosol size distribution was measured using a passive cavity aerosol spectrometer probe, a type of optical particle counter. The passive cavity aerosol spectrometer probe detected the PM distributions of particle sizes between 0.05 µm and 1.5 µm in radius. An integrating nephelometer 356 was used to measure the total scattering properties of the PM particles at the 450 nm, 550 nm and 700 nm wavelengths. The optical extinction for absorption at 567 nm wavelength was measured using a radiance research particle soot absorption photometer. Measurements were taken on-board an aircraft, while flying over the burning source.

PM measurements were taken at Mongu in Zambia in August and September 2000 as part of the SAFARI 2000 research campaign (Billmark *et al.* 2003). A high volume sampler pump was used to collect aerosol samples for further analysis on PM concentration and composition. Gas chromatography was used to determine the composition of the PM samples collected. HYbrid Single-Particle Lagrangian Integrated Trajectory (HYSPLIT) trajectories were used to determine the transport of PM laden air masses.

Air samples were measured from an aircraft flying over Cape Town in order to determine the PM properties during brown haze conditions in July and August 2003 (Gwaze *et al.* 2007). PM samples were collected using streaker samplers. PM size distribution properties were determined using a Passive Cavity Aerosol Spectrometer Probe. The PM samples collected using streaker samplers were analysed using electron microscopy to determine PM size distribution, morphological and chemical properties.

As mentioned previously there are AERONET and MPLNET monitoring sites in Africa, of which some of them are located in South Africa. The AERONET sites are located in

Bethlehem (Winkler *et al.* 2008), Elandsfontein (Laakso *et al.* 2012), Johannesburg (Sivakumar *et al.* 2009), Pietersburg (Elias *et al.* 2003), Pretoria (Sivakumar *et al.* 2009) and Skukuza (Kumar *et al.* 2014). The only MPLNET site in South Africa is located in Skukuza (Campbell *et al* 2001).

MPLNET and AERONET sites have been used in conjunction with satellite data within the study of PM properties in South Africa. Tesfaye *et al.* (2011) used 10 years of MISR AOD data to assess the PM climatology over Southern Africa on board the TERRA satellite. Over Southern Africa, during the SAFARI 2000 aerosol research campaign, the retrievals from MODIS and MISR were used in the assessment of PM properties over the region (Diner *et al.* 2001; Ichoku *et al.* 2003). MISR retrievals correlated well with AERONET over the Southern African region for the dry season period for the SAFARI 2000 study (Diner *et al.* 2001). Aerosol data retrieved over South Africa, from the CALIPSO satellite had a correlation of $R = 0.509$ when compared to *in situ* measurements of aerosols from AERONET (Schuster *et al.* 2012). When dust and marine aerosols were removed from the correlation analysis, the R decreased to $R = 0.483$ (Schuster *et al.* 2012).

2.8. Summary

Aerosol compositional effects which are determined from the source types of PM emissions include those of anthropogenic and natural origin. PM composition directly impact overall radiative effects which is indicated by the AOD. The aerosol source types that contribute to total PM loading in the atmosphere are more regional than the source types represented by PM. PM particles types are largely of anthropogenic origin due to the case studies measuring PM being located in communities affected by adverse health impacts due to poor air quality, and this is easier to determine due to the localised nature of sampling. *In situ* measurements of AOD have the same advantage as that of PM sampling due to the localised siting of sampling stations. There is greater uncertainty for AOD retrievals from satellites with retrievals representative of the total atmospheric column. Hence the aerosols which effect light extinction, could be from distant sources and nearby emission sources, which are not discernible from the AOD sampling alone.

Local meteorological effects and land cover characteristics disperse and distribute PM within the boundary layer and the extent to which vertical mixing occurs is determined by the strength of the local atmospheric stability. MLH directly impacts the extent of vertical mixing and increasing MLH is favourable for good AOD-PM_{10} correlations. Increasing

RH directly impacts aerosol size distribution, modifying the aerosol loading characteristics of the atmosphere indicated by increasing AOD. Rainfall increases wet deposition and lessens the aerosol loading in the atmosphere, decreasing the AOD. Increasing temperatures, increases vertical mixing of air and improves aerosol distribution throughout the atmosphere. Increasing temperatures also increase evaporation from soil surfaces and aids in aerosol emissions from bare soil surfaces. Increasing wind speeds aid in pollution dispersion and distribution of pollution throughout the atmosphere. Mesoscale meteorological affects also aid in local-regional distribution of aerosols through upslope and downslope winds that circulate pollutants between higher altitude areas and lower lying areas.

Synoptic scale meteorological systems drive the regional circulation of aerosols largely through the large scale movement of air masses. The international studies have found that high PM episodes are dominated by high pressure systems in the northern hemisphere for which will differ seasonally from region to region in terms of frequency, scale of geographic impact and intensity. Likewise low PM episodes are associated more with low pressure systems in the northern hemisphere. The most frequent synoptic systems in South Africa are the subtropical anticyclones which distribute aerosols regionally via stable layers in the atmosphere on days associated with clear calm conditions. Also attributable to the clear conditions that form due to anticyclonic systems, are the subsidence inversions which trap PM closer to the surface and result in increasing PM concentrations without affecting the AOD. Convergent conditions associated with low pressure systems which are associated with cloudy skies prevent satellite retrievals of AOD. Thus it is not possible to determine the AOD-PM$_{10}$ relationship for all synoptic conditions.

The AOD-PM$_{10}$ relationship will vary between stations and between countries. More case studies have been completed for the Asian continent than in Europe. The correlations typically did not exceed an R of 0.7. The case studies reviewed highlighted the importance of integrating meteorological confounders into the AOD-PM$_{10}$ relationship in order to obtain good correlations. The only study to have determined a very high correlation was Nordio *et al.* (2013). The study was unique in that a number of additional coefficients including PM emissions, elevation, roads and population density were included along with the AOD and the meteorology.

Effects on the AOD-PM$_{10}$ correlation are interlinked to each other. For some cases, the AOD-PM$_{10}$ relationship is impacted indirectly through effects on either the AOD or PM$_{10}$. In most cases, the effects impact both AOD and PM$_{10}$, weakening the AOD-PM$_{10}$ correlation. South Africa has a subtropical climate with high RH conditions. As such it is important to account for RH effects on the AOD-PM$_{10}$ correlation. Due to the frequent occurrence of subsidence inversions and the formation of stable layers aloft in the atmosphere it is also important to account for MLH effects on the AOD-PM$_{10}$ relationship. In doing so, it would be possible to optimise the AOD-PM$_{10}$ correlation.

The measurements of aerosol properties on the ground, AOD included, largely employed photometric technology such as sun photometers for both passive sampling and long term sampling. Within South Africa, studies that have measured aerosol optical properties have been located mostly over the north eastern regions of the country. There is limited knowledge of the regional aerosol properties over the Western Cape, Eastern Cape, KwaZulu-Natal and the Northern Cape regions of the country. Satellite measurements of AOD over these regions need to be validated using *in situ* AOD measurements before they can be used with greater certainty. The measurement of PM on the ground, largely employed gravimetric methods for passive sampling and used TEOM extensively for long term measurements at AQM stations in South Africa and abroad. The use of most types of TEOM samplers have the limitation that semi-volatile and volatile PM species are not sampled.

Sensors on board different satellites retrieve AOD at different times of the day for the same location and represent separate AOD measurements based on the characteristics of the sensor, the satellite and the retrieval algorithms used to measure AOD. Generally when evaluating the weaknesses of satellite remote sensing for application within environmental studies, sensor and satellite platform characteristics and level 0 image processing algorithms need to be acknowledged as sources of uncertainty propagation within environmental data. Specifically for aerosol remote sensing, the characteristics of the algorithm that facilitates AOD retrieval needs to be acknowledged as a source of uncertainty within AOD data in addition to the general sources of uncertainty. While the previous satellite sensors have not be specifically designed to measure pollution, this is expected to change with the launch of the Multi-Angle Imager for Aerosols (MAIA) satellite instrument which has been designed specifically to monitor small particles (Cole, 2016).

CHAPTER 3: RESEARCH METHODOLOGIES

3.1. Introduction

Measures of aerosols in the atmosphere include total aerosol loading and aerosol concentration that can be measured by instruments on the ground, airborne platforms (for example aircraft) and on board satellites in space.

In this study, AOD data were used from the MODIS sensor on board the AQUA and TERRA satellites and *in situ* TEOM measurements of PM_{10} for the towns of George and Malmesbury for the year 2011. In this chapter the background of the MODIS AOD data retrieval strategy, method and validation are presented and the measurements of ambient PM concentrations using TEOM instruments are described. Furthermore, the background to the case study areas and the measurement of PM loading, PM_{10} concentration and meteorology for the case study areas is presented. Finally the tools and statistical procedures used to analyse the PM_{10} concentrations, MODIS AOD and meteorological data is outlined.

3.2. MODIS Retrievals of Aerosol Loading from Space

3.2.1. Overall Strategy of TOA Retrieval

The Top of Atmosphere (TOA) reflectance at a specified wavelength band explained by equation 1 can be determined from the reflectance of radiation in the atmosphere before reaching the surface (ρ_λ^*), transmittance of radiation downwards and upwards without the effect of reflectance at the surface (T_λ), the reflectance of radiation at the surface for a specified wavelength (ρ_λ^s), the atmospheric backscattering ratio (s_λ) (Levy, 2009). These parameters of the TOA reflectance are related to the solar and satellite zenith and azimuth angles. Each of the parameters of the TOA reflectance with the exception of radiation reflected at the surface are dependent upon the degree of PM composition, PM size distribution and loading in the atmosphere, additional to Rayleigh light scattering. Thus the parameterisation of the TOA reflectance allows for the determination of interactions of incoming and outgoing solar radiation with the atmosphere and the surface and is the foundational basis for the determination of the AOD.

$$\rho_\lambda^*(\theta_0, \theta, \phi) = \rho_\lambda^a(\theta_0, \theta, \phi) + \frac{T_\lambda(\theta_0) T_\lambda(\theta) \rho_\lambda^s(\theta_0, \theta, \phi)}{1 - s_\lambda \rho_\lambda^s(\theta_0, \theta, \phi)}$$

Equation 1

By accounting for the reflectance of radiation at the surface, by assuming that the surface reflectance is 0 for a dark surface, the reflectance of radiation by PM particles and other molecules in the atmosphere can be eventually estimated (Levy, 2009). Further assumptions and simulations of radiative interactions in the atmosphere result in the retrieval of PM properties. The simulation of atmospheric reflectance properties that contribute to the reflectance measured by the satellite sensor are achieved using LUTs.

The algorithms used to retrieve PM optical properties from the MODIS sensor consist of separate terrestrial and oceanic algorithms due to the differing surface reflectance properties. The first part of the processing of imagery is to distinguish between terrestrial and oceanic surfaces as well to distinguish other large water bodies (Levy, 2009). Over land surfaces the MODIS over land dark target algorithm is applied. The algorithm tries to resolve the PM optical properties by using PM models which are either fine or coarse dominated in order to estimate the surface reflectance such that it closely resembles the actual surface reflectance. PM properties are retrieved from three wavelength channels at 470 nm, 660 nm and 2130 nm by retrieving PM and surface properties from the 2130 nm and using the constant surface reflectance ratios between 470 nm, 2130 nm, 660 nm and 2130 nm to derive PM and surface optical properties for the 470 nm and 660 nm wavelength channels. The AOD at 550 nm, the fine aerosol weighting (η) at 550 nm and the surface reflectance at 2130 nm are retrieved through an inversion procedure of the PM and surface optical properties at the three wavelength channels. More detailed information on the algorithm is provided in Levy *et al.* (2009).

One of the sub-datasets used in this study included the Corrected_Optical_Depth_Land sub dataset for the AOD retrieved using the dark target algorithm (summarised above) at 550 nm which previous air quality studies used including Ballard *et al.* (2008); Tian and Chen (2010); Jennings (2013); Llamas *et al.* (2013); Saide *et al.* (2013); Saide *et al.* (2014); Toth *et al.* (2014) ; Zeeshan and Oanh (2015). The second sub-dataset used was the Deep_Blue_Aerosol_Optical_Depth_550_Land sub dataset which provided the AOD at 550 nm retrieved using the deep blue algorithm was used in previous studies including Justice *et al.* (2009); Strawa *et al.* (2011) and Onishi *et al.* (2012). The third sub-dataset

used in this study was the Cloud_Mask_QA subdataset which provided cloud cover information which has been used previously in air quality studies including Gupta and Christopher (2008); Harbula (2010); Kim *et al.* (2013); Higgs *et al.* (2015).

3.2.2. Validation of AOD Retrievals from Space

The AERONET, a network of ground based instruments has traditionally facilitated the validation of remotely sensed estimations of AOD (Holben *et al.* 1998). Fixed sun photometers or sun and sky scanning spectral radiometers are used within the AERONET (Holben *et al.* 1998). This has proven to be an efficient validation procedure for regional to global aerosol studies (Kaufman *et al.* 2002).

An AERONET station will not retrieve an AOD measurement, during the specific time of satellite overpass for the same air parcel for which a MODIS AOD value was recorded (Remer *et al.* 2005). By accounting for the speed of this air parcel, a balance is found between the temporal resolution of AERONET measurements and the spatial resolution of a MODIS image (Ichoku *et al.* 2002). The MODIS AOD product of 10 km spatial resolution was averaged in Ichoku *et al.* (2002) to a 50 km grid resolution and compared to AERONET measurements which are hourly averaged. Variations of this method are typically implemented to compare satellite AOD with ground measured AOD (see Jiang *et al.* 2007 and LiLi *et al.* 2007).

AERONET stations are mostly located within North America and Europe. However AERONET stations have been located in all major continents in order to represent a variety of land surfaces and aerosol modes (Levy *et al.* 2007). MODIS retrievals of dark target AOD have been validated against global AERONET measurements (Remer *et al.* 2008). Representative of Southern African aerosol, are the AERONET stations in Skukuza and Mongu (Chu *et al.* 2002). Correlations between MODIS AOD at 550 nm and AERONET AOD at 550 nm were 0.93 for AOD from the MODIS sensor on board the TERRA satellite (AOD_{terra}) and 0.91 for AOD from the MODIS sensor on board the AQUA satellite (AOD_{aqua}) (Remer *et al.* 2008). Levy *et al.* (2010) quantified the correlations between MODIS AOD and AERONET AOD which ranged between 0.79 and 0.91 for MODIS AOD retrievals with quality levels ranging from low to high confidence. This suggests that the MODIS AOD are generally good for use for global aerosol studies.

Levy *et al.* (2010) determined that the MODIS dark target retrieved AOD compares better with AERONET sites where the reflectance at 2119 nm range between 0.1-0.15 and the normalized differential index (NDVI) at short wave infra-red wavelengths ranged between 0.3-0.4 for cases of low aerosol loading (AOD less than 0.15). Levy *et al.* (2010) provided examples of these locations where MODIS dark target retrieved AOD compares better with AERONET sites which included Southern Africa, the eastern region of the United States and the western region of Europe. There were other regions for which the AOD was over or under-estimated for low aerosol loading events including the central Asian region and the northern region of Australia.

For cases of higher PM loading (AOD greater than 0.4), better correlations with AERONET were determined for which the fine PM were predominant over locations such as in the western regions of Europe and the eastern coastal region of the United States. For circumstances when coarse mode PM particles contribute significantly to the PM loading such as in Southern Africa for high PM loading events, the MODIS AOD is underestimated.

It is suggested that the MODIS AOD is sufficiently comparative to ground surface measurements of the AOD from the AERONET. Furthermore, based upon Levy *et al.* (2010) it is suggested that the number of AERONET stations in Southern Africa is limited, and that variation of the seasonal PM climatology in Southern Africa may differ to those observed at the AERONET stations in Southern Africa. The use of MODIS AOD data was expected to be sufficient for the comparison of the AOD-PM$_{10}$ correlations determined in this study due to the generally good correlation at the global spatial scale between MODIS and AERONET AOD (Levy *et al.* 2010). The evaluation of the extent that MODIS AOD could be used within air quality analysis of PM$_{10}$ was to be achieved in this study by comparing the AOD-PM$_{10}$ correlations determined in this study to correlations from previous studies which have used MODIS AOD and PM$_{10}$.

The advantage of using established AERONET stations for validation is the provision of ground data with a long archived record (Holben *et al.* 1998), however, where such stations are sparse they are still used for validation (de Almeida Castanho *et al.* 2008). One validation site was used by Liu *et al.* 2002 obtaining 6 AOD measurements for the validation of AOD retrievals from 6 SPOT 5 images. A 30 km pixel window was used around the ground AOD site to verify retrieved SPOT 5 AOD for Liu *et al.* (2002). A

single validation point is insufficient according to Hadjimitsis (2009) where a ground based network of fixed sun photometers should be used for the validation of AOD from satellite images.

However in the absence of a network for fine to urban scale AOD studies, alternative validation procedures have been used (Wang *et al.* 2010). A network of portable sun photometers provided ground AOD data for de Almeida Castanho *et al.* (2007). Calibration of satellite AOD retrievals for de Almeida Castanho *et al.* (2007), employed similar space and time averaging techniques utilised by Ichoku *et al.* (2002). The air borne LIDAR system used in Lewis *et al.* (2010) had the advantage of recording AOD retrievals with greater spatial coverage, allowing for greater comparison with satellite AOD retrievals. These few examples represent some of the routes through which ground measurements of AOD are achieved.

Lidar technology is most often used to obtain vertical PM profiles because ground layer AOD has to be distinguished from other aerosol layers captured within satellite derived AOD (Lewis *et al.* 2010). The alternative is the use of atmospheric chemistry and transport models to simulate the PM column profile (Liu *et al.* 2007). The drawback of such models is their spatial limitation of 1 km (Seamen, 2000) and where a finer resolution is possible; more data inputs are required when the necessary information may not be available (Jerret *et al.* 2005). When data availability is limited for fine scale studies (Liu *et al.* 2007), by using a global to regional chemical transport model, it is still possible to estimate the effect of vertical atmospheric aerosols variation (Liu *et al.* 2009).

3.3. Monitoring of PM$_{10}$

The PM$_{10}$ measurements were taken using TEOM 1400a PM$_{10}$ monitors. Figure 2 represents an overview of the instrument components (Wu *et al.* 2002). Air flows through the sampling inlet which separates the PM$_{10}$ aerosols from the aerosols of other sizes with a flow rate at 3L/min. The PM$_{10}$ aerosols collect on a filter connected to the tapered oscillating microbalance. The mass concentration is computed from the fluctuation in the oscillation of the microbalance prior to and after the deposition of PM$_{10}$ aerosols onto the filter (Jerez et al 2006).
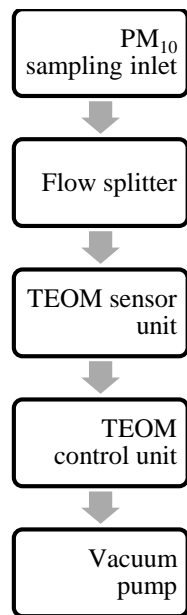
Figure 2: Schematic diagram of main TEOM sampling components (Wu *et al.* 2003).

3.4. Case Study Area

In this study, the towns of Malmesbury and George were selected as case studies (Figure 3). The AQM stations located in George and Malmesbury are regionally representative stations within the air quality network operated by the Western Cape Department of Environmental Affairs and Development Planning (DEADP) (DEADP, 2012a; DEADP, 2012b). Malmesbury has a mediterranean climate (Rubel and Kotek, 2010). The Malmesbury AQM station is located within the town of Malmesbury which lies within the Swartland Local Municipality which has the most precipitation occurring between April and September months, with agriculture being the main land use type within the municipality (Halpern and Meadows, 2013). The Swartland Local Municipality forms a part of the greater West Coast District Municipality with the Cedarberg Mountains located on the eastern boundary of the district municipality and is one of the most economically active and populous municipalities within the district region (Fouché, 2007).
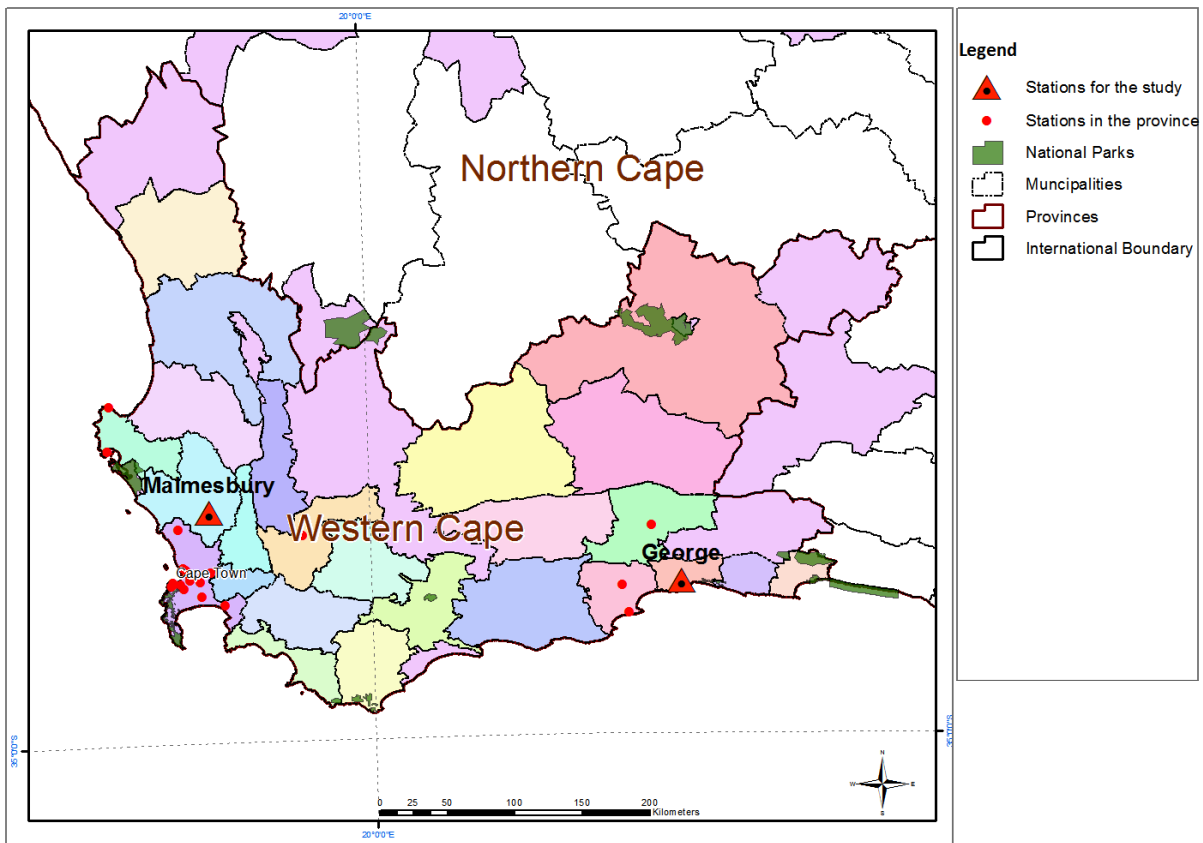
Figure 3: The locations of AQM stations in the Western Cape Province used in this study.

The George AQM station is situated within the George Local Municipality with its northern boundary the Outeniqua Mountains and its southern boundary the Indian Ocean. Precipitation in the municipality is high and occurs during most seasons (Faling *et al.* 2012) and the municipality has an oceanic climate (Rubel and Kotek, 2010). Cold fronts are the characteristic synoptic features which affect the municipality (Pool and Ronde, 2002). George lies within the greater Eden District Municipality, and is one of the most economically active and populous municipalities within the district region with both urban, manufacturing and agriculture major land uses within the municipality (Faling *et al.* 2012).

The two case studies chosen are characterised by different climate types. Urban activity is not the dominant land use activity within the municipalities contrasting to major metropolitans such as the City of Cape Town. Mountain ranges border both municipalities and are likely to have a role in the meso-scale distribution of air masses over these municipalities. Significant pollution sources include transboundary impacts from the City of Cape Town for Malmesbury and manufacturing activities for George (Scott 2010).

3.4.1. Monitoring of AOD over the Western Cape

The TERRA and AQUA satellites are equipped with MODIS sensors which retrieved radiance measurements used to determine the AOD. The TERRA satellite crossed over the Malmesbury station between 8 and 9:40 am in the morning and the George station between 7:50 and 9:35 am. The AQUA satellite crossed over the Malmesbury AQM station between 11:55 and 13:25 pm in the afternoon and crossed over the George AQM station between 11:40 am and 13:15 pm. On most days the satellites crossed over the general Western Cape region which included both AQM stations at the same time. MODIS AOD data over the two AQM stations for the period January to December 2011 were used in this study.

The validation of MODIS AOD retrieved over the case study areas was not included in this study. There was insufficient ground truth data available as aerosol monitoring instruments such as sun photometers and LIDAR instruments were not employed to measure aerosol properties in the case study areas of Malmesbury and George in the Western Cape. However, there is sufficient evidence to support the use of MODIS AOD data without additional field validation (for example Kim *et al.* 2013; Liu *et al.* 2009 and Grguric *et al.* 2013).

3.4.2. Monitoring of Ambient Particulate Matter and Meteorology

PM_{10} mass concentrations were measured continuously using TEOM 1400a PM_{10} monitors from January 2008 by the DEADP (DEADP, 2012a; DEADP, 2012b). PM_{10} concentrations and meteorological data measured at the George and Malmesbury AQM stations for the period January to December 2011 was used in this study. Factors that were considered by the DEADP when selecting the location of the AQM stations (Figure 4) included topography, artefacts such as trees, power lines and buildings that could of altered the direction of flow of air masses making it difficult to distinguish the contribution of local emission sources to the air quality measured at the station. Once the AQM stations had been established by the DEADP and the TEOM measurements were operational, calibration checks were undertaken by the DEADP including fortnightly zero and span checks as well as dynamic calibration checks every three months. The TEOM instruments were operated in a temperature controlled environment. The data collected by the DEADP using the TEOM monitors were centrally collected by a data logging system kept by the DEADP.

Meteorological parameters were measured by the DEADP using a single automatic weather station at the AQM stations (DEADP, 2012a; DEADP, 2012b). Parameters measured included the solar radiation, temperature, rainfall, barometric pressure, RH, wind speed and wind direction. To prevent storms from disturbing the measurements, a 10 m metal tower (Figure 4) was connected to the weather station by the DEADP (DEADP, 2012a; DEADP, 2012b).

Figure 4: Ambient air quality monitoring stations in a) Malmesbury (DEAD, 2012a) and b) George Local Municipality (DEADP, 2012b).

3.5. Tools and procedures

3.5.1. Satellite Data

MODIS AOD was retrieved from the Level 1 and Atmospheric Archive and Distribution System (LAADS) for the year 2011. Files were retrieved using a bounding box over the Western Cape Region with the northern most latitude -30° S , the southernmost latitude -35° S, the westernmost longitude 17° E and the easternmost longitude 25° E. Files were acquired in Hierarchical Data Format (HDF) covering a temporal period from the 1 January 2011 to the 31 December 2011.

Sub-datasets from the HDF files were retrieved using ENVI v4.7 and IDL v7.1.2 with a batch processing retrieval script. Separate retrievals of sub-datasets were done for the data collected for different months and satellite data sources. The data collection comprised of the AOD retrieved using the dark target algorithm ("Corrected_Optical_Depth_Land"), the AOD retrieved using the deep blue algorithm ("Deep_Blue_Aerosol_Optical_Depth_550_Land"), the angstrom exponent retrieved over terrestrial areas ("Angstrom_Exponent_Land") and the cloud cover ("Cloud_Mask_QA") sub-datasets. The processing included the spatial projection of the sub-datasets to Universal Transverse Mercator (UTM) with the datum WGS -84 and the zone 36S. The log processing file after each retrieval was stored to track the processing identification number of each HDF file. Outputs of the retrieval process were raster image sub-dataset files in IMG file format.

To extract the values from the processed sub-datasets over the spatial locations of the AQM stations, ArcGIS v10.1 was used. The spatial analyst tool Extract values to Points tool was used to extract the values from the raster data to vector data format over the spatial locations of the Malmesbury AQM station with latitude -33.455362°S and longitude 18.731913°E and the George AQM station with latitude -33.979375°S and longitude 22.472917°E. The processing identification number was used to identify the associated filename of the HDF image file. The HDF image filename contained identifiers of the satellite source, data, time and satellite product type of the image retrieval.

Values were extracted from the sub-datasets in vector format in Microsoft Excel. The processing identification number and the filename identifiers were used to collate the values within a database. Databases were created in separate spreadsheets for data for each AQM station and satellite source.

3.5.2. Ambient PM$_{10}$ and Meteorological Data

PM$_{10}$ mass concentration data and meteorological data were retrieved from the monthly air quality reports from the DEADP for the Malmesbury AQM station and the George AQM station for the year 2011. The processing of the data extraction was done using Adobe Acrobat XI pro version 11.09.09. Data were extracted from the reports which were in pdf format and processed to a Microsoft Excel spreadsheet format.

The data were extracted from the reports including the hourly averaged PM_{10} mass concentration ($\mu g/m^3$), solar radiation ($W.m^{-2}$), wind speed ($m.s^{-1}$), wind direction (°), RH (%), temperature (°C), rainfall (mm) and Barometric Pressure (hPa). The mean 24 hour averages of the PM_{10} concentrations and the meteorological data were calculated from the hourly data to aggregate the data to a daily temporal resolution. Quality control was used when averaging all the data temporally by requiring the data to be 70% complete as was applied in Garland and Sivakumar (2012). The hourly PM_{10} concentrations, meteorological data, 24 hour averaged PM_{10} concentrations and 24 hour averaged meteorological data were temporally collocated with the retrieved MODIS AOD to the hour of satellite overpass.

3.5.3. Statistical Procedures

The statistical analysis of the PM_{10} and MODIS AOD data included the analysis of temporal trends and statistical tests to compare the data. When statistical analysing the PM_{10} and MODIS AOD data, it was assumed that the data were parametric. This is similar to other studies which have previously explored the AOD-PM_{10} relationship for example Emili *et al.* (2010) and Vidot *et al.* (2007). When comparing the PM_{10} data to meteorological data, it was assumed that the data were non-parametric due to the non-linearity of the meteorological parameters. This statistical approach was similar to that used by Gounden (2007).

Analysis of the PM_{10} concentrations measured at the Malmesbury and George AQM stations included the temporal analysis of the PM_{10} data. Diurnal profiles of the PM_{10} concentrations were determined and compared seasonally and to the annual average using the Tukey HSD post hoc test. Diurnal profiles were typically plotted in air quality studies for example Querol *et al.* (2001) and Grivas *et al.* (2008). The diurnal PM_{10} profiles were also plotted to characterise the temporal trends. The PM_{10} concentrations on weekends and weekdays were also compared using an independent samples t-test. Weekday and weekend diurnal PM_{10} concentrations have previously been compared in Engelbrecht *et al.* (2000) and Grivas *et al.* (2008).

The number of exceedances of the NAAQS (DEA, 2009) and the WHO guidelines for the 24 hour averaged PM_{10} concentrations (WHO, 2006) were determined by comparison of the standards and guidelines to the daily averaged PM_{10} concentrations at each AQM

station. This was done to compare the PM_{10} air quality at each AQM station at a national and global scale similar to Kassomenos *et al.* 2011, Moodley (2008) and Gounden (2007).

The daily averaged PM_{10} data were compared between different months and seasons. Seasonal trend analysis of PM was done previously by Sgrigna *et al.* (2015) to characterise the seasonal variability of PM deposition and by Triantafyllou and Biskos (2012) and Gounden (2007) to characterise the seasonal variability of PM_{10} mass concentration. This was done to determine the presence of seasonality of the PM_{10} concentrations. In this study, the PM_{10} data were compared between months and between seasons using the Tukey HSD post hoc test.

The AOD data retrieved over each AQM station were analysed to determine the temporal trends of the AOD over each station. The AOD data analysed including those retrieved from the AQUA satellite using the dark target algorithm ($AOD_{aqua.dt}$), and the deep blue algorithm ($AOD_{aqua.db}$) in addition to the AOD retrieved from the TERRA satellite using the dark target algorithm ($AOD_{terra.dt}$). The AOD was compared to the annual averaged AOD to determine the temporal fluctuations of the AOD during the year by determining the frequency of the AOD retrievals, below and above the annual averaged AOD. The AOD data were compared for differences between seasons using the Tukey HSD post hoc test. The temporal trend analysis of AOD has been done in previous studies for example Queface *et al.* (2011) and Kumar *et al.* (2014).

The AOD-PM_{10} relationship over each AQM station was statistically explored using linear regression analysis. Regression analysis included the correlation of AOD with hourly averaged and daily averaged PM_{10} concentrations. Linear analysis was done to determine the annual, weekly, monthly and seasonal AOD-PM_{10} relationship. Analysis of the AOD-PM_{10} relationship at different temporal scales had been done before for example by Kumar *et al.* 2008, Emili *et al.* (2010) and Hashim *et al.* (2011). A filtering procedure was adapted from Barladeanu *et al.* (2012) and employed in this study to determine the relationship between the AOD and the daily averaged PM_{10} concentrations above and below the annual average AOD and PM_{10} concentrations. The AOD and PM_{10} data were also averaged between the two AQM stations in order to upscale the annual AOD-PM_{10} relationship determined using linear regression. Spatial up-scaling of the AOD-PM_{10} relationship was previously employed in Emili *et al.* (2010) and Koelemeijer *et al.* (2006).

The trends of the meteorological parameters included in the study were also determined temporally. Diurnal profiles of the wind speed, temperature, RH and solar radiation were plotted and compared seasonally using the Kruskal Wallis post hoc test. Diurnal profiling of meteorological parameters had previously been done in Ningwei *et al.* (2012). The monthly averaged meteorological parameters were plotted along with monthly averaged PM_{10} concentrations to track and compare the seasonal monthly variations between meteorological parameters and PM_{10} concentrations similar to Chen and Xie (2013). Seasonal wind rose plots were created using WR PLOT v7. The daily averaged meteorological parameters including wind speed, rainfall, solar radiation, RH and temperature in each season were compared to daily averaged PM_{10} concentrations in each season using spearman rank correlation analysis. Correlation analysis between PM_{10} concentrations and meteorological analysis using a non-parametric approach was previously done in Gounden (2007). The results of the correlation analysis were compared together with the wind rose plots to explore the seasonal meteorological effects on PM_{10} concentrations similar to the comparative approach used in Gounden (2007)

In the final part of the study the $\log_{10}$ transformed PM_{10} data were used for the purposes of the multiple linear regression and comparative correlation analysis between PM_{10} and various possible predictors. These predictors included the AOD, daily averaged RH, daily averaged temperature, daily averaged wind speed and daily averaged wind direction. Furthermore the adjusted AOD was also included in this analysis namely AOD/RH. The AOD was adjusted by the division of the AOD with RH. This approach was adapted from Dinoi et al (2010) which adjusted the AOD using the product of the averaged MLH and the average wind speed. Correlation analysis between daily averaged PM_{10} concentrations and temporally co-located predictors for the whole year was included to evaluate the linear relationship of PM_{10} with its predictors. Linear regression models were determined in this analysis, one which included AOD as a predictor and the other which used AOD/RH. This approach was similar to Gounden (2007), which used multiple linear regression to assess the overall effect of meteorological parameters on PM_{10} concentrations.

3.6. Summary

Due to the use of the methods outlined in this study, the PM_{10} concentrations, the AOD and meteorology were characterised for the towns of George and Malmesbury for the year 2011. Furthermore, additional analysis was possible which included the determination of the linear relationship between PM_{10} and its main predictors including the AOD, RH,

AOD/RH, temperature, wind speed and wind direction. This has served the purpose to determine the extent; AOD could be used as a proxy for air quality analysis of PM pollution in the Western Cape, South Africa. Furthermore, it was possible to highlight the specific meteorological conditions which may act as confounders of the AOD-PM_{10} relationship in the Western Cape.

CHAPTER 4: RESULTS AND DISCUSSION

4.1. Introduction

Pollutant sources of PM_{10} can be found in all urban environments from motor vehicles exhausts, biomass fuel burning activities in households, veld and agriculture burning and from industrial combustion processes. No threshold has been determined for PM_{10} ambient air quality beyond which adverse health effects on the population will occur. Even the lowest concentrations of PM_{10} in the atmosphere will contribute to negative population health impacts.

It is important to investigate PM_{10} ambient air quality in all areas of the Western Cape. Additionally PM_{10} particles can stay aloft in the atmosphere for days and can travel long distances in the atmosphere to affect the air quality of distant areas in the Western Cape. Case studies of ambient air quality in the Western Cape have mainly been carried out in the City of Cape Town (for example Wichmann, 2006; White *et al.* 2009; Wichmann and Voyi, 2012; Niyobuhungiro and von Blottnitz, 2013). This chapter characterises the PM_{10} ambient air quality measured at the AQM stations in two other towns in the Western Cape, that is, Malmesbury[1] and George[2].

This chapter explores the meteorological characteristics of the case study area and quantitatively determines the relationship between meteorological conditions and PM_{10} concentrations at the case study sites. The AOD characteristics over the AQM stations are discussed. The main focus of the chapter is the relationship between the satellite retrieved AOD over the AQM stations and the PM_{10} measured at the stations. Lastly the effects of meteorological factors on the AOD-PM_{10} are examined.

4.2. High PM_{10} Concentrations

Scott (2010) observed that air quality is a potential issue within the towns of Malmesbury and George. The study highlighted the transboundary pollution impacts from the city of Cape Town on the neighbouring town of Malmesbury which forms a part of the Swartland Municipality. Furthermore the contribution of heavy industries in the town of George to air pollution in the area was also highlighted (Scott, 2010).

---

[1] Malmesbury is a town on the periphery impacted by transboundary air pollution.
[2] George is a larger town with a mixture of residential, land use and industrial activities occurring in the town, such that the town has the potential to be affected by poor air quality due to the number of air pollution sources in the area

The PM$_{10}$ data for 2011 was analysed to identify occurrences when the PM$_{10}$ concentration exceeded safe levels according to the ambient air quality standards or air quality guidelines. The DEA (2009) NAAQS daily averaged PM$_{10}$ limit is 120 µg/m^3, for which no exceedances occurred in Malmesbury and George in 2011. The use of the daily average WHO (2006) guideline for PM$_{10}$ is useful in comparing air quality case studies at a global level and is 50 µg/m^3. Seven exceedances of this guideline occurred in Malmesbury and George (Figures 5 and 6), indicating that there is a PM air quality problem within the two towns.

A small number of exceedances have been observed in cities with similar climate types as Malmesbury and George including in New Zealand (Brown *et al.* 2005) at a station with an urban residential background and in Spain (Escudero et al, 2007) at rural background stations. In comparison to these case study examples, the number of exceedances observed at George and Malmesbury AQM stations were not unusual. Kassomenos *et al.* (2011) observed many more exceedances in Greece at an urban traffic station and urban background station. It was determined from these case studies that the number of exceedances vary depending on the location of the AQM station and the representative background sources being measured.

The WHO guidelines for average annual PM$_{10}$ concentrations is 20 µg/m^3. The average annual PM$_{10}$ concentration for 2011 at the Malmesbury AQM station is 21µg/m^3 and at the George AQM station the annual average PM$_{10}$ concentration is 20 µg/m^3. This indicates that the annual average PM$_{10}$ concentrations at George and Malmesbury are comparable to the WHO annual average guideline and may be of concern as an air quality issue. At the country level, the annual concentrations at George and Malmesbury AQM stations are on par with South Africa's annual average PM$_{10}$ concentrations in 2009 (21-30 µg/m^3) (Fajersztajn *et al.* 2013). The annual PM$_{10}$ concentrations at George and Malmesbury were lower than those observed in townships such as Khayalitsha (Tessema, 2011), Leandra (Mugabo, 2011) and Marikana (Venter, 2013). Hence, this suggested that the PM$_{10}$ concentrations at George and Malmesbury AQM stations are locally representative of the concentrations where the stations are sited and that there is local scale variability of the PM$_{10}$ concentrations at localities a distance away from the Malmesbury and George AQM stations.

The occurrence of exceedances during the dry period at the Malmesbury AQM station are linked with the seasonal variability. Seasonal variability is tied to both meteorological effects and to human activities. Lower rainfall in the dry season, increases the persistence of aerosols aloft in the atmosphere (Sharon *et al.* 2006) and this is indicated by a negative correlation between rainfall and PM_{10} concentrations (for example Vardoulakis and Kassomenos, 2008), while biomass burning increases the quantity of PM from burning sources (for example Diab *et al.* 2003). The burning season in the south-western Cape falls within the summer and autumn months according to van Wilgen *et al.* (2012). Our study confirmed this with the dry season for 2011 observed in this study by rainfall variations measured at the Malmesbury AQM station which occurred in the summer months and autumn months. The drier period at the Malmesbury AQM station is also characterised by warmer temperatures and greater solar radiation compared to the remaining seasons.

The occurrence of exceedances at the George AQM station in the late winter season are also linked with the seasonal variability. However unlike the Malmesbury AQM station, a greater number of exceedances occurs after the peak monthly rainfall in June during a period of declining rainfall. Additionally the exceedances occur out of the typical burning season which occurs from November to April. More than 50% of the exceedances occurred in winter. Engler *et al.* (2012) suggested that the greater number of exceedances in winter in Leipzig, Germany were due to the greater frequency of surface inversions and burning of fuel in the residential sector due to the colder temperatures. Thus greater fuel combustion in the residential sector for heating purposes and the frequency of surface inversions are suggested to be possible factors which favour greater PM_{10} concentrations in winter measured at the George AQM station.

For Mediterranean climates, Escudero *et al.* (2007) observed that most exceedances occurred in the summer and autumn months for rural background AQM stations in Spain. This was similar to what was observed in Malmesbury with most exceedances occurring in the summer and autumn months. At urban background AQM stations, the opposite occurred with mid - winter and spring months in Thessaloniki, Greece having more frequent exceedances (Kassomenos et al, 2011). Rodriguez *et al.* (2001) also observed similar trends with exceedances at Spanish urban and industrial background AQM stations with frequent exceedances in winter, in addition to the exceedances in summer. At the rural background AQM station studied by Rodriguez *et al.* (2001), exceedances in summer were the most frequent. Similarly Toro *et al.* (2014) observed more frequent exceedances

in winter months (April to September) in Santiago, Chile at urban background stations for a city in a Mediterranean climate. Hence it is apparent that there are seasonal differences in exceedances between urban and rural background AQM stations due to levels of anthropogenic activity. Thus it is likely that the AQM station in Malmesbury represents rural background sources rather than urban background sources.
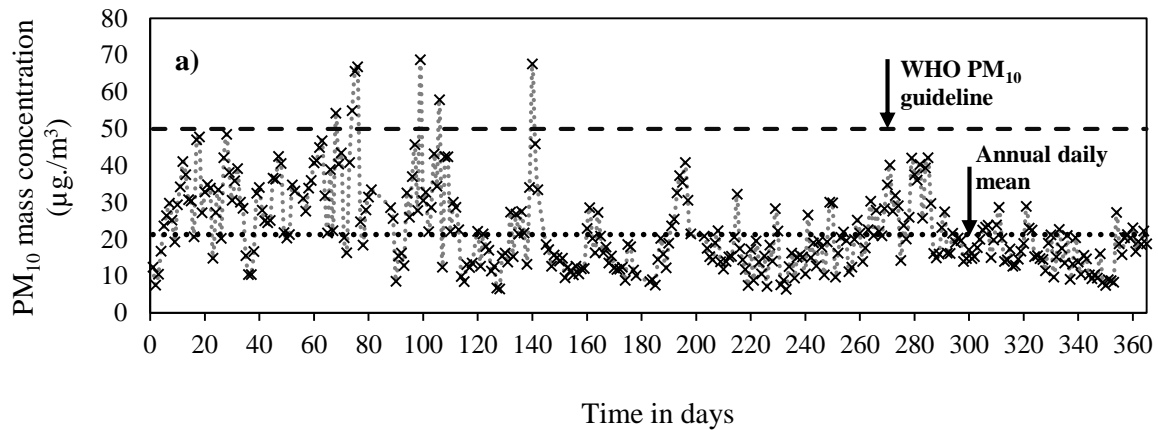
Figure 5: 24 hourly averaged hourly PM$_{10}$ concentrations at the Malmesbury AQM station in 2011, compared to the annual daily mean PM$_{10}$ concentration and the WHO air quality guideline for daily mean PM$_{10}$ concentrations.
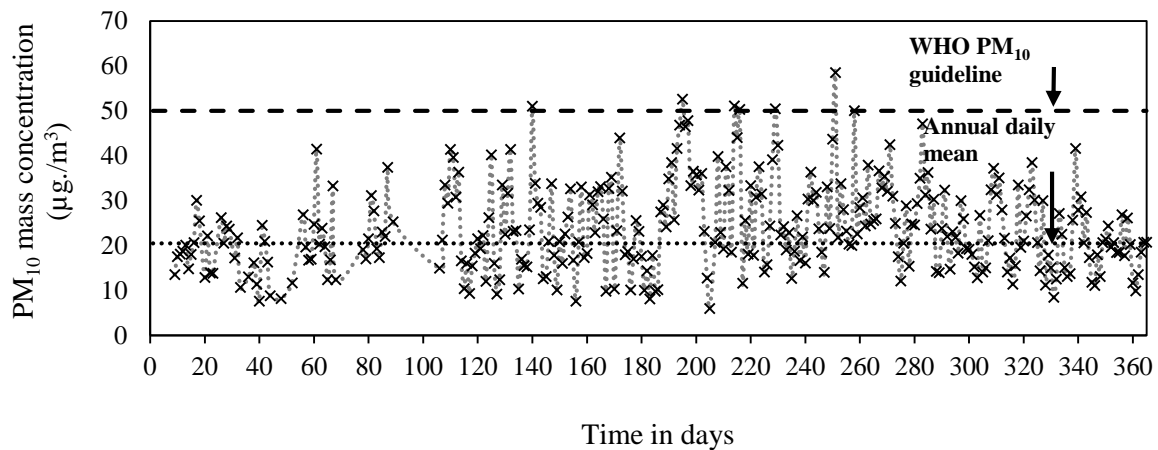
Figure 6: 24 hourly averaged hourly PM$_{10}$ concentrations at the George AQM station in 2011, compared to the annual daily mean PM$_{10}$ concentration and the WHO air quality guideline for daily mean PM$_{10}$ concentrations.

For the George station, most of the exceedances occurred in winter-spring months. Other studies also observed that many exceedances occurred in winter for example in New Zealand (Brown *et al.* 2005), in Belgium (Maenhaut *et al.* 2012) and in France (Poggi and Portier, 2011). Therefore the occurrence of exceedances in the winter-spring months is a common occurrence for regions with an oceanic climate.

Thus the comparisons of case studies for PM_{10} trends observed for stations in a Mediterranean climate indicate the effect of anthropogenic activity on the occurrence of exceedances which is likely to be of more importance than seasonal meteorological effects. This is not observed for case studies which observe PM_{10} trends for stations in ocean climate regions. This is due to the occurrence of favourable meteorological conditions such as frequent surface inversions and increased anthropogenic activity occurring in the same season (for example Maenhaut *et al.* 2012).

4.3. Characteristics of Diurnal Mean PM_{10} and Meteorology

4.3.1. Seasonal Characteristics

The diurnal mean PM_{10} concentrations at Malmesbury (Figure 7) and George (Figure 8) AQM stations peaked twice, in the morning and in the evening. The mean PM_{10} concentrations in spring at the George AQM were characterised by a third peak at around midday. However it is unlikely that the meteorological drivers contributed to the peaks in mean PM_{10} concentrations at the Malmesbury AQM station. At the George AQM station, it was possible to compare the mean PM_{10} concentrations to the mean diurnal meteorological conditions in spring as insufficient data were available to characterise the mean PM_{10} concentrations in other seasons. Mean diurnal wind speed trends (Figure 9); temperatures (Figure 11); RH conditions (Figure 13) and solar radiation levels (Figure 15) measured at the Malmesbury AQM station were not characterised by noticeable fluctuations around the time mean PM_{10} concentrations peaked. Low wind speeds, low temperatures and low solar radiation levels were likely to contribute to favourable conditions for the morning peak in diurnal PM_{10} concentrations monitored at the Malmesbury AQM station. It is likely that the peak in PM_{10} concentrations at Malmesbury AQM station coincide with anthropogenic emission sources such as traffic activity similar to case studies in Lebanon and Chile (Saliba *et al.* 2006 and Gramsch *et al.* 2006). The peak in PM_{10} concentrations during the midday at the George AQM station in spring is likely due to the decrease in vertical air mixing as a result of the increasing wind speeds (Figure 10) and temperatures (Figure 12) which remain relatively cold. This contrasts with the greater atmospheric turbulence due to warmer temperatures in summer in Spain which coincided with reduced PM_{10} concentrations (Barerro *et al.* 2015). It is likely that greater atmospheric turbulence during the day at the Malmesbury AQM station due to increasing solar radiation levels and temperatures favoured the lower PM_{10} concentrations during the

days similar to the explanation provided by Barerro *et al.* (2015) for low PM_{10} concentrations in Spain during the day. The relatively lower RH conditions and greater wind speeds at the Malmesbury AQM station during the day also favoured the suspension of PM_{10} particulates such as soil (Hien *et al.* 2002).

Mean diurnal PM_{10} concentrations in winter at the Malmesbury AQM station were significantly different and mostly lower than the mean PM_{10} concentrations in other seasons including summer ($Q = 4.33$, $p < 0.0005$), autumn ($Q = 5.24$, $p < 0.0005$) and spring ($Q = 2.99$, $p = 0.027$) (Table 2). The differences between the high mean diurnal PM_{10} concentrations in summer and in autumn were negligible ($Q = 0.91$, $p = 0.894$). This suggests a bi-seasonal pattern of the mean diurnal PM_{10} concentrations in 2011 for PM_{10} concentrations at the Malmesbury AQM station in summer, autumn and spring collectively and PM_{10} concentrations in winter on its own. At the George AQM station, mean diurnal PM_{10} concentrations in summer were mostly lower and significantly different from the diurnal PM_{10} concentrations in winter ($Q = 4.45$, $p < 0.0005$) and in spring ($Q = 4$, $p = 0.001$). Although the peak mean diurnal concentrations in winter were relatively much higher than the peak mean diurnal concentrations in spring, the differences between the mean diurnal concentrations for these seasons were negligible at the George AQM station ($Q = 0.44$, $p = 0.970$). Diurnal PM_{10} concentrations monitored at the George AQM station remained somewhat stable for the duration of the afternoon compared to the increasing trend of diurnal PM_{10} concentrations monitored at the Malmesbury AQM station in the afternoon. The stabilised trend of the diurnal PM_{10} concentrations monitored at the George AQM station are more apparent in spring. Diurnal meteorology monitored at the George station were affected by poor data completeness. This is indicted by the missing wind speed data, temperature data, RH data (Figure 14) and solar radiation data (Figure 16). The declining wind speeds in the afternoon in George in spring and the cooler temperatures relative to those measured in Malmesbury are likely to have contributed to the favourable conditions for the stabilised but elevated diurnal PM_{10} concentrations in the afternoon.

Table 2: Intra-annual seasonal comparisons of diurnal PM$_{10}$ concentrations at Malmesbury and George AQM stations and comparison to the annual diurnal signature in 2011.

Comparison	Tukey HSD post-test – Malmesbury AQM station	Tukey HSD post-test – George AQM station
annual vs. summer	Q = 1.2; p = 0.754	Q = 2.2; p = 0.131
annual vs autumn	Q = 2.1; p = 0.23	In sufficient data in autumn
annual vs. winter	Q = 3.13; p = 0.02	Q = 2.25; p = 0.117
annual vs. spring	Q = 0.14; p = 1	Q = 0.18; p = 0.276
summer vs. autumn	Q = 0.91; p = 0.894	In sufficient data in autumn
summer vs. winter	Q = 4.33; p < 0.0005	Q = 4.45; p < 0.0005
summer vs. spring	Q = 1.33; p = 0.67	Q = 4; p = 0.001
autumn vs. winter	Q = 5.24; p < 0.0005	In sufficient data in autumn
autumn vs. spring	Q = 2.24; p = 0.17	In sufficient data in autumn
winter vs. spring	Q = 2.99; p = 0.027	Q = 0.44; p = 0.970
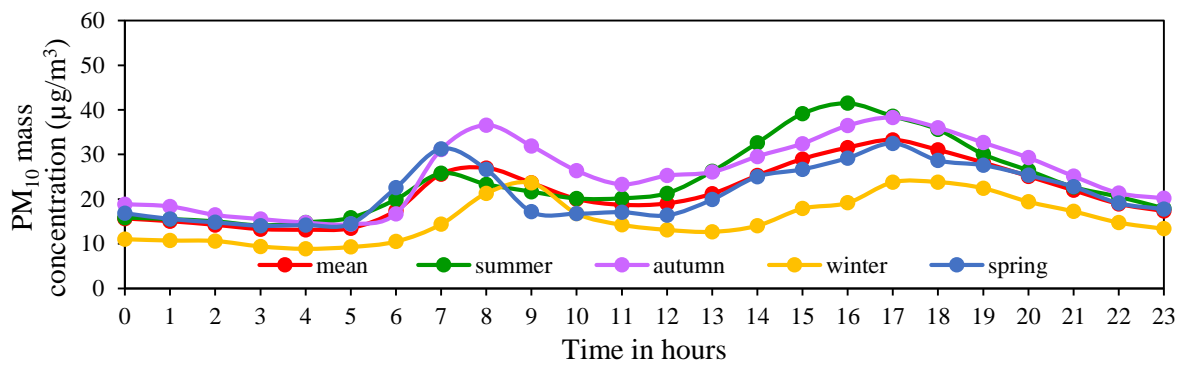
Figure 7: Mean diurnal PM$_{10}$ mass concentrations (µg/m^3) at the Malmesbury AQM station in 2011 with annual and seasonal mean concentrations.
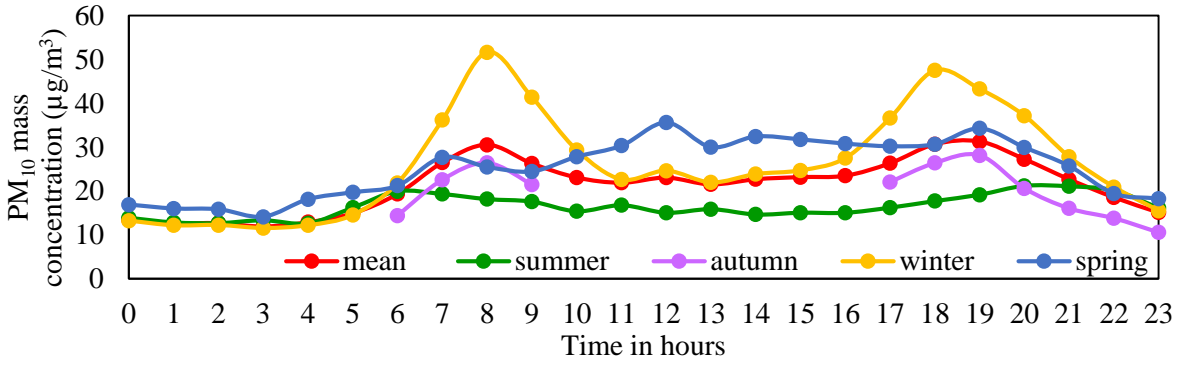
Figure 8: Mean diurnal PM$_{10}$ mass concentrations (µg/m^3) at the George AQM station in 2011 with annual and seasonal mean concentrations.
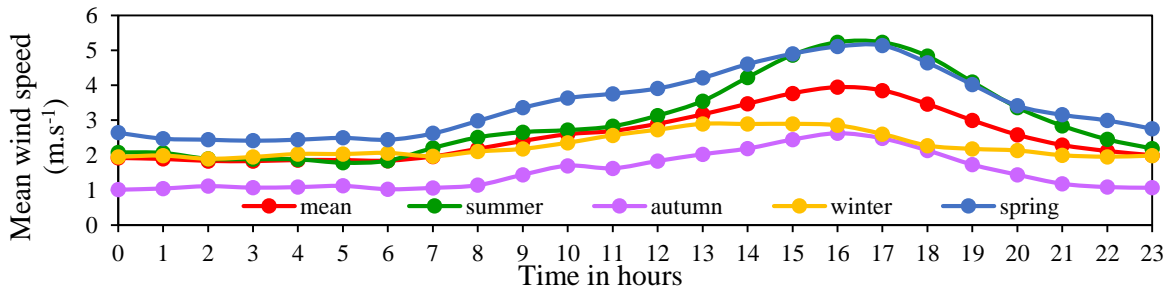
Figure 9: Diurnal averaged wind speed conditions at the Malmesbury AQM station in 2011.
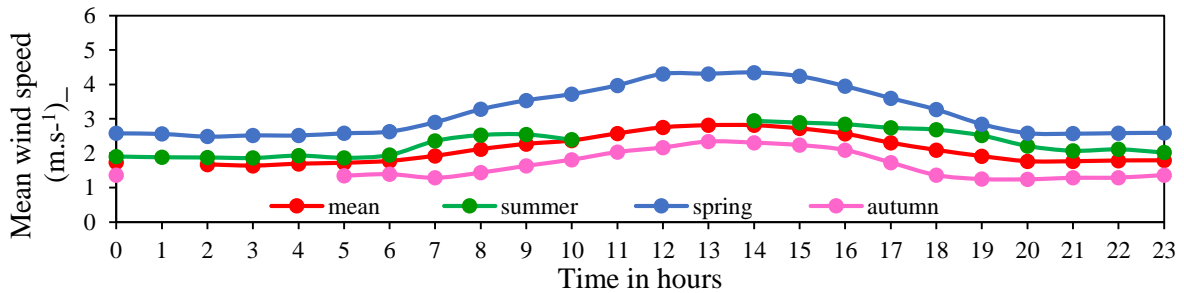
Figure 10: Diurnal averaged wind speed conditions at the George AQM station in 2011.
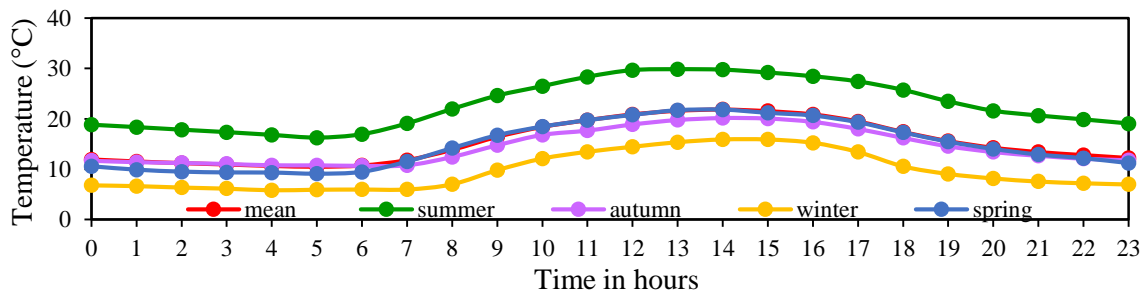
Figure 11: Diurnal mean temperatures at the Malmesbury AQM station in 2011.
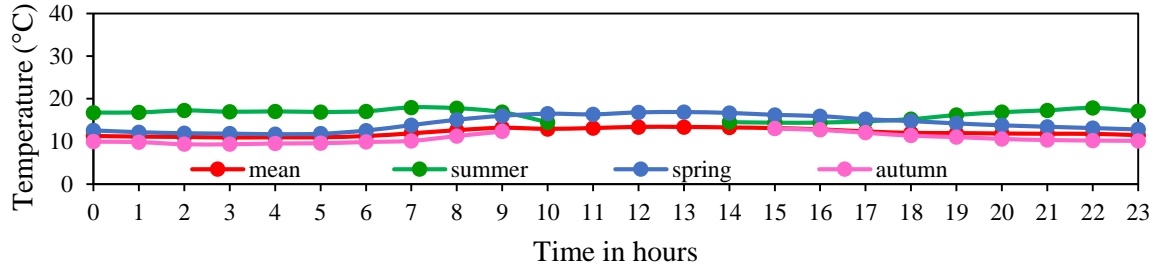
Figure 12: Diurnal mean temperatures at the George AQM station in 2011.
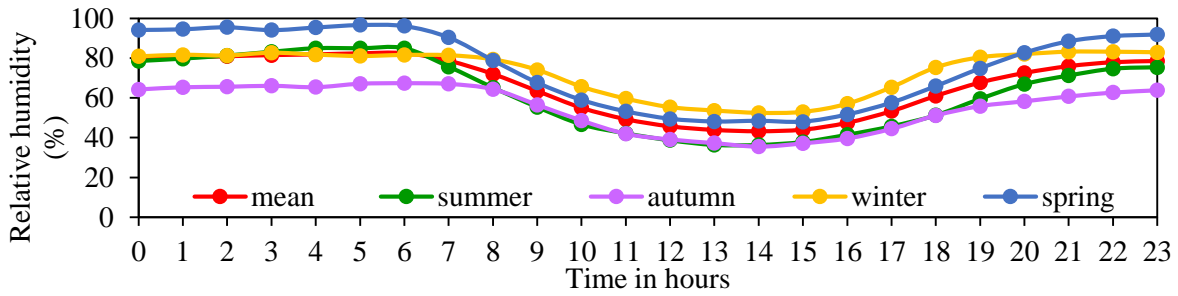
Figure 13: Diurnal RH conditions at the Malmesbury AQM station in 2011.
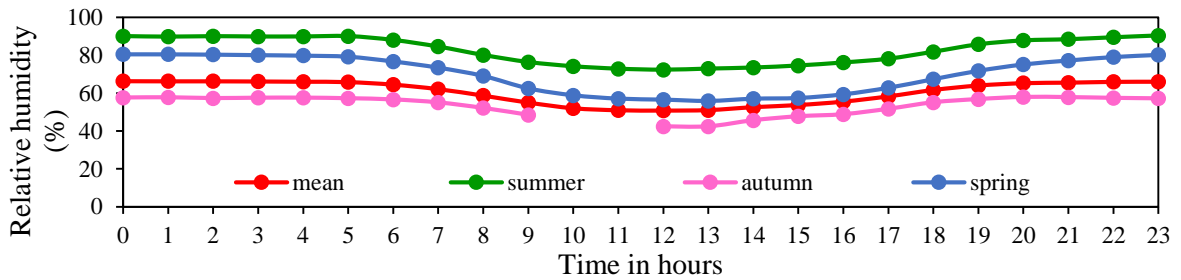
Figure 14: Diurnal RH conditions at the George AQM station in 2011.
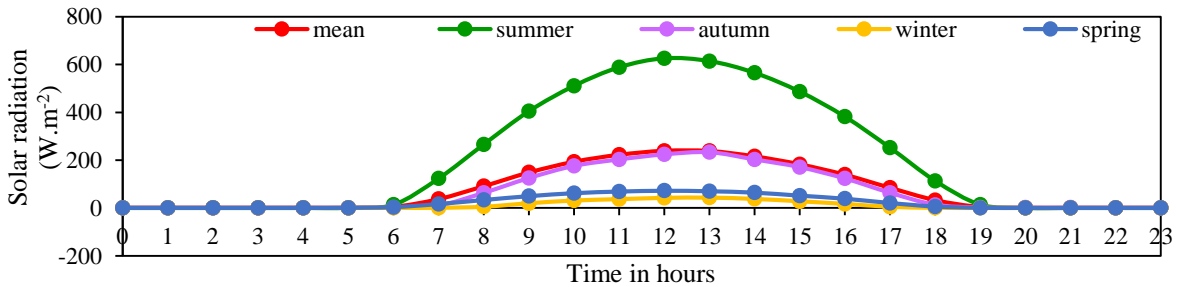
Figure 15: Diurnal seasonal solar radiation trends at the Malmesbury AQM station in 2011.
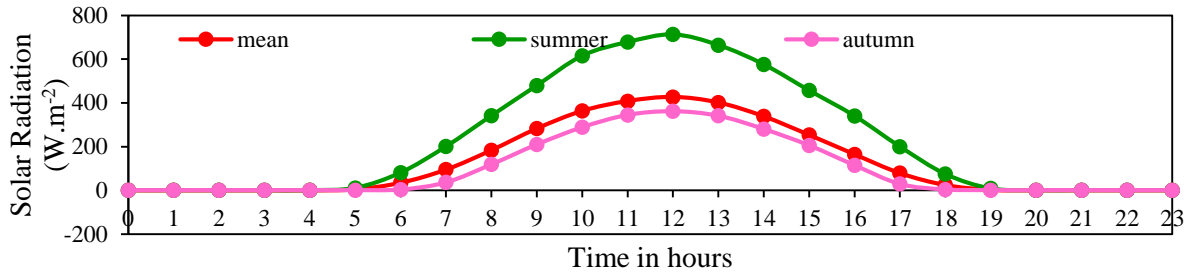
Figure 16: Diurnal seasonal solar radiation trends at the George AQM station in 2011.

4.3.2. Weekdays and Weekends

The weekend diurnal mean PM_{10} concentrations were also calculated at Malmesbury and George AQM stations (Figure 17 and Figure 18). A difference was determined between mean PM_{10} concentrations on weekdays and on weekends at the Malmesbury AQM station ($t = 2.2$; $p=0.033$) with greater PM_{10} concentrations during weekdays. Although mean PM_{10} concentrations at the George AQM station were slightly greater for most hours on weekdays and the morning peak PM_{10} concentrations were much greater on weekdays relative to weekends, the difference between weekend and weekday mean PM_{10} concentrations was insignificant ($t = 1.939$, $p = 0.059$). Previous studies in Europe and the USA have found that PM_{10} concentrations were higher on weekdays rather than weekends and were attributed to greater traffic and human activity (Lonati *et al.* 2006; Grivas *et al.* 2004 and Motallebi *et al.* 2003). Thus the differences between weekday and weekday PM_{10} concentration levels at the Malmesbury AQM station were likely due to varying intensities of anthropogenic emission sources near the AQM station. The differences in intensities of emissions sources near the George AQM station were likely to be negligible on weekdays and weekends.
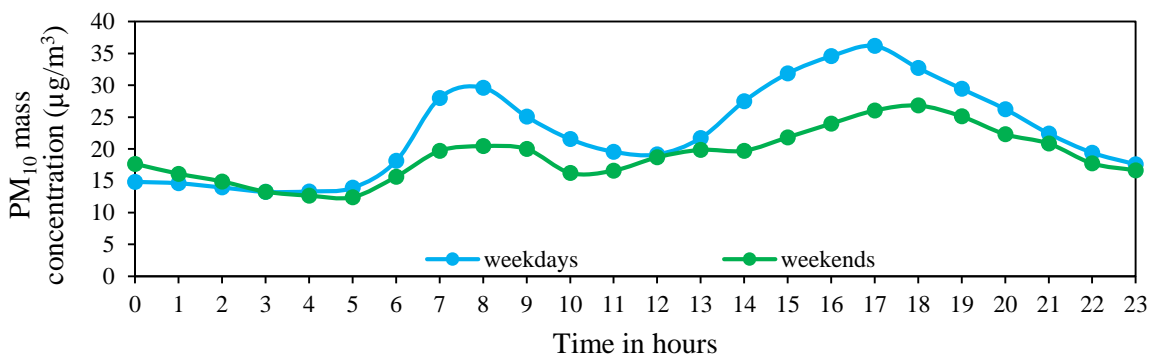
Figure 17: Weekend and weekday diurnal mean PM_{10} concentrations at the Malmesbury AQM station in 2011.
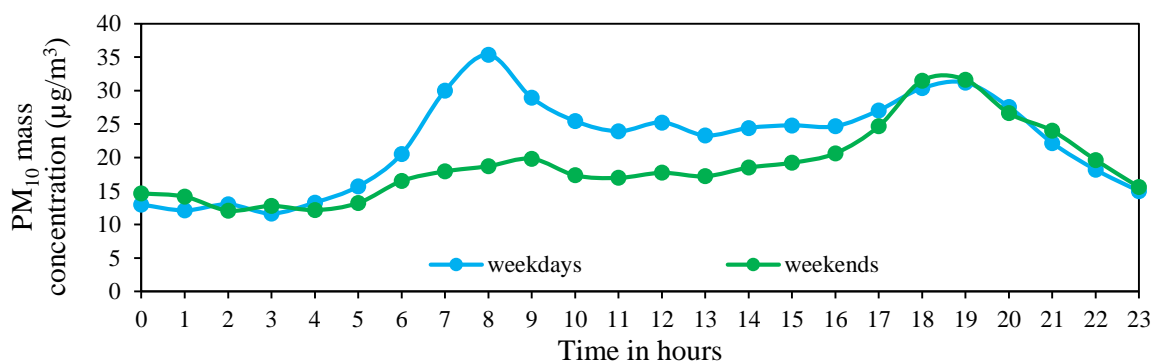
Figure 18: Weekend and weekday diurnal mean PM₁₀ concentrations at the George AQM station in 2011.

4.4. Monthly and Seasonal PM$_{10}$ Concentrations and Meteorology

At the Malmesbury AQM station, mean daily PM$_{10}$ concentration levels in summer were similar to those in autumn (Table 3). The PM$_{10}$ concentration trends in spring were also similar to those in summer. It was observed that daily concentrations of PM$_{10}$ were similar for January - April months when PM$_{10}$ concentrations were relatively high (Figure 19) and mostly similar for May - December months when PM$_{10}$ concentrations were generally lower suggesting a bi - seasonal cycle of the PM$_{10}$ concentration at the Malmesbury AQM station (Table 4). Inter-seasonal PM$_{10}$ concentration trends were observed, a winter - spring increase (August - October), a spring - summer decrease (October to December), a summer to autumn plateau with high PM$_{10}$ concentrations (January - April) and an autumn - winter decrease (April to June). The highest monthly mean hourly PM$_{10}$ concentrations were also observed in the January - March months. Monthly mean hourly averaged PM$_{10}$ concentrations were lower for other months of the year. A rainfall trough occurred (Table 5) during the same period of the summer - autumn PM$_{10}$ plateau (January - April) which proceeded to an autumn - winter peak in monthly rainfall during the same period of the autumn - winter decrease in PM$_{10}$ concentrations. The winter-spring increase in PM$_{10}$ concentrations (August - October) was accompanied by decreasing monthly rainfall. The spring - summer decrease in PM$_{10}$ concentrations was accompanied by a tertiary peak in monthly rainfall. The period of the summer - autumn plateau was accompanied by a RH plateau which fluctuated at higher RH for the rest of the year for which lower PM$_{10}$ concentrations were frequent. Temperatures peaked over the January - April months, while wind speeds and solar radiation gradually declined. The prevailing wind direction for the January to April period was south westerly (Figure 21). Thus the January to April period at the Malmesbury station was characterised by high PM$_{10}$ concentrations, warmer

75

temperatures, dryer air (but still >50% RH), low rainfall, declining wind speeds with a predominant south westerly direction and greater solar radiation.

At the George AQM station, a bi - seasonal PM_{10} concentration trend was observed (Table 3). Mean daily PM_{10} concentrations in summer were significantly different to mean PM_{10} concentrations in autumn ($Q = 2.8$; $p = 0.027$), winter ($Q = 4.75$; $p < 0.0005$) and spring ($Q = 4.24$; $p < 0.0005$). Mean daily PM_{10} concentrations in autumn, winter and spring were similar to each other. Summer mean monthly PM_{10} concentrations were much lower than PM_{10} concentrations in autumn, winter and spring (Figure 20). The highest mean monthly PM_{10} concentrations occurred in winter and spring but were slightly higher in winter. There was less than 70% data coverage for PM_{10} data in the autumn months such that the mean monthly PM_{10} concentrations in March and April were not calculated. The low mean monthly PM_{10} concentrations in summer coincided with the highest mean monthly RH conditions and lowest mean monthly rainfall levels at the George AQM station. The higher mean monthly PM_{10} concentrations in winter coincided with the highest monthly mean rainfall, the lowest solar radiation levels and the lowest mean monthly temperatures (Table 6). The predominant wind direction were westerlies at the George AQM station in winter (Figure 22). Prevailing wind directions in summer were westerlies, easterlies and south easterlies. Possible sources which may have contributed to the higher concentrations in winter includes the greater burning of fuel sources for heating due to the colder weather in winter. A possible meteorological driver of the higher PM_{10} concentrations in winter includes the greater frequency of surface inversions favoured by lower temperatures in winter.

Table 3: Intra-annual seasonal comparisons of daily PM_{10} concentrations at the Malmesbury AQM station and the George AQM station in 2011.

Seasonal comparison	Tukey HSD post hoc test-Malmesbury AQM station	Tukey HSD post hoc test-George AQM station
summer and autumn	$Q = 2.23$; $p = 0.118$	$Q = 2.8$; $p = 0.027$
summer and winter	$Q = 4.59$; $p < 0.0005$	$Q = 4.75$; $p < 0.0005$
summer and spring	$Q = 1.75$; $p = 0.299$	$Q = 4.24$; $p < 0.0005$
autumn and winter	$Q = 6.73$; $p < 0.0005$	$Q = 1.54$; $p = 0.412$
autumn and spring	$Q = 3.97$; $p = 0.001$	$Q = 1.1$; $p = 0.693$
winter and spring	$Q = 2.90$; $p = 0.021$	$Q = 0.49$; $p = 0.961$

Table 4: Significance of the intra-monthly multiple comparisons of daily averaged PM$_{10}$ concentrations at Malmesbury AQM station in 2011*.

Month	JAN	FEB	MAR	APR	MAY	JUN	JUL	AUG	SEP	OCT	NOV	DEC
JAN	■	1.000	0.395	1.000	0.020	<0.0005	0.014	<0.0005	0.099	0.392	0.001	<0.0005
FEB	1.000	■	0.222	1.000	0.109	<0.0005	0.081	<0.0005	0.343	0.758	0.007	<0.0005
MAR	0.395	0.222	■	0.156	<0.0005	<0.0005	<0.0005	<0.0005	<0.0005	0.000	<0.0005	<0.0005
APR	1.000	1.000	0.156	■	0.109	<0.0005	0.081	<0.0005	0.352	0.778	0.007	<0.0005
MAY	0.020	0.109	<0.0005	0.109	■	0.598	1.000	0.613	1.000	0.989	0.999	0.585
JUN	<0.0005	<0.0005	<0.0005	<0.0005	0.598	■	0.767	1.000	0.233	0.043	0.976	1.000
JUL	0.014	0.081	<0.0005	0.081	1.000	0.767	■	0.786	1.000	0.970	1.000	0.763
AUG	0.000	0.000	<0.0005	<0.0005	0.613	1.000	0.786	■	0.234	0.040	0.982	1.000
SEP	0.099	0.343	<0.0005	0.352	1.000	0.233	1.000	0.234	■	1.000	0.960	0.215
OCT	0.392	0.758	0.000	0.778	0.989	0.043	0.970	0.040	1.000	■	0.644	0.035
NOV	0.001	0.007	<0.0005	0.007	0.999	0.976	1.000	0.982	0.960	0.644	■	0.978
DEC	<0.0005	<0.0005	<0.0005	<0.0005	0.585	1.000	0.763	1.000	0.215	0.035	0.978	■

*Orange are cells with daily mean PM$_{10}$ concentrations which are similar; Green are cells with daily mean PM$_{10}$ concentrations which are different; significant @ $p < 0.05$.
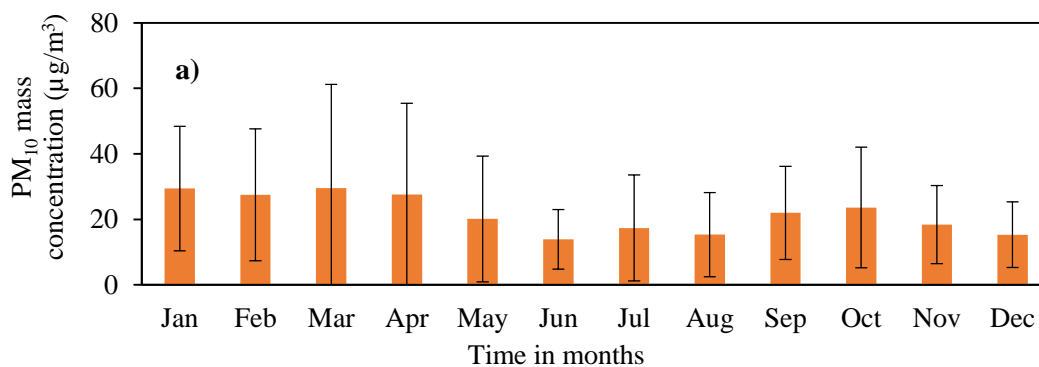
Figure 19: Monthly hourly averaged PM$_{10}$ concentrations at the Malmesbury AQM station in 2011.
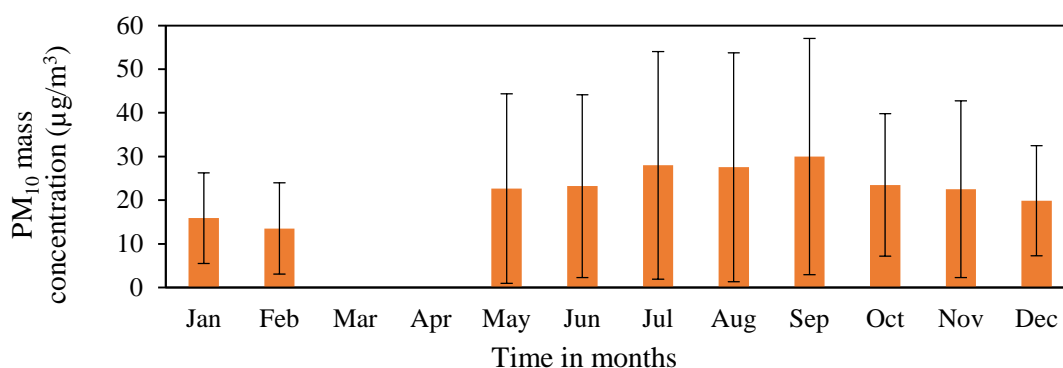
Figure 20: Monthly hourly averaged PM$_{10}$ concentrations at the George AQM station in 2011.

Previous case studies in Chile, Spain, Turkey and Khayalitsha, South Africa found that high PM$_{10}$ concentrations occurred mainly in winter but also in spring in regions with more pollutant sources such as the seasonal trends measured at urban and traffic background AQM stations (Wichmann, 2006; Moreno *et al.* 2006; Kocak *et al.* 2011 and Toro *et al.* 2014). In Spain, high PM$_{10}$ concentrations were observed at rural background stations mainly in summer and autumn but also in spring (Rodrıguez *et al.* 2002 and Querol *et al.* 2004) This suggested that the PM$_{10}$ concentrations observed at the Malmesbury AQM station were representative of regional or rural background concentrations. The autumn and winter months in Chile were affected by cooler temperatures, lower RH (still >50%) and slower wind speeds (Toro *et al.* 2014). The high PM$_{10}$ concentrations at Malmesbury in summer -autumn months share similar RH and wind speed trends with those observed in Chile, being associated with lower wind speeds and lower RH. Contrasting though is the associated higher temperatures in Malmesbury in summer - autumn months with higher PM$_{10}$ concentrations and associated lower temperatures in Chile in the autumn and winter months.

In England, high PM$_{10}$ concentrations occurred throughout the year at traffic and urban background AQM stations (Harrison *et al.* 2001; Charron *et al.* 2007; Bigi and Harrison, 2010 and Kassomenos *et al.* 2012). In Germany, at both traffic and rural stations, higher PM$_{10}$ concentrations occurred in winter, spring and autumn months and lower concentrations occurred in summer for exceedance days (Engler *et al.* 2012). However the seasonal trends of daily PM$_{10}$ concentration in Germany were not apparent for non-exceedance days which made up the bulk of each year's daily PM$_{10}$ concentrations. In Canada, PM$_{10}$ concentrations were higher in summer months and lower in winter months (McKendry, 2000). Aldabe *et al.* 2011 determined that the highest PM$_{10}$ concentrations measured in Spain were in winter. There is no apparent seasonal similarity for PM$_{10}$

78

concentrations measured in oceanic climates in different countries. This suggests that seasonal PM_{10} concentrations in oceanic climates vary for different geographic locations and that the seasonal characteristics of PM_{10} concentrations at the George AQM station are specific to the town of George only.

The results in this study indicated correlations between rainfall and PM_{10} in all seasons at the George and Malmesbury AQM stations. This suggests that PM_{10} is negatively correlated with rainfall in all seasons at George and the Malmesbury AQM stations. Positive correlations were observed between PM_{10} and solar radiation. At the Malmesbury AQM station, solar radiation and temperature had a substantial effect on PM_{10} concentrations in summer and autumn, the seasons with the higher PM_{10} concentrations. Temperature also had a substantial correlation on PM_{10} concentrations in winter when the PM_{10} concentrations were low. Winter is the season with the highest PM_{10} concentrations at the George AQM station, and it was observed that meteorology has a substantial effect on PM_{10} concentrations in this season including rainfall, wind speed and temperature compared to other seasons.

At the Malmesbury AQM station, although the highest PM_{10} concentrations occurred in autumn, none of the five meteorological variables were either the highest or lowest in this season. PM_{10} concentrations had correlations greater than 50% with temperature and solar radiation. The highest correlation between RH and PM_{10} occurred in autumn. The lowest PM_{10} concentrations occurred in winter, with the correlation between PM_{10} and temperature greater than 50%. Winter had the coldest temperatures, coldest solar radiation and the highest RH.

When the results of this study are compared to a Durban case study, we observe that meteorological drivers have a varied effect on PM_{10} for different AQM sites in different cities. In Durban, Gounden (2010) observed strong correlations for RH at three Durban AQM station and for only one site a strong correlation between rainfall and PM_{10}. Hence meteorology has a substantial effect on PM_{10} concentrations at the Malmesbury and George AQM stations, however the meteorological effects vary between the two AQM stations.

The range of correlations of temperature and PM_{10} concentrations at the Malmsesbury AQM station were lower (0.33 - 0.60) to the correlation of temperature and PM_{10} concentrations (0.60) observed in Spain (Galindo *et al.* 2011). Galindo *et al.* (2011) determined higher correlations between solar radiation and PM_{10} concentrations than the correlations between solar radiation and PM_{10} concentrations determined in this study. The correlations between relative humidity and PM_{10} concentration were higher in this study. Wind speed correlations with PM_{10} concentrations in Galindo *et al.* (2011) were both negative and positive, while the correlations in this study between wind speed and PM_{10} concentration were negative.

In Turkey, Şahin *et al.* (2011) determined weak correlations between PM_{10} concentrations at AQM stations and meteorological parameters. The highest correlations mentioned in Şahin *et al.* (2011) are for wind speed (0.3 - 0.4) and for rainfall (0.10 - 0.2). The correlations in this study are somewhat higher than these. Vardoulakis and Kassomenos (2008) determined correlations between PM_{10} concentrations and meteorological parameters for England and Greece AQM stations for the long term 2001 - 2003. In this study, weak correlations were determined between wind speed and PM_{10} concentrations in the warmer seasons (summer and spring) at the Malmesbury AQM and this is also observed at the Greece AQM stations. The higher correlations between wind speed and PM_{10} concentrations were for the England AQM stations in the cold season and this is similar to this study where the higher correlations at the George AQM station (higher correlations than Malmesbury) are in the cold season (autumn and winter). While positive high correlations between temperature and PM_{10} concentrations were observed for most of the year at the Malmesbury AQM station the correlations between temperature and PM_{10} concentrations at the Greece AQM stations were weakly positive for most of the year and even weaker at the England AQM stations. Also of interest are the negative weak correlations between temperature and PM_{10} concentrations at the England AQM stations for the cold season which was not similar to this study. The findings in this study determined higher correlations between temperature and PM_{10} concentrations at the Malmesbury AQM station (mediterranean type) and lower correlations between temperature and PM_{10} concentrations at the George AQM station (oceanic station). Similarly Vardoulakis and Kassomenos (2008) determined higher correlations between temperature and PM_{10} concentration at the Greece AQM stations (mediterranean) than at the England AQM stations (oceanic climate) between temperature and PM_{10} concentrations. In our study weak correlations were determined between RH and PM_{10}

concentrations at both George and Malmesbury AQM stations. Similarly Vardoulakis and Kassomenos (2008) determined weak correlations between RH and PM_{10} concentrations at the Greece and England AQM stations. In Vardoulakis and Kassomenos (2008) although weak, the correlations between rainfall and PM_{10} concentrations at the England AQM stations were higher than those at the Greece AQM stations. This is also similar to our findings where the correlations between rainfall and PM_{10} concentrations although weak were somewhat higher at the George AQM station than at the Malmesbury AQM station. Positive correlations between solar radiation and PM_{10} concentration were determined at the Malmesbury AQM station in contrast to the negative and positive correlations between solar radiation and PM_{10} concentrations observed at some Greece AQM stations.

The meteorological correlations with PM_{10} concentrations at the George and Malmesbury AQM stations differ to those observed for AQM stations in cities with different climates. For example Elminir (2008) observed a weakly positive correlation between PM_{10} and RH in Egypt and moderately negative correlations between PM_{10} and temperature. Ningwei *et al.* (2012) also observed a weak positive correlation between RH and PM_{10} but in China. Rajsic *et al.* (2004) observed a weak positive correlation between PM_{10} and RH in Belgrade, Serbia and weakly negative correlations between PM_{10} and temperature. Rajsic *et al.* (2004) also observed a negatively weak relationship between wind speed and PM_{10} which is similar to what was observed at AQM stations in Malmesbury and George and for AQM stations in Greece and England (Vardoulakis and Kassomenos (2008). This would suggest that wind speed typically has a generally weakly negative correlation with PM_{10}.

Table 5: Correlations of daily mean PM_{10} concentration with daily means of meteorological parameters measured at Malmesbury AQM station in 2011.

Months	Meteorological variable	Mean	N	Spearman correlation meteorological variable and daily PM_{10}
January, February, December	Wind speed (m.s^{-1})	3.09±0.91	87	Rho = -0.402; p<0.0005
	Temperature (°C)	23.26±4.33	87	Rho = 0.601; p<0.0005
	Relative humidity (%)	63.66±11.48	87	Rho = -0.389; p<0.0005
	Solar radiation (W.m^{-2})	209.21±139.22	87	Rho = 0.608;p<0.0005
	Rainfall (mm)	0.101±0.674	88	Rho = -0.32;p=0.002
March, April, May	Wind speed (m.s-^{1})	1.85±0.71	70	Rho = -0.045; p=0.713
	Temperature (°C)	18.23±6.19	70	Rho = 0.516; p<0.0005
	Relative humidity (%)	69.34±16.6	70	Rho = -0.478; p<0.0005
	Solar radiation (W.m^{-2})	82.83±104.06	70	Rho = 0.576;p<0.0005
	Rainfall (mm)	0.027±0.09	83	Rho = -0.426;p<0.0005

Table 5: continued

Months	Meteorological variable	Mean	N	Spearman correlation meteorological variable and daily PM_{10}
June, July, August	Wind speed (m.s^{-1})	2.63±1.04	77	Rho = -0.007; p=0.951
	Temperature (°C)	10.83±2.49	81	Rho = 0.591; p<0.0005
	Relative humidity (%)	81.48±12.2	81	Rho = -0.277; p=0.012
	Solar radiation (W.m^{-2})	12.66±4.11	81	Rho = 0.193, p=0.085
	Rainfall (mm)	0.072±0.2	82	Rho = -0.238;p=0.031
September, October, November	Wind speed (m.s^{-1})	3.44±0.69	91	Rho = -0.224; p=0.033
	Temperature (°C)	14.85±3.47	91	Rho = 0.33; p=0.001
	Relative humidity (%)	75.62±11.64	91	Rho = -0.213; p=0.043
	Solar radiation (W.m^{-2})	23.53±7.19	91	Rho = 0.255;p=0.015
	Rainfall (mm)	0.022±0.077	90	Rho = -0.533;p<0.0005

Table 6: Correlations of daily mean PM_{10} concentration with daily means of meteorological parameters measured at George AQM station in 2011.

Months	Meteorological variable	Mean	N	Spearman correlation meteorological variable and daily PM_{10}
January, February, December	Wind speed (m.s^{-1})	2.9±1.19	66	Rho = 0.133; p=0.288
	Temperature (°C)	18.18±2.03	66	Rho = 0.334; p=0.006
	Relative humidity (%)	79.89±8.13	66	Rho = -0.228; p=0.065
	Solar radiation (W.m^{-2})	209.55±102.55	66	Rho = 0.440;p<0.0005
	Rainfall (mm)	0.059±0.125	66	Rho = -0.5;p<0.0005
March, April, May	Wind speed (m.s-^{1})	2.2±1.2	63	Rho = -0.317; p=0.011
	Temperature (°C)	15.63±3.11	62	Rho = 0.304; p=0.016
	Relative humidity (%)	74.53±13.17	62	Rho = -0.14; p=0.276
	Solar radiation (W.m^{-2})	131.12±59.96	65	Rho = 0.298; p=0.016
	Rainfall (mm)	0.067±0.183	66	Rho=-0.42;p<0.0005
June, July, August	Wind speed (m.s^{-1})	2.13±1.49	52	Rho = -0.536; p<0.0005
	Temperature (°C)	12.77±2.67	53	Rho = 0.446; p=0.001
	Relative humidity (%)	70.25±16.18	53	Rho = -0.413; p=0.002
	Solar radiation (W.m^{-2})	100.04±29.17	53	Rho = 0.634, p<0.0005
	Rainfall (mm)	0.148±0.535	91	Rho = -0.564;p<0.0005
September, October, November	Wind speed (m.s^{-1})	3.57±1.33	81	Rho = -0.109; p=0.333
	Temperature (°C)	15.63±2.15	81	Rho=0.106; p=0.348
	Relative humidity (%)	72.7±8.79	81	Rho = -0.098; p=0.384
	Solar radiation (W.m^{-2})	235.52±77.78	50	Rho = -0.062;p=0.668
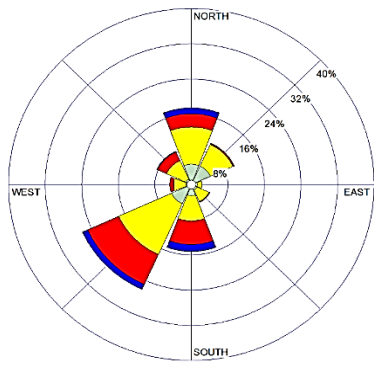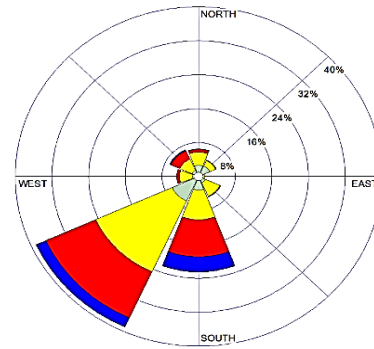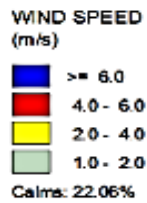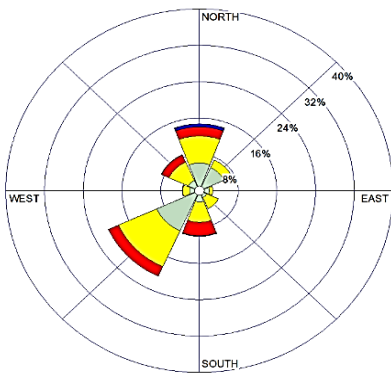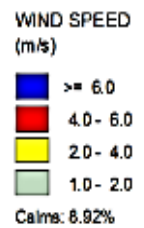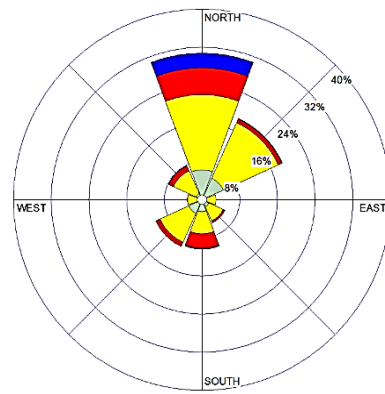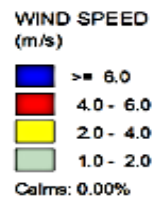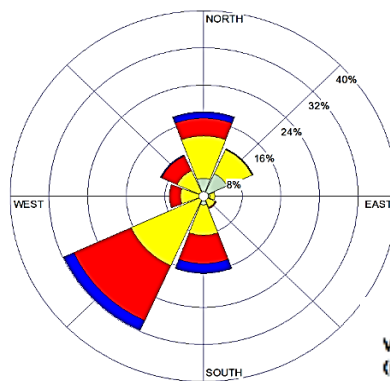
Figure 21: Wind rose plots for winds at Malmesbury AQM station in 2011 for a) the whole year b) summer c) autumn d) winter and e) spring.
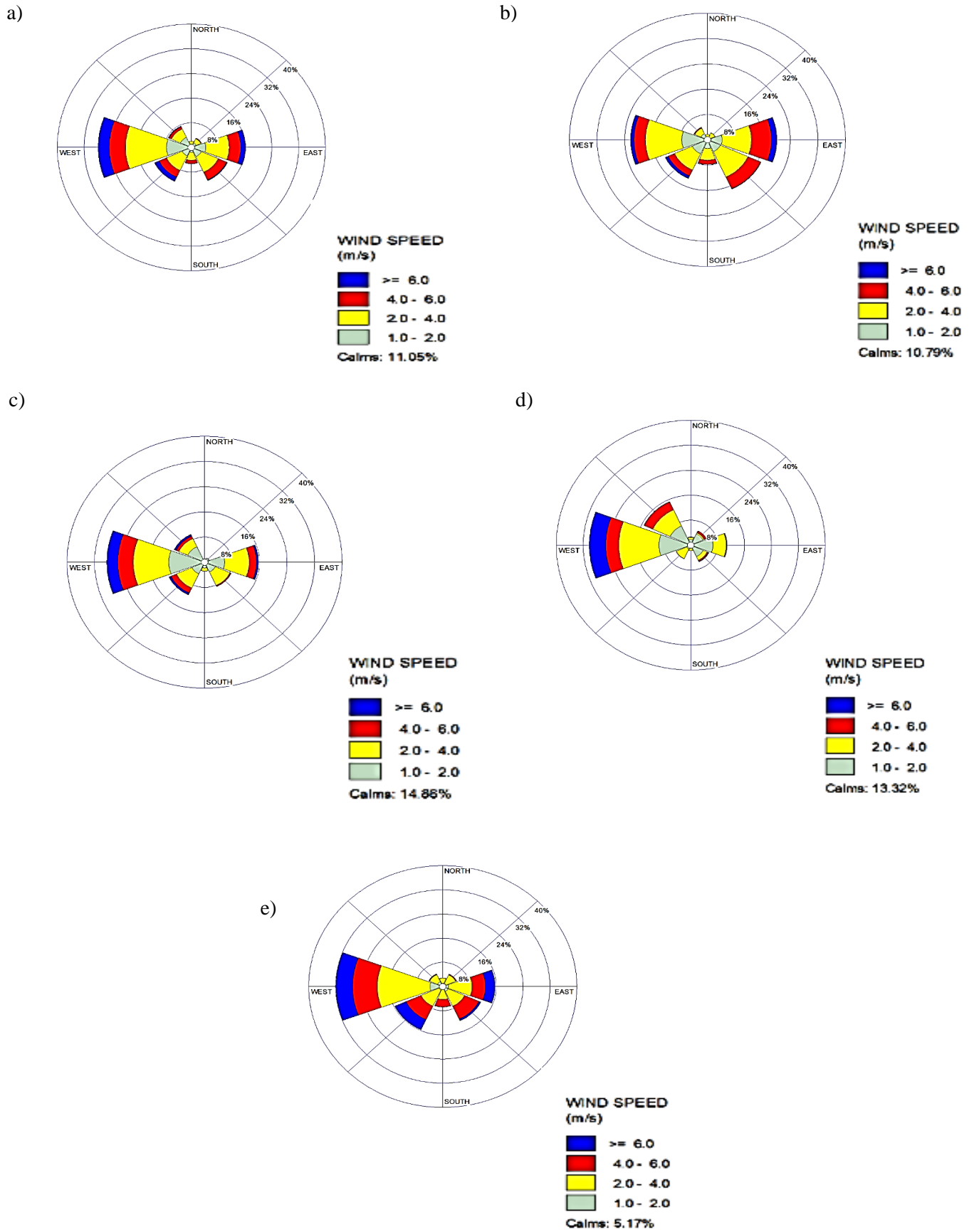
Figure 22: Wind rose plots for winds at George AQM station in 2011 for a) the whole year b) summer c) autumn d) winter and e) spring.

4.5. AOD characteristics

The trends of the AOD over the Malmesbury and George AQM stations was an indicator of the total aerosol loading in the atmosphere over the AQM stations. Two AOD datasets were used in the analysis; from MODIS retrievals on board the TERRA satellite using the dark target algorithm ($AOD_{terra.dt}$) and from MODIS retrievals on board the AQUA satellite using the dark target algorithm ($AOD_{aqua.dt}$). AOD using the deep blue algorithm ($AOD_{aqua.db}$) was excluded due to poor data completeness for many months during the year in 2011. The time range of satellite overpass for the TERRA satellite over the Malmesbury AQM station occurred between 8:00 am and 9:40 am and between 7:50am and 9:35 am over the George AQM station. The time range of satellite overpass for the AQUA satellite over the Malmesbury AQM station occurred between 11:55 am and 13:25 pm and between 11:40 am to 13:15 pm over the George AQM station.

It was possible to test the AOD data over Malmesbury and George AQM stations for seasonal differences using the Tukey's HSD post hoc test. Although the $AOD_{terra.dt}$ over Malmesbury AQM station showed a declining trend in the AOD for the duration of the year (Figure 23), there were no seasonal differences (Table 7). A declining trend was also observed for $AOD_{aqua.dt}$ over Malmesbury however the trend ends in August with declining trends in the AOD observed in each season with increasing AOD towards the end of each season. No seasonal trends were apparent for $AOD_{aqua.dt}$ with $AOD_{aqua.dt}$ in most seasons similar. Both the $AOD_{aqua.dt}$ and $AOD_{terra.dt}$ trends over Malmesbury AQM station were characterised by relatively higher AODs in summer and autumn months similar to what was observed for PM_{10} concentrations measured at the AQM station. Over the George AQM station, no seasonal trends were apparent for either $AOD_{aqua.dt}$ or $AOD_{terra.dt}$ (Figure 24), with AOD mostly similar between seasons (Table 8). A spike in the AOD was observed in summer when PM_{10} concentrations were low. The spike in the AOD in summer may be due to the transport of PM over the George AQM from distant sources. Another spike in the AOD was observed during the winter and spring months when PM_{10} concentrations were high.

Using a long term $AOD_{terra.dt}$ data from 2000 - 2005, the AOD trends over Greece were determined in Kaskaoutis *et al.* 2007. It was observed that the highest AOD occurred in summer and the lowest AOD occurred in winter (Kaskaoutis *et al.* 2007). This was different to what was observed in this study over the Malmesbury AQM station for which

the AOD$_{terra.dt}$ were highest in summer and autumn and lowest in spring. The AOD referred to in Kaskaoutis *et al.* 2007 was retrieved from satellite imagery over the City of Athens, which show a different seasonal AOD trend relative to Malmesbury due to the greater contribution of anthropogenic aerosol sources to PM pollution in the city of Athens. The high AOD in summer and autumn over Malmesbury is likely to be enhanced by the veld fires that occur during the summer and autumn months (van Wilgen *et al.* 2012).

The AOD seasonal trends over the George AQM station were similar to the typical seasonal trends observed over the Czech Republic/Poland for which a peak was observed in winter (Koelemeijer *et al.* 2006). However the seasonal trends over the George AQM station were different to those over Netherlands/Belgium which peaked in the spring and summer months (Koelemeijer *et al.* 2006). The AOD over Spain/Portugal peaked in the summer months which were similar to the AOD$_{aqua.dt}$ trend over the Malmesbury AQM station but different to the AOD$_{terra.dt}$ trend over the Malmesbury AQM station for which the AOD peaked in autumn (Koelemeijer *et al.* 2006).

The analysis of the AOD trends over the Malmesbury and George AQM stations was limited by the low temporal frequency of AOD data. The AOD trends could not be characterised at the same temporal scales that the PM$_{10}$ concentrations were characterised at, which included diurnal and daily temporal variations. Additionally, comparisons of the AOD trends were limited due to the use of different satellite products. The observations of the monthly AOD trends at the 10 km by 10 km resolution and wind speeds measured at the station were not similar, which suggested that wind speeds may affect AOD at a regional rather than local scale similar to the findings of Tesfaye *et al.* (2011).
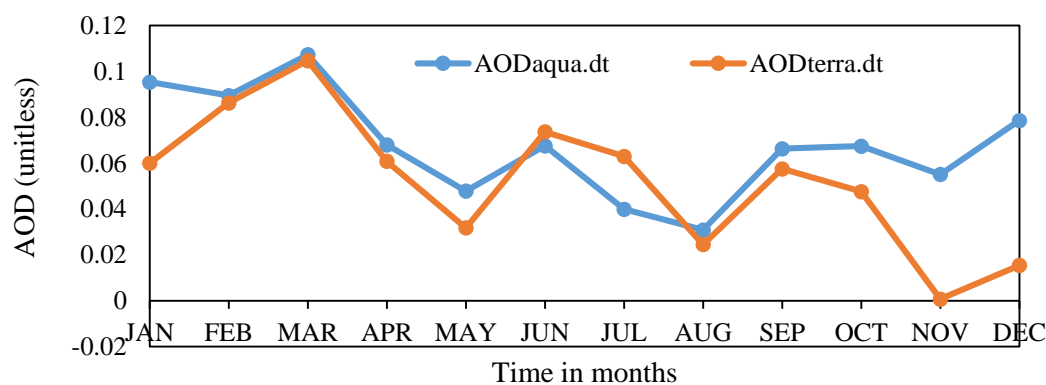
Figure 23: Monthly mean AOD over the Malmesbury AQM station for 2011.

86
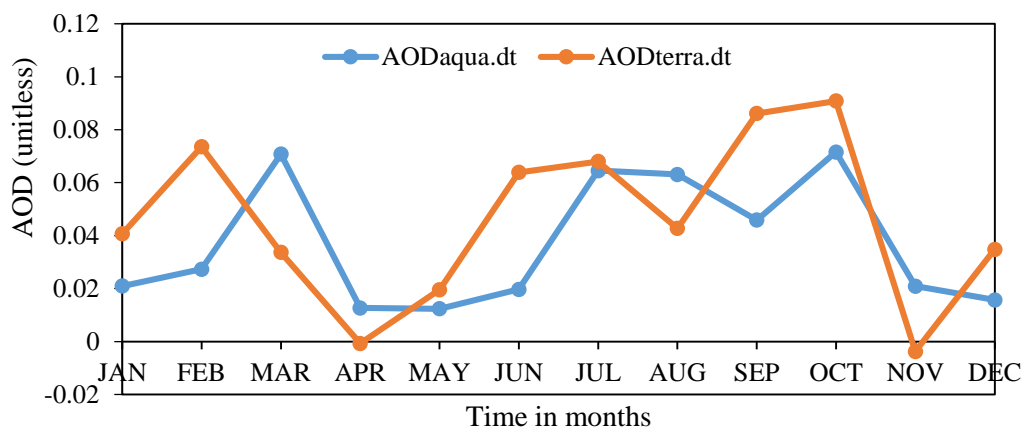
Figure 24: Monthly mean AOD over the George AQM station for 2011.

Table 7: Intra-annual comparison of AOD over Malmesbury AQM station between seasons in 2011 using the Tukey's HSD post hoc test.

Seasonal comparison	$AOD_{aqua.dt}$		$AOD_{terra.dt}$		$log_{10}AOD_{aqua.db}$	
	Tukey Q score	p	Tukey Q score	p	Tukey Q score	p
summer and autumn	0.732	0.884	1.194	0.632	1.782	0.287
summer and winter	3.321	0.006	0.010	1.000	9.512	0.000
summer and spring	1.837	0.260	1.051	0.720	1.052	0.719
autumn and winter	1.973	0.203	0.203	0.630	7.382	0.000
autumn and spring	0.776	0.865	2.104	0.157	0.172	0.998
winter and spring	1.487	0.448	1.071	0.708	4.330	0.000

Table 8: Intra-annual comparison of AOD over George between seasons in 2011 using the Tukey's HSD post hoc test.

Seasonal comparison	$AOD_{aqua.dt}$		$AOD_{terra.dt}$	
	Tukey Q score	p	Tukey Q score	p
summer and autumn	2.183	0.132	1.194	0.632
summer and winter	2.323	0.098	0.952	0.777
summer and spring	2.325	0.097	0.785	0.861
autumn and winter	1.52	0.428	2.796	0.029
autumn and spring	1.598	0.383	2.610	0.048
winter and spring	0.224	0.996	0.112	0.999.

4.6. Correlations between AOD and PM$_{10}$ Concentrations

4.6.1. Correlations between AOD and Hourly Averaged PM$_{10}$ Concentrations

The differences observed in terms of $AOD_{aqua.dt}$-PM$_{10}$ correlations and $AOD_{terra.dt}$-PM$_{10}$ correlations were attributed to the differences between the AOD retrieved from sensors

onboard different satellites and the PM_{10} measured at different sites. $AOD_{aqua.dt}$ observed in this study over the Malmesbury AQM station were higher than $AOD_{terra.dt}$ over the Malmesbury AQM station. Similarly other locations have observed the same difference between $AOD_{aqua.dt}$ and $AOD_{terra.dt}$ (Koejoelmiere *et al.* 2006 and Ichoku *et al.* 2005). The causes of the differences between AOD observations are varied but mainly attributed to differences due to the MODIS sensors being mounted on different satellites (Yoon *et al.* 2012). One such example of differences between satellites are the different times at which AOD is remotely sensed.

The hourly PM_{10} concentrations at Malmesbury and George stations for the period of AQUA satellite overpass were generally lower than the PM_{10} concentrations during the period of TERRA satellite overpass. The time of TERRA satellite overpass was generally coincident just after the morning diurnal peak in PM_{10} concentration, while the time of AQUA satellite overpass was coincident to the period of lowest diurnal PM_{10} concentrations. This was contrasting to AOD comparisons with AOD from the AQUA satellite higher than the AOD from the TERRA satellite. This suggests that the AOD was not a good indicator of hourly PM_{10} concentration as it was not sensitive to the diurnal differences of the PM_{10} concentrations. Ichoku *et al.* (2005) highlighted that AOD from the AQUA satellite were higher than the AOD from the TERRA satellite. This is further supported by a finding in Ma *et al.* (2013). This is likely due to the aerosols in the afternoon experiencing greater dispersal to the upper atmosphere enhanced by convective mixing which would indicate a higher AOD relative to aerosols being trapped nearer the surface in the morning.

The observed correlations (R) over the Malmesbury AQM station for hourly PM_{10} was 0.35 (p < 0.0005) for $AOD_{aqua.dt}$ (Figure 25) and 0.33 (p < 0.0005) for $AOD_{aqua}.db$ (Figure 26), indicating weak but significant correlations. There was no significant linear correlation between $AOD_{terra.dt}$ and hourly $\log_{10}PM_{10}$ (p = 0.315) (Figure 27). The findings indicated that the AOD which used the dark target algorithm were slightly better correlated to hourly PM_{10} concentrations than the AOD retrieved using the deep blue algorithm over the Malmesbury AQM station.

Figure 25: Linear correlation between one hourly PM$_{10}$ and AOD$_{aqua.dt}$ for the Malmesbury AQM station.
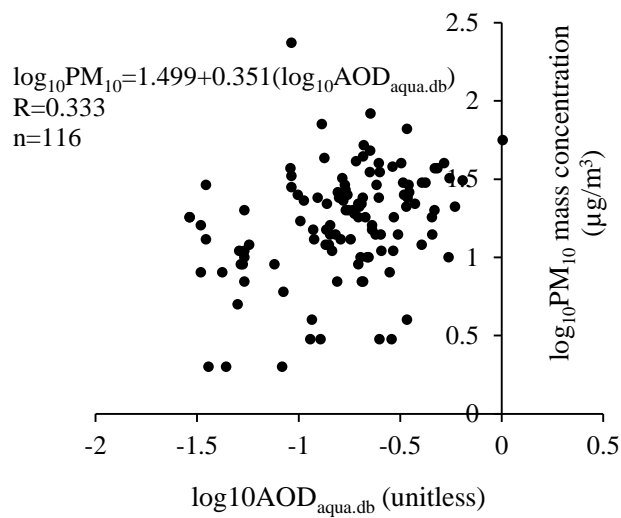
Figure 26: Linear correlation between one hourly log$_{10}$ transformed PM$_{10}$ and log$_{10}$ transformed AOD$_{aqua.db}$ for the Malmesbury AQM station.
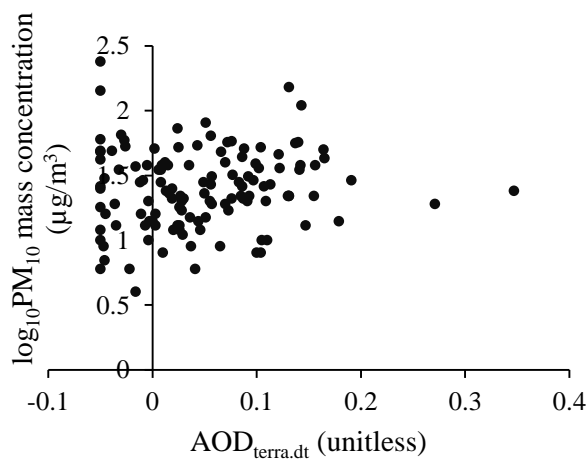
Figure 27: Linear correlation between one hourly log$_{10}$ transformed PM$_{10}$ and AOD$_{terra.dt}$ for the Malmesbury AQM station.

The observed correlations for hourly PM_{10} over the George AQM station, was 0.32 (p = 0.001) for $AOD_{aqua.dt}$ (Figure 28) which was lower than the correlation over the Malmesbury AQM station. There was no significant linear correlation between $AOD_{terra.dt}$ and hourly $log_{10}PM_{10}$ (p = 0.653) (Figure 29) over the George AQM station. The AOD-PM_{10} correlation over the George and Malmesbury stations were lower to those observed over Switzerland in 2008 by Emili *et al.* (2010). Over Switzerland, greater correlations were observed for hourly PM_{10} which were 0.34 - 0.52 for AOD_{SEVIRI} and 0.42- 0.46 for AOD_{MODIS} which varied due to differences in topography (Emili *et al.* 2010). In the case of Emili *et al.* (2010), the AOD–PM_{10} correlation benefited from the inclusion of the MLH into the linear PM_{10} model. The AOD-PM_{10} correlations determined in Emili *et al.* (2010) included the measurements from a number of AQM stations and thus comparatively differ to the correlations determined in this study over individual AQM stations.
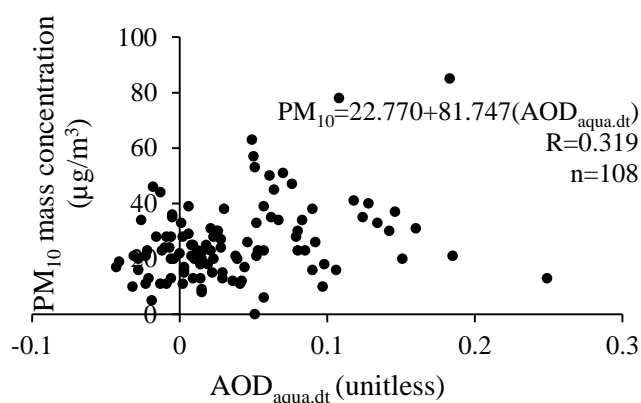
Figure 28: Linear correlation between one hourly PM_{10} and $AOD_{aqua.dt}$ for George AQM station.
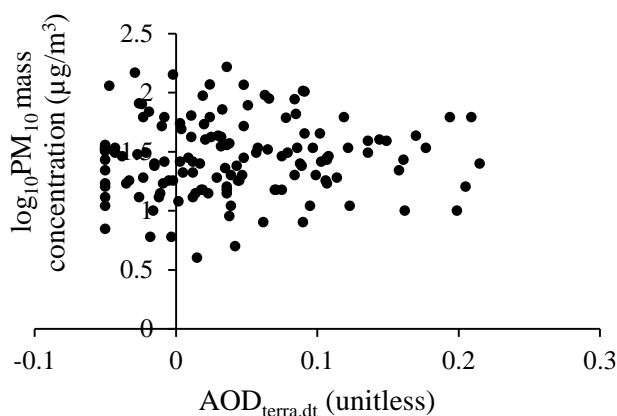
Figure 29: Linear correlation between one hourly log transformed PM_{10} and $AOD_{terra.dt}$ for George AQM station.

In this study the use of the cloud mask did not substantially change the correlation, for example over the Malmesbury AQM station the use of cloud screening slightly decreased the correlation from 0.37 (Table 9) to 0.35 when cloud free AOD data were used. This suggests that the level of cloudiness within AOD pixels are not adequately determined by the MODIS algorithm. Similarly a previous study found that the use of cloud screening did not improve the AOD-PM_{10} correlation over Thailand (Sukitpaneenit and Oanh, 2013).

Table 9: Correlation between AOD and one hourly PM_{10} over Malmesbury and George before cloud screening.

Satellite AOD	Correlation over Malmesbury			Correlation over George		
	Correlation before cloud screening	n	p value	Correlation before cloud screening, (significance)	n	P value
AODaqua.dt	0.371	137	p < 0.0005	0.362	86[c]	0.001
AODaqua.db	0.344[a]	118	p < 0.0005	Not applicable	Not applicable	Not applicable
AODterra.dt	0.081[b]	132	P = 0.353	0.083	148[d]	0.313

a: $\log_{10}PM_{10}$, $\log_{10}AOD$;
b: $\log_{10}PM_{10}$
c: $\log_{10}PM_{10}$, $\log_{10}AOD$
d: $\log_{10}PM_{10}$

Over Thailand, for all the AQM stations used in the study the correlations for AOD_{terra} − PM_{10} (0.34) and AOD_{aqua}-PM_{10} (0.34) were similar (Zeeshan and Oanh, 2014) to the correlations observed over the Malmesbury and George AQM stations for $AOD_{aqua.dt}$. However when the $AOD_{aqua.dt}$-PM_{10} correlation was up scaled by obtaining mean AOD and PM_{10} from Malmesbury and George data on the same days, the correlation for $AOD_{aqua.dt}$-PM_{10} was greater (0.48) and was similar to those determined by Emili *et al.* (2010). Zeeshan and Oanh, 2014 apportioned the AOD-PM_{10} correlations at different sites using meteorological effects by cluster analysis. The clustering approach used was not intended to improve the AOD-PM_{10} correlation but rather to improve its use for air quality analysis.

In this study, it was found that that the daily mean PM_{10} concentrations at the George and Malmesbury AQM stations were weakly correlated. In the up scaled analysis it was determined that a better $AOD_{aqua.dt}$-PM_{10} correlation was determined than what was determined individually over the Malmesbury and George AQM stations. However it was also determined that the $AOD_{aqua.dt}$ over the stations and the PM_{10} measured at the stations

were different. Thus the upscaled AOD-PM$_{10}$ correlation was not applicable for air quality studies in this case.

A filtering procedure was applied to determine the AOD-PM$_{10}$ correlations for high and low AODs and for high and low PM$_{10}$ concentrations over Malmesbury and George. An interesting finding from this analysis using hourly averaged PM$_{10}$ data was the determination of a significant AOD$_{aqua.dt}$-PM$_{10}$ correlation with low PM$_{10}$ concentrations over the Malmesbury AQM station while a significant correlation was determined for AOD$_{aqua.dt}$-PM$_{10}$ at high PM$_{10}$ concentrations over the George AQM station.

For the previous case studies in Europe and in Asia, it was observed that the correlations between 0.4 and 0.5 were more abundant than correlations between 0.7 and 0.9 (Koelemeijer *et al.* 2006; Emili *et al.* 2010; Sukitpaneenit and Oanh, 2013; Wu *et al.* 2012). This suggests that the AOD-PM$_{10}$ relationship itself can be used as an indicator of PM$_{10}$ pollution distribution within a region which may not require very strong AOD-PM$_{10}$ correlations such as the case of Mahmud (2013) rather than as predictive proxy indicator for PM$_{10}$ as an air quality pollutant over region such as the case of Emili *et al.* (2010). The correlations determined over the Malmesbury and George AQM stations were weak. Thus it is suggested that further work is required to further explore methods to optimise the hourly AOD-PM$_{10}$.

4.6.2. Correlations between AOD and Daily Averaged PM$_{10}$ Concentrations

This study observed significant daily correlations over the Malmesbury AQM station for AOD$_{aqua.dt}$-PM$_{10}$, AOD$_{terra.dt}$-PM$_{10}$ and AOD$_{aqua}$.db-PM$_{10}$. The correlations were the highest for AOD$_{aqua.dt}$-PM$_{10}$ (R = 0.36 and p < 0.0005) (Figure 30) and for AOD$_{aqua.db}$-PM$_{10}$ (R = 0.33 and p < 0.0005) (Figure 31) which were similar to hourly AOD-PM$_{10}$ correlations. The correlation was lowest for AOD$_{terra.dt}$-PM$_{10}$ (R = 0.24 and p = 0.006) (Figure 32) but still significant as no significant correlation was observed for hourly correlations. The findings of the study indicated that the AOD which used the dark target algorithm was slightly better correlated to hourly PM$_{10}$ concentrations than the AOD retrieved using the deep blue algorithm over the Malmesbury AQM station.
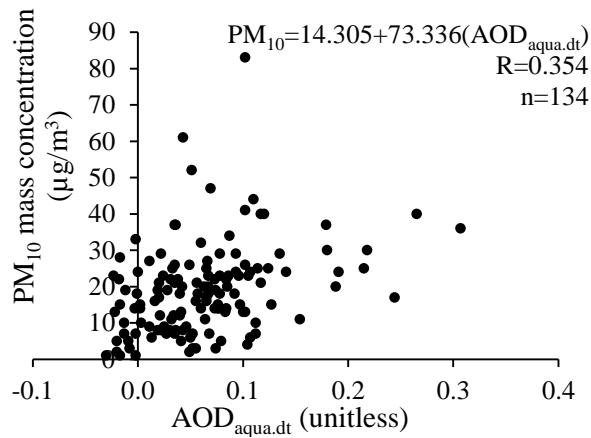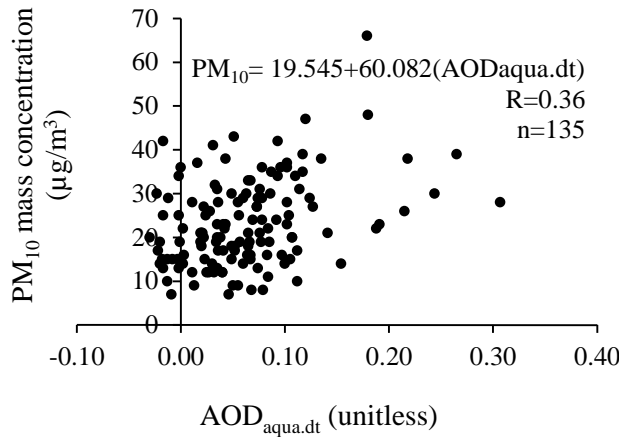
**Figure 30: Linear correlation for 24 hour averaged PM$_{10}$ and AOD$_{aqua.dt}$ for the Malmesbury AQM station.**
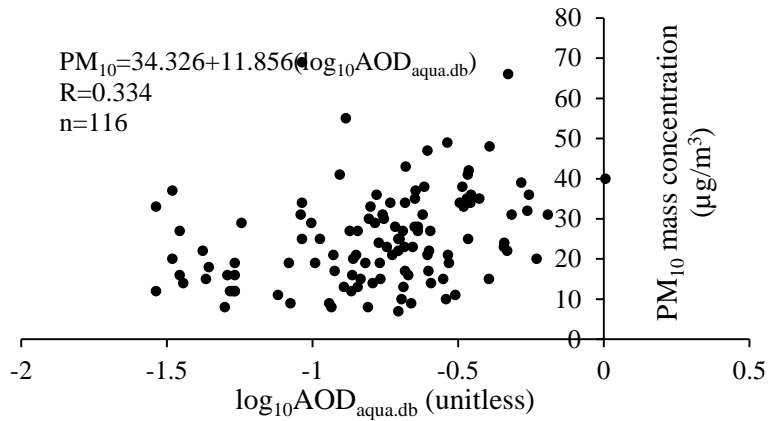
Figure 31: Linear correlation for 24 hour averaged PM$_{10}$ and AOD$_{aqua.db}$ for the Malmesbury AQM station.
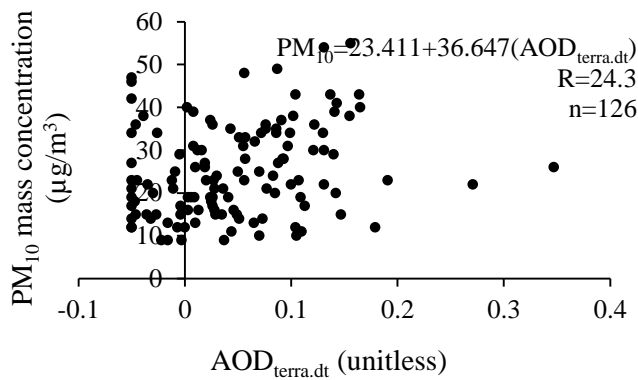
Figure 32: Linear correlation for 24 hour averaged PM$_{10}$ and AOD$_{terra.dt}$ for the Malmesbury AQM station.

This study observed a correlation over the George AQM station for AOD$_{aqua.dt}$-PM$_{10}$ which was 0.24 (Figure 33) and this was lower than the observed hourly AOD-PM$_{10}$ correlation.

This suggests the $AOD_{aqua.dt}$ –daily averaged PM_{10} relationship to be weaker over the George AQM station. There was no significant correlation determined between $AOD_{terra.dt}$ and the daily mean PM_{10} concentrations over the George AQM station (Figure 34).

$PM_{10}=34.328+4.619(\log_{10}AOD_{aqua.dt})$
R=0.236
n=80
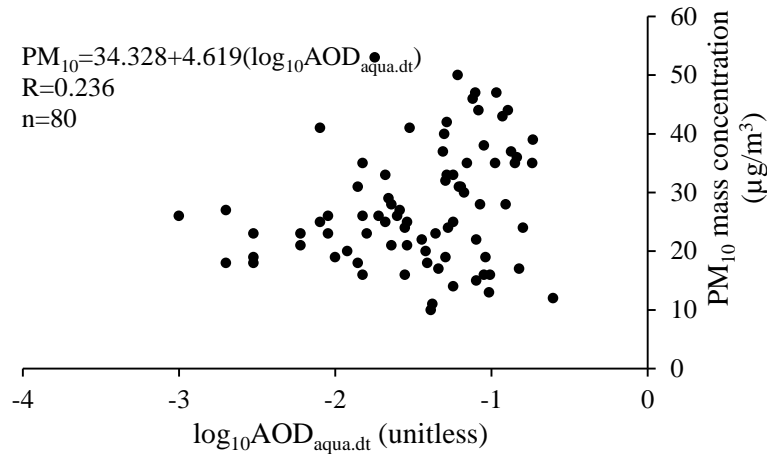
Figure 33: Linear model between $AOD_{aqua.dt}$ and 24 hourly averaged PM_{10} for the George AQM station.
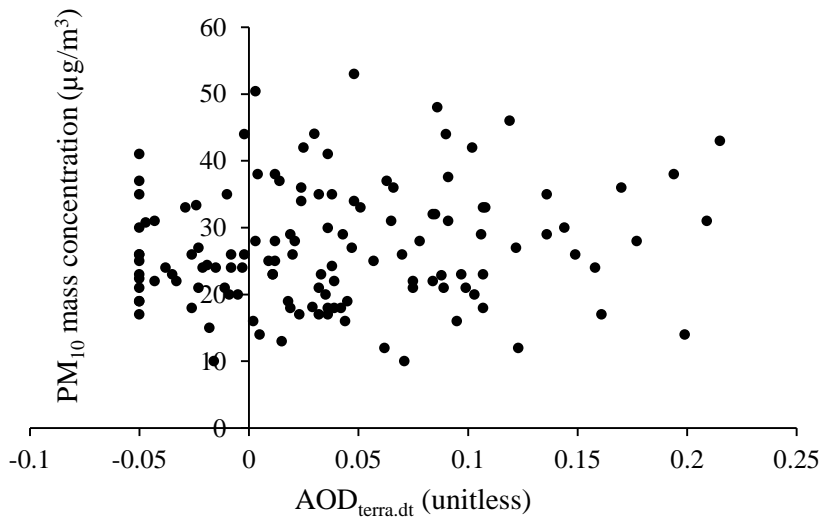
Figure 34: Linear model between $AOD_{terra.dt}$ and 24 hourly averaged PM_{10} for the George AQM station.

Similar to what was observed between the correlation of AOD and hourly PM_{10} concentration, introducing a cloud mask cloud screening procedure decreased the correlation for $AOD_{aqua.dt}$-PM_{10} slightly from 0.39 (Table 10) to 0.36 over Malmesbury. Similarly for George the use of cloud screening decreased the correlation slightly from 0.28 before cloud screening to 0.24 after cloud screening. Gupta and Christopher (2008) suggested that the use of the MODIS quality flags did not affect the AOD-$PM_{2.5}$

relationship significantly. Dinoi *et al.* (2010) used a different cloud cover dataset, and found that the AOD-PM$_{10}$ correlation over Italy improved with the use of cloud screening. This suggests that the issue of cloud contamination is not entirely resolved by the use of the MODIS sub datasets to assess cloud contamination (Dinoi *et al.* (2010). Similar to Gupta and Christopher (2008) the results in this study also indicated that the use of quality flags did not substantially improve the relationship. Hence the AOD retrieved in this study could benefit from an alternative cloud screening procedure based upon *in situ* measurements of cloudiness.

Table 10: Correlation between AOD and 24 hourly PM$_{10}$ over Malmesbury and George before cloud screening.

| Satellite AOD | Correlation over Malmesbury | | | Correlation over George | | |
	Correlation before cloud screening	n	P value	Correlation before cloud screening, (significance)	n	P value
AODaqua.dt	0.387	138	P < 0.0005	0.279[b]	87	0.009
AODaqua.db	0.301[a]	120	0.001	Not applicable	Not applicable	Not applicable
AODterra.dt	0.270	131	0.002	0.168	136	0.05

a: log$_{10}$AOD
b: log$_{10}$AOD

Greater correlations were determined in this study between AOD from the AQUA satellite using the dark target retrieval algorithm and the daily PM$_{10}$ concentrations. The AOD-PM$_{10}$ correlations over the Malmesbury AQM station were greater than the AOD-PM$_{10}$ correlations over the George AQM station. The differences are likely to be directly attributable to differences in AOD and daily PM$_{10}$ concentrations between George and Malmesbury AQM stations. Emili *et al.* (2010; 2011) were examples of studies which determined strong AOD-PM$_{10}$ correlations by adjusting the AOD using the MLH.

4.6.3. Correlations between Weekly Averaged AOD and PM$_{10}$ Concentrations

The weekly AOD-PM$_{10}$ correlation was included in this study as the PM$_{10}$ and the AOD have observable weekly trends as was observed for example by Qin *et al.* 2004 for PM$_{10}$ concentrations and by Xia *et al.* (2008) for the AOD. Over the Malmesbury AQM station, varied correlations were determined for weekly averaged AOD and weekly averaged hourly PM$_{10}$ concentrations. The AOD$_{aqua.dt}$-PM$_{10}$ correlation was moderate at 0.49 (Table

11), while the correlation for $AOD_{terra.dt}$ was 0.36 and a strong correlation was observed for AOD_{aqua}.db (0.61).

Over the George AQM station, a significant correlation between the weekly averaged $AOD_{aqua.dt}$ and the weekly averaged hourly PM_{10} was not determined. However a significant but weak correlation for weekly averaged $AOD_{terra.dt}$ and weekly averaged daily PM_{10} (0.35) was determined which was similar to what was determined over the Malmesbury AQM station. The $AOD_{terra.dt}$ result was similar to what was observed at a monthly temporal scale over George.

The results in this study suggest that the weekly AOD observed by the AQUA satellite using the dark target algorithm, is well correlated with weekly PM_{10} concentration trends over the Malmesbury AQM station but not over the George AQM station. The results also suggest that the weekly averaged AOD observed by the TERRA satellite using the dark target algorithm was similarly correlated with weekly averaged PM_{10} over the Malmesbury and George AQM stations.

Table 11: Correlations between weekly averaged AOD and PM_{10} over the Malmesbury and George AQM stations.

AOD-PM_{10} relationship	Over the Malmesbury AQM station.		Over the George AQM station.	
	Pearson correlation	n	Pearson correlation	n
$AOD_{aqua.dt}$	R= 0.481; p < 0.0005	49	R = 0.290; p = 0.069	40
$AOD_{terra.dt}$	R=0.363; p = 0.012	47	R = 0.354; p = 0.021	42
$AOD_{aqua.db}$	R=0.611; p < 0.0005	31	*	*

*Insufficient data available over George for $AOD_{aqua.db}$

4.6.4. Correlations between Monthly Averaged AOD and PM_{10} Concentrations

The previous studies which have determined the monthly AOD-PM_{10} have indicated a range of correlations varying from weak to strong relationships with the most substantial correlations a result of large multiyear datasets from observations from multiple AQM sites. In this study AOD-PM_{10} correlations were determined from a dataset of AOD and PM_{10} observations for 1 year. Over the Malmesbury AQM station, strong monthly mean correlations from daily averaged PM_{10} and monthly PM_{10} (Table 12) for $AOD_{aqua.dt}$ (0.67), for AOD_{aqua}.db (0.78) but not for $AOD_{terra.dt}$ (0.36) were observed. The presence of an AOD-PM_{10} relationship for AOD_{aqua} over the Malmesbury AQM station suggested the

potential for a stronger AOD-PM_{10} relationship being determined using AOD from the AQUA satellite. Over the George AQM station, no significant monthly AOD-PM_{10} relationship was observed with correlations determined with a low sampling number.

At a continental scale, the PM_{10}-AOD relationship determined by Koelemeijer *et al.* (2006) is moderately strong at 0.47 for Europe. At the regional scale the AOD-PM_{10} correlations varied, the lowest for the Netherlands and Belgium region (0.22) and the highest for the Spain and Portugal regions (0.88). Barnaba *et al.* (2010) determined R^2 coefficients for Ispra and Modena AQM stations in Italy for the AOD-PM_{10} relationship for 2006-2007. The coefficients were weak, 0.12 at Ispra and 0.3 for Modena. The satellite AOD was validated against the MODIS AOD in Barnaba *et al.* (2010). Over Delhi, Kumar *et al.* (2008) determined a strong coefficient for the monthly AOD-PM_{10} relationship of 0.53 for a longer period between 2000 and 2005.

Similar to Barnaba *et al.* (2010) the strength of the AOD –PM_{10} relationship varies for different sites (Malmesbury and George AQM stations). The results in this study suggest that the monthly AOD-PM_{10} relationship is weaker over George and stronger over Malmesbury. The monthly AOD-PM_{10} relationship is useful to determine the presence of AOD-PM_{10} relationship at less aggregated monthly temporal scales. However the monthly AOD-PM_{10} has limited usefulness for air quality management where the focus is upon 24 hour averaged and annual exceedances (WHO, 2006).

Table 12: Correlations between monthly averaged AOD and PM_{10} over the Malmesbury AQM station.

AOD-PM_{10} relationship	Over the Malmesbury AQM station. Pearson correlation	n	Over the George AQM station. Pearson correlation	n
$AOD_{aqua.dt}$	R = 0.672; p = 0.017	12	R = 0.679; p = 0.064	8
$AOD_{terra.dt}$	R = 0.556; p = 0.061	12	R = 0.398; p = 0.329	8
$AOD_{aqua.db}$	R = 0.776; p = 0.014	9	*	*

*Insufficient data available over George for $AOD_{aqua.db}$

4.6.5. Correlations of Seasonal AOD and PM_{10} Concentrations

The tracking of seasonal PM_{10} concentrations is useful for identifying the season with the highest PM_{10} concentration, associating trends with meteorological drives of PM_{10} over the region and for suggesting possible pollutant sources for seasons with high

concentrations (for example McKendry 2000, Juneng *et al.* 2011). Ideally it is advantageous to track seasons with high PM_{10} concentrations and to identify the possible pollutant sources so as to identify possible interventions to reduce the associated risks from poor air quality.

Over the Malmesbury AQM station significant correlations were determined in winter (0.64) and in autumn (0.43) for $AOD_{aqua.dt}$ and hourly PM_{10} concentrations (Table 13). For $AOD_{aqua.dt}$ and daily averaged PM_{10} (Table 14), a significant correlation was observed in summer (0.43) and also for $AOD_{aqua.db}$ and daily PM_{10} (0.34). The strongest correlation occurs in winter, for which the lowest PM_{10} concentrations were observed, which has limited usefulness for air quality monitoring. Correlations in summer and in autumn were observed and this suggests that $AOD_{aqua.dt}$ has the potential to monitor PM_{10} concentration in these months which have high PM_{10} concentrations.

Over the George AQM station, the seasons with the highest PM_{10} concentration were winter and spring. The AOD-PM_{10} correlation in spring for $AOD_{aqua.dt}$ and hourly PM_{10} (Table 15) was significant (0.43). The correlation in winter for $AOD_{aqua.dt}$ and daily PM_{10} (Table 16) was significant (0.41). A significant AOD-PM_{10} correlation for AOD_{terra} and daily PM_{10} (0.47) in spring was determined, however this has limited usefulness due to the weak correlations of AOD_{terra} with PM_{10} measurements over the George AQM station for other seasons.

For both towns, significant but weak AOD-PM_{10} correlations were determined for the seasons that have high PM_{10} concentrations. The highest AOD-PM_{10} correlation was determined over Malmesbury in winter, a season which is associated with low PM_{10} concentrations. However this does not have much significance for air quality analysis, and it is suggested that additional characterisation of the AOD-PM_{10} relationship is needed to limit the effect of confounders, for example the use of the MLH (Gupta and Christopher, 2009). Overall there is no consistency for the AOD-PM_{10} correlations which occurred in seasons of high PM_{10} concentrations. This inconsistency is particularly apparent for $AOD_{aqua.dt}$. Overall, this suggests that the seasonal AOD-PM_{10} relationship is weak.

Table 13: Correlations between seasonal AOD and one hourly PM_{10} over the Malmesbury AQM station.

Seasonal period	$AOD_{aqua.dt}$-1 hour PM_{10} seasonal relationship		$AOD_{terra.dt}$-1 hour PM_{10} seasonal relationship		$AOD_{aqua.db}$-1 hour PM_{10} seasonal relationship	
	Pearson correlation	n	Pearson correlation	n	Pearson correlation	n
January, February, December	R = 0.148; p = 0.398	35	R = -0.028; p = 0.874	35	R = 0.199; p = 0.112	65
March, April, May	R = 0.433; p = 0.093	16	R = -0.172; p = 0.382	28	R = 0.040; p = 0.838[b]	28
June, July, August	R = 0.635; p < 0.0005	41	R = 0.096; p = 0.576	36	R = 0.422; p = 0.092[b]	17
September, October, November	R = 0.148; p = 0.357	41	R = 0.155; p = 0.431[a]	28	N/A[c]	0

a. log_{10} transformation used on PM_{10} subset

b. log_{10} transformation used on AOD subset.

c.   No data for this period

Table 14: Correlations between seasonal AOD and daily PM_{10} over the Malmesbury AQM station.

Seasonal period	$AOD_{aqua.dt}$-daily hour PM_{10} seasonal relationship		$AOD_{terra.dt}$- daily PM_{10} seasonal relationship		$AOD_{aqua.db}$- daily PM_{10} seasonal relationship	
	Pearson correlation	n	Pearson correlation	n	Pearson correlation	n
January, February, December	R = 0.43; p = 0.009	36	R = 0.204; p = 0.241	35	R = 0.344; p = 0.005	64
March, April, May	R = 0.444; p = 0.085	16	R = 0.383; p = 0.048	27	R = 0.250; p = 0.2a	28
June, July, August	R = 0.287; p = 0.075	42	R = 0.240; p = 0.158	36	R = 0.047; p = 0.853a	18
September, October, November	R = 0.073; p = 0.650	41	R = 0.126; p = 0.521	28	N/A b	0

a. log_{10} transformation used on AOD subset

b.   No data for this period

Table 15: Correlations between seasonal AOD and one hourly PM$_{10}$ over the George AQM station.

Seasonal period	AOD$_{aqua.dt}$-1 hour PM$_{10}$ seasonal relationship		AOD$_{terra.dt}$-1 hour PM$_{10}$ seasonal relationship	
	Pearson correlation	n	Pearson correlation	n
January, February, December	R = 0.104; p = 0.712	15	R = 0.00; p = 1.00	40
March, April, May	R = 0.250; p = 0.191	29	R = 0.083; p = 0.344[a]	34
June, July, August	R = 0.338; p = 0.055	33	R = 0.168; p = 0.269	36
September, October, November	R = 0.433; p = 0.015	31	R = -0.189; p = 0.424	30

a. log$_{10}$transformation of PM$_{10}$ subset

Table 16: Correlations between seasonal AOD and daily PM$_{10}$ over the George AQM station.

Seasonal period	AOD$_{aqua.dt}$-daily PM$_{10}$ seasonal relationship		AOD$_{terra.dt}$-daily PM$_{10}$ seasonal relationship	
	Pearson correlation	n	Pearson correlation	n
January, February, December	R = -0.229; p = 0.376	17	R= -0.034; p = 0.859	29
March, April, May	R = -0.053; p = 0.787	29	R = -0.171; p = 0.343	33
June, July, August	R = 0.411; p = 0.017	33	R = 0.147; p = 0.393	36
September, October, November	R = 0.328; p = 0.072	31	R = 0.465; p = 0.01	30

4.7. Meteorological Effects on the AOD-PM$_{10}$ Relationship

Previous studies which have determined the AOD-PM$_{10}$ relationship for various locations around the globe, have integrated meteorological parameters using three approaches. The first approach is the adjustment of the AOD using either or both the MLH and the RH. Emili *et al.* (2010), Emili *et al.* (2011) and Dinoi *et al.* (2010) were examples of studies which used this approach. The second approach, was the inclusion of the AOD and the meteorological parameters into a statistical multivariate model which estimated PM$_{10}$ concentrations. Statistical approaches such as neural networks (for example Wu *et al.* 2012) and linear regression (for example Grguric *et al.* 2013) have been used to model PM$_{10}$ concentrations. The third approach involved the clustering of PM$_{10}$ episodes according to the occurrences of different weather systems defined by the meteorological parameters as descriptors of the different weather systems and the determination of AOD-PM$_{10}$ relations within each of the classes (for example Wang *et al.* 2013; Zha *et al.* 2010). The first approach was advantageous in that the effect of individual meteorological effects on the AOD-PM$_{10}$ were determined, and required minimal meteorological data inputs were determined. The latter approaches were advantageous in that meteorological effects were

considered integratively since meteorological parameters do not act independently of each other for effects on air pollutants. However these approaches were more data intensive since multiple meteorological datasets were required. In this study the first and second approaches were found to be of interest due to the number of meteorological parameters analysed in this study. Malmesbury and George was used as case studies, including parameters $AOD_{aqua.dt}$, daily averaged PM_{10} concentration, the hourly averaged RH adjusted AOD (AOD/RH), daily averaged temperature, daily averaged wind speed, daily averaged wind direction and daily averaged RH.

The independent variables were first correlated individually with the PM_{10} (Table 17). The technique was adapted from Kumar *et al.* (2008). Kumar *et al.* (2008) included regression of PM_{10} concentration with RH and sea level pressure. Previously the $AOD_{aqua.dt}$ correlation with daily averaged PM_{10} was 0.36. A log transformed $AOD_{aqua.dt}$ was used in this part of the study and the AOD-PM_{10} correlation was lower over Malmesbury (R = 0.30) and was not significant over George which is likely partly due to the sensitivity of the AOD to sample size which decreased. However when AOD/RH was used instead, the AOD-PM_{10} correlation slightly increased over Malmesbury (R = 0.37) and over George (R = 0.34). The approach to adjust the AOD with hourly averaged RH was adapted from Dinoi *et al.* (2010) which adjusted the AOD by dividing the AOD with the product of averaged MLH and averaged wind speed. In this study, it was determined that adjustment of AOD with surface measurements of the RH did increase the AOD-PM_{10} correlation. Firstly Malmesbury and George was found to be highly humid throughout the year. Correlations were found between RH and PM_{10} concentrations in section 4.4 which indicates that RH does have an effect on PM_{10} concentration. The effect of RH on the AOD-PM_{10} correlation was discussed in section 2.3.4.2. Two studies previously discussed had different findings. Guo *et al.* (2009) determined that the adjustment of the AOD using the RH did not substantially increase the AOD-PM_{10} correlation over China. Emili *et al.* (2010) found that the adjustment of the AOD with RH had a smaller relative effect on the AOD-PM_{10} relationship over Switzerland relative to the adjustment of the AOD with the MLH. An alternative to the adjustment of the AOD with RH, was to use the meteorological parameters as a supplementary descriptor of the AOD-PM_{10} for different PM_{10} episodes (for example Kim *et al.* 2013).

In this study it was previously determined in section 4.4, that the temperature had a better correlation with PM_{10} (R = 0.1 - 0.6) in all seasons than the AOD (R=no significant

correlation -0.43) in Malmesbury and George. Furthermore it was previously determined in this study that temperature was better correlated with PM_{10} than RH in all seasons in Malmesbury and George. The results in this part of the study also determined that temperature was better correlated with PM_{10} (R = 0.42) than the AOD (R=0.3) and the RH (R= no significant correlation) in Malmesbury (Table 17). In George, the RH was better correlated with PM_{10} (R = 0.3) than the AOD (R = no significant correlation) and temperature (R = no significant correlation). The wind direction was weakly correlated with PM_{10} in Malmesbury but no significant correlation was found in George between wind direction and PM_{10}. The wind speed was not significantly correlated with PM_{10} in Malmesbury but was weakly correlated with PM_{10} in George (R = -0.3).

A linear regression analysis was run for parameters monitored in Malmesbury. The wind direction was not a significant predictor when incorporated into the linear regression analysis with the AOD or AOD/RH and temperature as independent parameters. Using temporally co-located temperature, AOD/RH and AOD observations, the number of samples decreased further. This has an impact on the correlation. For example the correlation between daily averaged temperatures decreases from 0.42 in Table 17 to 0.36 in Table 18 due to a decrease in the sample size. This indicates that the sample size is not large enough for the correlation between temperature and PM_{10} concentration to stabilize.

The correlations did not change when the temperature was the sole predictor or when temperature and the AOD were co-predictors with the correlation remaining about 0.4 (Table 18). However when both the temperature and AOD/RH were used in the statistical model for Malmesbury, the correlation increased to 0.45 (Table 19). This suggests that the RH has a complementary but indirect effect when used in a multi-linear model with temperature.

A linear regression analysis was also run for wind speed and AOD/RH monitored in George AQM station. The wind speed was not significant when included as a predictor with AOD/RH in a linear regression model and had to be log transformed. The correlation between the log transformed wind speed and PM_{10} concentration was 0.3 (Table 20). The correlation increased to 0.4 when AOD/RH was included as a predictor to the statistical model along with wind speed.

Previous studies suggest that even with different statistical approaches, incorporating multiple meteorological parameters with the AOD to estimate PM_{10} concentrations yields a wider variation in correlations with the PM_{10} (for example Zha *et al.* 2010) and for some regions better correlations with PM_{10} concentrations (for example Nordio *et al.* 2013). Overall, previous studies found that the AOD-PM_{10} correlations with multiple meteorological independents range widely for different regions and with different statistical approaches, suggesting that the findings were not unusual. Despite the weak correlations determined, the findings do support the consideration of integrating meteorological effects into the AOD-PM_{10} relationship over Malmesbury and George, such that the masking effect of these meteorological confounders on the AOD-PM_{10} are minimised.

Table 17: Correlation analysis between annual daily averaged PM_{10} concentrations, the AOD and meteorological parameters over the Malmesbury AQM station.

Daily averaged meteorological and aerosol parameters	Daily mean PM_{10} concentration in Malmesbury		Daily mean PM_{10} concentration in George	
	Pearson correlation	n	Pearson correlation	n
AOD	R = 0.303; p = 0.001	112	R = 0.184; p = 0.138	66
AOD/RH	R = 0.368; p < 0.0005	132	R = 0.335; p = 0.002	84
Temperature	R = 0.416; p < 0.0005	132	R = 0.147; p = 0.171	89
Wind speed	R = -0.088; p = 0.315	132	R = -0.274; p = 0.009	91
Wind direction	R = 0.236; p = 0.002	132	R = -0.019; p = 0.858	91
RH	R = -0.154; p = 0.078	132	R=-0.281; p=0.007	90

Table 18: Linear Correlation Coefficient, Slope, and Intercept for Multivariate Models to Estimate daily averaged PM_{10} Mass Concentration using Temperature and AOD over Malmesbury AQM station.

Model	Independent variable	R	Change in R (%)	Slope; significance	Intercept	n
1	Temperature	0.355	-	0.449; p < 0.0005	0.787	
2	Temperature AOD	0.397	11.8	0.353; p = 0.004 0.096; p = 0.046	1.025	111

Table 19: Linear Correlation Coefficient, Slope, and Intercept for Multivariate Models to Estimate daily averaged PM$_{10}$ Mass Concentration using Temperature and AOD/RH over Malmesbury AQM station.

Model	Independent variable	R	Change in R (%)	Slope; significance	Intercept	n
1	Temperature	0.416	-	0.498; p < 0.005	0.727	
2	Temperature AOD/RH	0.449	7.9	0.367 41.239	0.845	131

Table 20: Linear Correlation Coefficient, Slope, and Intercept for Multivariate Models to Estimate daily averaged PM$_{10}$ Mass Concentration using log$_{10}$ wind speed and AOD/RH over George AQM station.

Model	Independent variable	R	Change in R (%)	Slope; significance	Intercept	n
1	log10 wind speed	0.331	-	-14.446 ; p < 0.005	30.546	
2	log10 wind speed AOD/RH	0.424	28.1	-11.903; p = 0.012 2611.590; p=0.007	28.384	83

4.8. Summary

High PM$_{10}$ concentrations at the Malmesbury AQM station occurred in AOD and hourly or daily averaged PM$_{10}$ concentrations at Malmesbury and George AQM stations were weakly correlated (0.24-0.36). AOD$_{aqua.dt}$ were better correlated with PM$_{10}$ concentrations over Malmesbury and George (0.24-0.36) than AOD$_{terra.dt}$ (no significant correlation − 0.24). The AOD-PM$_{10}$ relationship over Malmesbury improved from 0.36 to 0.45 when RH adjusted AOD and temperature were used together using multiple linear regression. Seasonally, temperature and solar radiation were most commonly strongly correlated with PM$_{10}$ concentrations at the Malmesbury AQM station in summer and autumn. While at the George AQM station, rainfall, wind speed and solar radiation were strongly correlated with PM$_{10}$ concentrations in winter.

CHAPTER 5: CONCLUSION

5.1. Introduction

The aim of this study was to determine the extent to which AOD is useful for air quality analysis of PM_{10} related air pollution within the Western Cape Province. This chapter assesses whether the aims and associated objectives were attained within the conceptual framework of the study. The chapter further discusses and evaluates the limitations of the study and then lastly presents the recommendations for future studies.

PM is a health risk, even at low ambient concentrations in the atmosphere, however the cost to monitor or to model surface concentrations is high. The analysis of ambient PM concentration is important for air quality management in South Africa in order to suggest recommendations for pollution abatement. Satellite remote sensing retrievals of AOD are cost effective and have been used previously in conjunction with meteorological drivers of PM pollution particularly MLH and RH for regional air quality studies (example Dinoi *et al.* 2010; Emili *et al.* 2010 and Wu *et al.* 2012). .

Air quality in George and Malmesbury are of concern, since several exceedances of the WHO (2006) guidelines were observed. The PM_{10} concentrations were observed to exceed both the WHO guideline for annual average PM_{10} concentrations and daily average PM_{10} concentrations. A higher seasonal frequency of exceedances in Malmesbury occurred in summer and autumn while at George a greater number of exceedances occurred in winter particularly the July and August months. It was suggested that local pollution sources that contribute to the high PM_{10} concentrations at George and Malmesbury were somewhat different. It is likely that veld fires favoured by the warmer and drier conditions may be dominant pollution sources in the summer and autumn months at the Malmesbury station. It is likely that residential biomass burning sources and possibly more frequent surface inversions contributed to the higher concentrations in the winter and spring months at the George station which were colder than other months.

Information about PM_{10} concentrations in Malmesbury and George did not benefit from the analysis of AOD. A temporal mismatch was observed between seasonal PM_{10} concentrations and the AOD at both Malmesbry and George. There were no seasonal differences observed between most of the AOD data.

Specific meteorological conditions were found to be important confounding factors when observing AOD and PM_{10} trends. The AOD-PM_{10} relationship over Malmesbury improved (R= 0.45) with the RH integration of the AOD and the integration of temperature using multiple linear regression. Cloud contamination of AOD retrievals were suggested to be inaccurate due to the AOD-PM_{10} relationship over George and Malmesbury not substantially changing when cloud screening was applied using the MODIS cloud mask sub-dataset. Differences between the $AOD_{aqua.dt}$-PM_{10} and $AOD_{terra.dt}$-PM_{10} relationship over Malmesbury and George suggested that meteorological conditions that characterised diurnal PM_{10} concentrations partly masked the AOD-PM_{10} correlations with the MLH being one of the predominant meteorological parameters. Meteorological processes have short term effects on the AOD-PM_{10} relationship. For, PM_{10} to be comparable to the AOD, meteorological processes should contribute to the upward dispersal of aerosols to the upper atmosphere. The algorithms employed and procedures used to retrieve the AODs used in this study had a confounding effect on the AOD-PM_{10} relationship as it directly contributed to the number of AOD observations retrieved within the year. Parameters such as the aerosol size distribution, extinction efficiency, refractive index and particle size all are considered within the aerosol retrieval algorithm and thus effect the AOD-PM_{10} relationship.

5.2. Summary of key findings

This study has an aim to discern the extent that AOD is useful within the air quality analysis of PM_{10} related air pollution especially within the Western Cape Province. The following sub-sections discuss the key findings with respect to each of the study's objectives.

- ***Assessment of the PM_{10} Concentrations Monitored in Malmesbury and George according to the WHO Guidelines for PM_{10} in 2011***

This objective was attained by the comparison of daily averaged PM_{10} concentrations monitored in Malmesbury and George to the WHO guideline for daily averaged PM_{10} concentrations which was 50 µg/m^3. The comparison was done in order to assess the severity of PM_{10} associated air quality in Malmesbury and George. This study found that there was an air quality issue in Malmesbury and George in 2011. In Malmesbury most of the exceedances of the WHO guideline occurred in the summer and autumn months. In

George most of the exceedances of the WHO guideline occurred in the winter – spring months. This finding supported the need to analyse the PM_{10} associated air quality in the towns of Malmesbury and George.

- ***Characterization of the Diurnal Trends of PM_{10} Associated Ambient Air Quality and Meteorology Monitored in George and Malmesbury in 2011***

An annual average PM_{10} concentration was calculated for each hour of the day for 2011. Seasonal average PM_{10} concentrations were also calculated for each hour of the day for 2011. Weekday and weekend diurnal PM_{10} were also calculated. Similar annual and seasonal averages were calculated for the meteorological parameters including the wind speed, temperature, RH and solar radiation. The analysis of diurnal PM_{10} concentrations allowed for the determination of the occurrence of peak PM_{10} concentrations during the day. The analysis of diurnal meteorology allows for the assessment of whether a favourable meteorological environment developed around the time of the peak PM_{10} concentrations. If this was not the case, then there is a possibility that anthropogenic activity was the main contributor to the increased PM_{10} concentrations.

This study found that PM_{10} concentrations in Malmesbury are greater on weekdays compared to weekends in 2011. There is no difference between PM_{10} concentrations in George on weekdays and weekend. Anthropogenic PM pollution sources do effect PM_{10} concentrations in Malmesbury on weekdays relative to weekends but have equal effect on PM_{10} concentrations in George on weekdays relative to weekends. Mean diurnal wind speed trends; temperatures; RH conditions and solar radiation levels measured at the Malmesbury AQM station were not characterised by noticeable fluctuations around the time mean PM_{10} concentrations peaked by the late afternoon. Low wind speeds, low temperatures and low solar radiation levels were likely to have contributed to favourable conditions for the morning peak in diurnal PM_{10} concentrations**.**

- *To Characterise the Monthly and Seasonal Trends of PM$_{10}$ Associated Ambient Air Quality and Meteorology Monitored in George and Malmesbury in 2011 and to assess the Correlations between the PM$_{10}$ Concentrations and the Meteorology Monitored in the Two Towns*

The monthly averages of PM$_{10}$ concentration were calculated from the hourly PM$_{10}$ data. The statistical tests were run using the daily average PM$_{10}$ concentrations to assess the seasonal trend in the data. Seasonal means of the meteorological parameters were calculated for wind speed, wind direction, solar radiation, rainfall, temperature and the RH. Statistical correlation analysis was run between daily averaged meteorology except wind direction and daily averaged PM$_{10}$ concentration separately for each season. Temporal trends of PM$_{10}$ included monthly and seasonal averages. The temporal characteristics of PM$_{10}$ in Malmesbury and George were assessed. This was done so as to determine the status quo of PM$_{10}$ air pollution in the two towns. Correlation analysis between PM$_{10}$ concentrations and meteorological drivers of pollution was conducted.

Higher PM$_{10}$ concentrations were recorded for the January to April period in Malmesbury relative to the rest of the year. Higher PM$_{10}$ concentrations in George were recorded for the June to August months relative to the December, January - February months which coincided with the lowest PM$_{10}$ concentrations. The January - April period in Malmesbury was characterised by higher PM$_{10}$ concentrations, warmer temperatures, dryer air (but still > 50% RH, low rainfall, declining wind speeds with a predominately south westerly direction and greater solar radiation relative to the rest of the year. The high monthly PM$_{10}$ concentrations in June - August months in George coincided with the highest rainfall, lowest solar radiation levels and the lowest temperatures relative to the rest of the year. The predominant wind direction during this period were westerlies. In both George and Malmesbury, solar radiation had a significant impact on PM$_{10}$ concentrations during the seasons with the higher PM$_{10}$ concentrations. There is a strong dependence of PM$_{10}$ concentrations on RH and temperature in Malmesbury which was not found in George.

- *To Characterise the Satellite AOD over Malmesbury and George*

The source of the AOD data was from satellite images retrieved from the MODIS sensor on board the TERRA and AQUA satellites which were downloaded from the LAADs system. The AOD was extracted from raster format data in ArcGIS and exported as vector

point form data. The vector data was subsequently extracted and compiled in Microsoft Excel. The AOD data consisted of 3 datasets, 2 AOD datasets from AQUA and TERRA satellites retrieved using the dark target algorithm and a 3rd dataset from the AQUA retrieved using the deep blue algorithm. This objective was significant in order to determine whether the AOD can be analysed to the same temporal extent that the PM_{10} data was analysed (diurnal, daily, monthly and seasonally).

The temporal trends of the AOD could be temporally analysed for monthly and seasonal trends only. There were no seasonal differences for $AOD_{terra.dt}$ over Malmesbury and George. There were mostly no seasonal differences for $AOD_{aqua.dt}$ over Malmesbury and no seasonal differences over George. There were seasonal differences in $AOD_{aqua.db}$ over Malmesbury with AOD in summer, spring and autumn different to the $AOD_{aqua.db}$ in winter in 2011. The deep blue algorithm is better equipped to distinguish between the surface reflectance of land surfaces including deserts, semi desert and urban areas and the surface reflectance of aerosols over these land surfaces compared to the dark target algorithm. Malmesbury is located in a semi desert area.

- ***To Assess the Correlations between Ambient Air Quality Monitored PM_{10} and Satellite AOD over Malmesbury and George***

To attain this objective, the PM_{10} concentrations (hourly, 24 hour averaged) were temporally collocated with the retrieved MODIS AOD to the hour of satellite overpass. The AOD-PM_{10} relationship over each AQM station was statistically explored using correlation and linear regression analysis. Linear analysis was done to determine the annual, weekly, monthly and seasonal AOD-PM_{10} relationship. The purpose of this analysis was to identify the temporal circumstances where the AOD could be used as a proxy of PM_{10} concentration. Correlations between the hourly and daily averaged AOD and PM_{10} concentration were weak (R=0.24-0.36). PM_{10} concentrations were better correlated with $AOD_{aqua.dt}$ (R=0.24-0.67) compared to $AOD_{terra.dt}$ (0.24-0.47) over Malmesbury and George. Correlations between AOD and PM_{10} concentration were stronger over Malmesbury (R=0.24-0.78) than over George (0.24-0.47). The use of cloud screening did not substantially improve the correlation between AOD and PM_{10} over George and Malmesbury. The upscaling of the AOD and the PM_{10} concentrations improved the AOD-PM_{10} correlation substantially.

- *To Determine the Effects of Meteorology Monitored in George and Malmesbury on the Relationship between Ambient Air quality Monitored PM$_{10}$ and Satellite AOD over Malmesbury and George*

To achieve this objective, both the PM$_{10}$ concentrations and meteorological data (hourly, 24 hour averaged) were temporally collocated with the retrieved MODIS AOD to the hour of satellite overpass. Multiple linear regression was run with the AOD, daily averaged RH, daily averaged temperature, daily averaged wind speed and daily averaged wind direction included as predictors of PM$_{10}$. The analysis intended to investigate the value of including meteorological parameters as coefficients alongside the AOD within a regression model to predict PM$_{10}$ concentration. The multiple linear regression to model PM$_{10}$ indicated that the correlation over Malmesbury increased significantly (R=0.45) when the AOD/RH and the temperature coefficients were introduced. The linear regression models for PM$_{10}$ concentrations over George indicated that the correlation increased significantly when the AOD/RH and the wind speed coefficients were introduced.

It was found that it is possible to conclude that the AOD is weakly correlated with PM$_{10}$ over Malmesbury and George. Therefore the AOD cannot be used as a proxy for PM$_{10}$ concentration solely on its own. However this does not mean that the AOD is not useful within the analysis of PM$_{10}$ related air pollution. This study has shown that it is possible to significantly increase the AOD-PM$_{10}$ correlation by integrating the meteorological confounders of the relationship within a linear regression model. The meteorological parameters considered as coefficients included the RH and the temperature. This study found that the use of the MODIS cloud cover mask to remove cloud contaminated AOD pixels did not significantly impact the AOD-PM$_{10}$ relationship over the two case study towns.

5.3. Limitations

The limitations highlighted could not be controlled for and pertain to the use of PM$_{10}$ concentration and AOD data. Only PM$_{10}$ concentration data over 1 year were used in this study. Temporal trends may not be evident within just 1 year of data and a trend can only be confirmed if it is repeated over multiple years. The method of data extraction to acquire PM$_{10}$ data were work intensive in this study and this meant that only data over 1 year

could be analysed, however subsequent studies can now benefit from the acquisition of air quality data from the South African Air Quality Information System.

AOD data are sparse and represents a single observation every day or every few days. Hourly and daily temporal trends cannot be detected from AOD data. Using AOD data from remotely sensed satellite imagery for over a one year period meant that there was an insufficient amount of observations to detect a seasonal trend. The extraction of AOD data is both time and work intensive due to the AOD data being contained within a layer of sub datasets within an hdf image file. The lack of seasonal variation in two of the data sets may also indicate that the AOD data requires validation using *in situ* surface measurements of the AOD.

Differences between AOD observations can result from differences between satellites due to the use of a range of polarisations, viewing angles, wavelengths, spatial and temporal resolutions to retrieve information about the atmosphere. The MODIS cloud mask was not effective in identifying sub pixel cloud contamination which can underestimate cloudiness in a satellite image. Hence erroneous AOD under cloudy conditions may have inadvertently been incorporated in the study during the analysis. The use of spatial upscaling in this study was limited due to the differences in PM_{10} concentrations between George and Malmesbury and the limited number of AQM stations included which were not spatially representative of Western Cape region.

5.4. Future Research

There is an air quality issue in Malmesbury and George. Malmesbury has a limited number of pollution sources, and it is more likely for transboundary air pollution from the City of Cape Town to affect the local air quality in Malmesbury. It is more likely that local air pollution sources affect the ambient air quality in George due to the presence of industrial, agricultural and urban air pollution sources. A study to do air quality modelling is proposed to determine the fate of air pollutants from the City of Cape Town and its contribution to air pollution in Malmesbury and the greater Swartland Local Municipality. A second air quality modelling study to model the dispersion of pollution from area, point and line sources within the George Local Municipality should be undertaken.

A study to analyse several years' worth of PM_{10} air quality data to determine the anthropogenic influences on weekday and weekend PM_{10} air pollution should be

undertaken. Traffic pollution sources are more likely to contribute to weekly fluctuations in PM_{10}. By understanding the annual trend in weekly PM_{10} fluctuations, it is possible to confirm the contribution of anthropogenic sources of air pollution to the PM_{10} levels in George and Malmesbury. Furthermore, analysing the temporal trends from multiple years worth of data will also assist in determining whether the PM_{10} seasonal trends in 2011 were similar to the seasonal trends in other years.

Most episodes of high PM_{10} levels occur within the January-April period in Malmesbury and the June-August period in George. Meteorology such as solar radiation is correlated significantly with PM_{10} concentrations. To determine the effect of meteorological drivers on PM_{10} air pollution, it is recommended that specific pollution episodes are studied. By understanding pollution episodes which coincide with favourable meteorological conditions, prediction models can be devised to determine when these pollution episodes will occur in the future. In addition pollution source contributions to pollution episodes can also be analysed. By isolating pollution episodes that are contributed for example by household fuel burning, it is possible to suggest suitable air quality management interventions such as alternative cleaner fuel sources.

In this study, seasonality was not detected for the AOD retrieved using the dark target algorithm. It is therefore beneficial to analyse the AOD temporal trends over multiple years, to determine the seasonality of the AOD over Malmesbury and George.

It was found in this study that the AOD temporal trends did not match the PM_{10} concentration temporal trends. This is partly explained by the MODIS AOD being globally validated but not validated regionally using surface measurements of the AOD in all regions of South Africa, with the Western Cape one of the regions without *in situ* AOD monitoring stations. Thus future field research could include regional *in situ* measurement of the AOD in the Western Cape and calibration of the satellite AOD retrieved by the MODIS sensor.

It was determined in this study that the use of the cloud mask sub dataset to remove the effects of cloudiness on AOD underestimated the effects of cloud contamination. Hence the AOD retrieved over Malmesbury and George could benefit from an alternative cloud screening procedure based upon *in situ* measurements of cloudiness

It was determined in this study that the AOD-PM$_{10}$ relationship over Malmesbury and George fluctuated temporally. The AOD-PM$_{10}$ relationship can be optimised under cloud free conditions and days when the aerosols are homogenously distributed with height in the atmosphere. Further investigation is needed to characterise the meteorological conditions including the mixing layer height and cloud cover at George and Malmesbury AQM stations which best represent the optimal conditions for the AOD-PM$_{10}$ relationship.

5.5. Concluding remarks

Despite the weaknesses of PM$_{10}$ estimation from satellite retrieved AOD identified in this study, there is still much interest in the use of satellite remote sensing of PM over areas with poor spatial coverage of AQM stations. The results from this study show that there is a linear relationship between the satellites retrieved AOD and PM$_{10}$ concentration in South Africa which is an initial step towards using the AOD to estimate PM$_{10}$ concentrations. This study has shown that it is important to consider the RH within the linear modelling of PM$_{10}$ concentrations.

Air quality managers face a number of challenges with understanding air quality in the jurisdictions they manage. Not all areas have an adequate baseline of the status of air quality. This prevents the status of health exposure to air pollution being quantified in all areas. In some areas, air quality studies whether passive or continuous are not possible in remote areas. Air quality data are affected by poor data quality or completeness. Access to air quality data is restricted due to the reluctance of local or district municipalities to share data. Continuous air quality monitoring is expensive to purchase, operate and to maintain. This therefore limits the extent to which air quality data is available in South Africa. Hence this limits the extent to which air quality managers can understand the air quality problem in the areas they have jurisdiction but also to pollution issues relating to transboundary pollution. So air quality managers need more air quality data which is inexpensive and that can cover areas where the air quality is not known at much larger spatial scales.

Satellite measurements of air pollution and of the environment in general have problems which reduce the appeal of the data for uptake by government institutions. Processing algorithms have not yet overcome the challenges of retrieving information over urban areas due to the geometric, textural and particularly the spectral characteristics of urban

areas. Cloud cover remains a problem for satellite observations and compounds the difficulties of monitoring over urban areas when pollution episodes occur on cloudy days. Satellite observations are not continuous in time posing difficulties in using the data for pollution monitoring. Satellite observations of pollution have a coarse spatial resolution which cannot be used for pollution monitoring at a local scale for example around hot spots.

Government institutions themselves experience challenges in the use of satellite data. Despite the affordability of satellite data, skilled expertise not always available within government is required to collect and to use the satellite data. The software required to process and to analyse satellite data is expensive and financial constraints of government institutions may make the attraction to use satellite data unappealing.

Satellite remote sensing of air pollution offers an opportunity to understand the status quo of PM related air quality across large spatial scales particularly in areas where there are no continuous AQM stations. However, the satellite retrieved AOD from the MODIS sensor cannot be used on its own as a proxy for PM_{10} concentrations to calculate exposure to PM_{10} pollution so as to inform the status quo for PM_{10} related air quality risk within towns in South Africa for air quality management policy. The satellite retrieved AOD must be validated against existing PM_{10} concentrations data together with measured meteorological parameters for example temperature, wind speed and RH. The AOD can be used in a linear model to predict PM_{10} concentrations, as long as meteorological parameters are included as well. This study also indicates that the composition of meteorological predictors used in the linear model for PM_{10} will not be the same for each case study area investigated. For the first time, a satellite will be launched in the future to monitor PM related air pollution; however the provisions identified in this thesis for the use of satellite data for pollution monitoring remain valid.

Resolving the effect of meteorological drivers of PM related air pollution within the statistical model calculated to estimate PM_{10} concentrations from satellite AOD is very important within South Africa. Even if the satellite AOD is validated against in situ AOD measurements, there will still be challenges to using the calibrated satellite AOD as a proxy for PM_{10} concentration. Therefore the effects of meteorological drivers on PM_{10} concentration must be resolved. To date, even air pollution dispersion models applied within South Africa, have had challenges to predicting PM_{10} concentrations within towns

and cities due to the challenges of resolving the effects of meteorological confounders on PM_{10} concentration. Firstly understanding the effect of meteorological drivers on PM related air pollution dispersion and distribution for a specific town or city is important, as the meteorological effects for one area will not be the same for another. Then a statistical model can be determined which best integrates the area specific meteorological effects along with the satellite data to estimate PM_{10} concentrations.

REFERENCES

Abel, S. J., Haywood, J. M., Highwood, E. J., Li, J., and Buseck, P. R. (2003). Evolution of biomass burning aerosol properties from an agricultural fire in southern Africa. *Geophysical Research Letters*, *30*(15).

Akimoto, H. (2003). Global air quality and pollution. *Science*, *302*(5651), 1716-1719.

Agarwal, R., Awasthi, A., Singh, N., Mittal, S. K., and Gupta, P. K. (2013). Epidemiological study on healthy subjects affected by agriculture crop-residue burning episodes and its relation with their pulmonary function tests. *International journal of Environmental Health Research*, *23*(4), 281-295.

Ahn, C., Torres, O., and Jethva, H. (2014). Assessment of OMI near-UV aerosol optical depth over land. *Journal of Geophysical Research: Atmospheres*, *119*(5), 2457-2473.

Aldabe, J., Elustondo, D., Santamaría, C., Lasheras, E., Pandolfi, M., Alastuey, A., ... and Santamaría, J. M. (2011). Chemical characterisation and source apportionment of $PM_{2.5}$ and PM_{10} at rural, urban and traffic sites in Navarra (North of Spain). *Atmospheric Research*, *102*(1), 191-205.

Alexandrov, M. D., Lacis, A. A., Carlson, B. E., and Cairns, B. (2002). Remote sensing of atmospheric aerosols and trace gases by means of Multifilter Rotating Shadowband Radiometer. Part II: climatological applications. *Journal of the Atmospheric Sciences*, *59*(3), 544-566.

Alghamdi, M. A., Shamy, M., Redal, M. A., Khoder, M., Awad, A. H., and Elserougy, S. (2014). Microorganisms associated particulate matter: a preliminary study. *Science of the Total Environment*, *479*, 109-116.

Ali, A., Amin, S. E., Ramadan, H. H., and Tolba, M. F. (2011, November). Ozone monitoring instrument aerosol products: Algorithm modelling and validation with ground based measurements over Europe. In *Computer Engineering and Systems (ICCES), 2011 International Conference on* (pp. 181-186). IEEE.

An, X. Q., Zhu, T., Wang, Z. F., Li, C. Y., and Wang, Y. S. (2007). A modelling analysis of a heavy air pollution episode occurred in Beijing. *Atmospheric Chemistry and Physics*, *7*(12), 3103-3114.

Ana, G., Adeniji, B., Ige, O., Oluwole, O., and Olopade, C. (2013). Exposure to emissions from firewood cooking stove and the pulmonary health of women in Olorunda community, Ibadan, Nigeria. *Air Quality, Atmosphere and Health*, *6*(2), 465-471.

Anderson, B. E., Grant, W. B., Gregory, G. L., Browell, E. V., Collins, J. E., Sachse, G. W., ... and Blake, N. J. (1996). Aerosols from biomass burning over the tropical South Atlantic region: Distributions and impacts. *Journal of Geophysical Research: Atmospheres (1984–2012)*, *101*(D19), 24117-24137.

Ballard, M., Newcomer, M., Rudy, J., Lake, S., Sambasivam, S., Strawa, A. W., ... and Skiles, J. W. (2007, December). Understanding the correlation of San Joaquin air quality monitoring with aerosol optical thickness satellite measurements. In *ASPRS 2008 Annual Conference Proceedings*.

Banks, J. R., and Brindley, H. E. (2013). Evaluation of MSG-SEVIRI mineral dust retrieval products over North Africa and the Middle East. *Remote Sensing of Environment*, *128*, 58-73.

Barladeanu, R., Stefan, S., and Radulescu, R. (2012). Correlation between the Particulate Matter (PM_{10}) mass concentrations and aerosol optical depth in Bucharest, Romania. *Romanian Reports in Physics*, *64*(4), 1085-1096.

Barnaba, F., Putaud, J. P., Gruening, C., and Dos Santos, S. (2010). Annual cycle in co-located *in situ*, total-column, and height-resolved aerosol observations in the Po Valley (Italy): Implications for ground-level particulate matter mass concentration estimation from remote sensing. *Journal of Geophysical Research: Atmospheres (1984–2012)*, *115*(D19).

Barrero, M. A., Orza, J. A. G., Cabello, M., and Cantón, L. (2015). Categorisation of air quality monitoring stations by evaluation of PM_{10} variability. *Science of the Total Environment*, *524*, 225-236.

Bauer, S. E., Koch, D., Unger, N., Metzger, S. M., Shindell, D. T., and Streets, D. G. (2007). Nitrate aerosols today and in 2030: a global simulation including aerosols and tropospheric ozone. *Atmospheric Chemistry and Physics*, *7*(19), 5043-5059.

Beh, B. C., Tan, F., Tan, C. H., Syahreza, S., Jafri, M. M., and Lim, H. S. (2013, May). PM_{10}, $PM_{2.5}$ and PM_1 distribution in Penang Island, Malaysia. In *AIP Conference Proceedings* (Vol. 1528, pp. 146-150).

Bellouin, N., Rae, J., Jones, A., Johnson, C., Haywood, J., and Boucher, O. (2011). Aerosol forcing in the Climate Model Intercomparison Project (CMIP5) simulations by HadGEM2-ES and the role of ammonium nitrate. *Journal of Geophysical Research: Atmospheres (1984–2012)*, *116*(D20).

Bencherif, H., Portafaix, T., Baray, J. L., Morel, B., Baldy, S., Leveau, J., ... and Diab, R. (2003). LIDAR observations of lower stratospheric aerosols over South Africa linked to large scale transport across the southern subtropical barrier. *Journal of Atmospheric and Solar-Terrestrial Physics*, *65*(6), 707-715.

Bernard, E., Moulin, C., Ramon, D., Jolivet, D., Riedi, J., and Nicolas, J. M. (2011). Description and validation of an AOT product over land at the 0.6 μm channel of the SEVIRI sensor onboard MSG. *Atmospheric Measurement Techniques*, *4*(11), 2543-2565.

Bigi, A., and Harrison, R. M. (2010). Analysis of the air pollution climate at a central urban background site. *Atmospheric Environment*, *44*(16), 2004-2012.

Billmark, K. A., Swap, R. J., and Macko, S. A. (2003). Characterization of sources for Southern African aerosols through fatty acid and trajectory analyses. *Journal of Geophysical Research: Atmospheres (1984–2012)*, *108*(D13).

Bocci, E., Bonafoni, S., Basili, P., Biondi, R., and Arino, O. (2009). Analysis of aerosol optical depth retrieved by MODIS and MERIS and comparison with photometer data. *Rivista italiana di Telerilevamento*, *41*(1), 5-10.

Bond, T. C., Doherty, S. J., Fahey, D. W., Forster, P. M., Berntsen, T., DeAngelo, B. J., ... and Zender, C. S. (2013). Bounding the role of black carbon in the climate system: A scientific assessment. *Journal of Geophysical Research: Atmospheres*, *118*(11), 5380-5552.

Booth, B., and Bellouin, N. (2015). Climate change: Black carbon and atmospheric feedbacks. *Nature*, *519*(7542), 167-168.

Boucher, O. (2015). *Atmospheric Aerosols: Properties and Climate Impacts*. Springer.

Boucher, O., Randall, D., Artaxo, P., Bretherton, C., Feingold, G., Forster, P., ... and Zhang, X. Y. (2013). Clouds and Aerosols. In: *Climate Change 2013: The Physical Science Basis. Contribution of Working Group I to the Fifth Assessment Report of the Intergovernmental Panel on Climate Change* [Stocker, T.F., D. Qin, G.-K. Plattner, M. Tignor, S.K. Allen, J. Boschung, A. Nauels, Y. Xia, V. Bex and P.M. Midgley (eds.)]. Cambridge University Press, Cambridge, United Kingdom and New York, NY, USA

Bréon, F. M., Vermeulen, A., and Descloitres, J. (2011). An evaluation of satellite aerosol products against sunphotometer measurements. *Remote Sensing of Environment*, *115*(12), 3102-3111.

Brown, L. E., Trought, K. R., Bailey, C. I., and Clemons, J. H. (2005). 2, 3, 7, 8-TCDD equivalence and mutagenic activity associated with PM_{10} from three urban locations in New Zealand. *Science of the Total Environment*, *349*(1), 161-174.

Burrows, S. M., Elbert, W., Lawrence, M. G., and Pöschl, U. (2009). Bacteria in the global atmosphere–Part 1: Review and synthesis of literature data for different ecosystems. *Atmospheric Chemistry and Physics*, *9*(23), 9263-9280.

Campbell, J. R., Welton, E. J., Spinhirne, J. D., Ji, Q., Tsay, S. C., Piketh, S. J., ... and Holben, B. N. (2003). Micropulse lidar observations of tropospheric aerosols over northeastern South Africa during the ARREX and SAFARI 2000 dry season experiments. *Journal of Geophysical Research: Atmospheres (1984–2012)*, *108*(D13).

Chadwick, O. A., Derry, L. A., Vitousek, P. M., Huebert, B. J., and Hedin, L. O. (1999). Changing sources of nutrients during four million years of ecosystem development. *Nature*, *397*(6719), 491-497.

Chaloulakou, A., Kassomenos, P., Spyrellis, N., Demokritou, P., and Koutrakis, P. (2003). Measurements of PM_{10} and $PM_{2.5}$ particle concentrations in Athens, Greece. *Atmospheric Environment*, *37*(5), 649-660.

Charron, A., Harrison, R. M., and Quincey, P. (2007). What are the sources and conditions responsible for exceedences of the 24h PM_{10} limit value ($50\mu g/m^3$) at a heavily trafficked London site? *Atmospheric Environment*, *41*(9), 1960-1975.

Chen, Y., and Xie, S. D. (2013). Long-term trends and characteristics of visibility in two megacities in southwest China: Chengdu and Chongqing. *Journal of the Air and Waste Management Association*, *63*(9), 1058-1069.

Chu, D. A., Kaufman, Y. J., Ichoku, C., Remer, L. A., Tanré, D., and Holben, B. N. (2002). Validation of MODIS aerosol optical depth retrieval over land. *Geophysical research letters*, *29*(12), MOD2-1.

Cohen, A. J., Ross Anderson, H., Ostro, B., Pandey, K. D., Krzyzanowski, M., Künzli, N., ... and Smith, K. (2005). The global burden of disease due to outdoor air pollution. *Journal of Toxicology and Environmental Health, Part A*, *68*(13-14), 1301-1307.

Cohen, A. J., Anderson, H. R., Ostro, B., Pandey, K. D., Krzyzanowski, M., Künzli, N., ... and Smith, K. R. (2004). Urban Air Pollution. In *Comparative Quantification of Health Risks: Global and Regional Burden of Disease Attributable to Selected Major Risk Favors, Vol. 2;* Ezzati, M.; Lopez, A.D.; Rodgers, A.; Murray, C.J.L., Eds.; World Health Organization: Geneva, Switzerland, 2004; pp 1353–1433

Cohen, B. (2006). Urbanization in developing countries: Current trends, future projections, and key challenges for sustainability. *Technology in Society*, *28*(1), 63-80.

Cole, S (2016). NASA selects instruments to study air pollution, tropical cyclones (2016, March 11), Retrieved from http://phys.org/news/2016-03-nasa-instruments-air-pollution-tropical.html, Accessed 24 July 2016.

Cosijn, C., and Tyson, P. (1996). Stable discontinuities in the atmosphere over South Africa. *South African Journal of Science*, *92*(8), 381-386.

Curier, R. L., Veefkind, J. P., Braak, R., Veihelmann, B., Torres, O., and De Leeuw, G. (2008). Retrieval of aerosol optical properties from OMI radiances using a multiwavelength algorithm: Application to Western Europe. *Journal of Geophysical Research: Atmospheres (1984–2012)*, *113*(D17).

Dai, T., Goto, D., Schutgens, N. A. J., Dong, X., Shi, G., and Nakajima, T. (2014). Simulated aerosol key optical properties over global scale using an aerosol transport model coupled with a new type of dynamic core. *Atmospheric Environment*, *82*, 71-82.

Dawson, J. P., Adams, P. J., and Pandis, S. N. (2007). Sensitivity of $PM_{2.5}$ to climate in the Eastern US: a modeling case study. *Atmospheric chemistry and physics*, *7*(16), 4295-4309.

de Almeida Castanho, A. D., Vanderlei Martins, J., and Artaxo, P. (2008). MODIS aerosol optical depth retrievals with high spatial resolution over an urban area using the critical reflectance. *Journal of Geophysical Research: Atmospheres (1984–2012)*, *113*(D2).

Deguillaume, L., Leriche, M., Amato, P., Ariya, P. A., Delort, A. M., Pöschl, U., ... and Morris, C. E. (2008). Microbiology and atmospheric processes: chemical interactions of primary biological aerosols. *Biogeosciences*, *5*, 1073-1084.

Department of Environmental Affairs (2009). National Environmental Management Air Quality Act, 2004 (Act no 39 of 2004) National Ambient Air Quality Standards. Government Gazette, no 32816.

Department of Environmental Affairs (2012). National Environmental Management Air Quality Act, 2004 (Act no 39 of 2004) National Ambient Air Quality Standard for Particulate Matter with Aerodynamic Diameter Less than 2.5 micron metres ($PM_{2.5}$). Government Gazette, no 35463.

Department of Environmental Affairs (2013). National Environmental Management Air Quality Act, 2004 (Act no 39 of 2004) National Dust Regulations. Government Gazette, no 36974.

Department of Environmental Affairs (2015). South African Air Quality Information System. Retrieved from http://www.saaqis.org.za/Mashup.aspx. Accessed 24 June 2015.

(DEADP) Department of Environmental Affairs and Development Planning (2012a). Air Quality Monitoring Monthly Report. Retrieved from https://www.westerncape.gov.za/assets/departments/environmental-affairs-development-planning/RN-120149-WCP-Monthly-Report-January-2012-Malmesbury-2012-04-30-AMENDED.pdf. Accessed 9 October 2012.

(DEADP) Department of Environmental Affairs and Development Planning (2012b). Air Quality Monitoring Monthly Report. Retrieved from https://www.westerncape.gov.za/assets/departments/environmental-affairs-

development-planning/RN-120162-WCP-Monthly-Report-January-2012-George-2012-04-30.pdf. Accessed 9 October 2012.

Denman, K. L., Brasseur, G., Chidthaisong, A., Ciais, P., Cox, P. M., Dickinson, R. E., ., ... Wofsy, S. C., and Zhang, X.: Couplings Between Changes in the Climate System and Biogeochemistry, *in: Climate Change 2007: The Physical Science Basis. Contribution of Working Group I to the Fourth Assessment Report of the Intergovernmental Panel on Climate Change* [Solomon, S., D. Qin, M. Manning, Z. Chen, M. Marquis, K.B. Averyt, M.Tignor and H.L. Miller (eds.)]. Cambridge University Press, Cambridge, United Kingdom and New York, NY, USA.

Dentener, F. J., Carmichael, G. R., Zhang, Y., Lelieveld, J., and Crutzen, P. J. (1996). Role of mineral aerosol as a reactive surface in the global troposphere. *Journal of Geophysical Research: Atmospheres*, *101*(D17), 22869-22889.

Diab, R. D., Rahman, M. Z., Moorgawa, A., and Freiman, M. T. (2003). First measurements of tropospheric aerosol profiles above Durban using a LIDAR: research letters. *South African Journal of Science*, *99*(3 and 4), p-168.

Diner, D. J., Abdou, W. A., Ackerman, T. P., Crean, K., Gordon, H. R., Kahn, R. A., ... and West, R.A. (2008). Level 2 aerosol retrieval algorithm theoretical basis. *Jet Propulsion Laboratory, California Institute of Technology*.

Diner, D. J., Abdou, W. A., Bruegge, C. J., Conel, J. E., Crean, K. A., Gaitley, B. J., ... and Holben, B. N. (2001). MISR aerosol optical depth retrievals over Southern Africa during the SAFARI-2000 dry season campaign. *Geophysical Research Letters*, *28*(16), 3127-3130.

Dinoi, A., Perrone, M. R., and Burlizzi, P. (2010). Application of MODIS products for air quality studies over Southeastern Italy. *Remote Sensing*, *2*(7), 1767-1796.

Elias, T., Piketh, S. J., Burger, R., and Silva, A. M. (2003). Exploring the potential of combining column-integrated atmospheric polarization with airborne *in situ* size distribution measurements for the retrieval of an aerosol model: A case study of a biomass burning plume during SAFARI 2000. *Journal of Geophysical Research: Atmospheres (1984–2012)*, *108*(D13).

Eliseev, A. V. (2015). Impact of tropospheric sulphate aerosols on the terrestrial carbon cycle. *Global and Planetary Change*, *124*, 30-40.

Ellison, G. B., Tuck, A. F., and Vaida, V. (1999). Atmospheric processing of organic aerosols. *Journal of Geophysical Research: Atmospheres*, *104*(D9), 11633-11641.

Elminir, H. K. (2007). Relative influence of air pollutants and weather conditions on solar radiation–Part 1: Relationship of air pollutants with weather conditions. *Meteorology and Atmospheric Physics*, *96*(3-4), 245-256.

Emeis, S. (2010). *Surface-based remote sensing of the atmospheric boundary layer* (Vol. 40). Springer Science and Business Media.

Emili, E., Popp, C., Petitta, M., Riffler, M., Wunderle, S., and Zebisch, M. (2010). PM 10 remote sensing from geostationary SEVIRI and polar-orbiting MODIS sensors over the complex terrain of the European Alpine region. *Remote Sensing of Environment*, *114*(11), 2485-2499.

Emili, E., Popp, C., Wunderle, S., Zebisch, M., and Petitta, M. (2011). Mapping particulate matter in alpine regions with satellite and ground-based measurements: An exploratory study for data assimilation. *Atmospheric Environment*, *45*(26), 4344-4353.

Engelbrecht, J. P., Swanepoel, L., Zunckel, M., Chow, J. C., Watson, J. G., and Egami, R. T. (2000). Modelling PM_{10} aerosol data from the Qalabotjha low-smoke fuels macro-scale experiment in South Africa. *Ecological modelling*, *127*(2), 235-244.

Engelbrecht, J. P., Swanepoel, L., Chow, J. C., Watson, J. G., and Egami, R. T. (2001). $PM_{2.5}$ and PM_{10} concentrations from the Qalabotjha low-smoke fuels macro-scale experiment in South Africa. *Environmental Monitoring and Assessment*, *69*(1), 1-15.

Engel-Cox, J. A., Holloman, C. H., Coutant, B. W., and Hoff, R. M. (2004). Qualitative and quantitative evaluation of MODIS satellite sensor data for regional and urban scale air quality. *Atmospheric Environment*, *38*(16), 2495-2509.

Engler, C., Birmili, W., Spindler, G., and Wiedensohler, A. (2012). Analysis of exceedances in the daily PM_{10} mass concentration (50 $\mu g/m^3$) at a roadside station in Leipzig, Germany. *Atmospheric Chemistry and Physics*, *12*(21), 10107-10123.

Escudero, M., Querol, X., Ávila, A., and Cuevas, E. (2007). Origin of the exceedances of the European daily PM limit value in regional background areas of Spain. *Atmospheric Environment*, *41*(4), 730-744.

Estelles, V., Martínez-Lozano, J. A., Pey, J., Sicard, M., Querol, X., Esteve, A. R., ... and Rocadenbosch, F. (2012). Study of the correlation between columnar aerosol burden, suspended matter at ground and chemical components in a background European environment. *Journal of Geophysical Research: Atmospheres (1984–2012)*, *117*(D4).

Fajersztajn, L., Veras, M., Barrozo, L. V., and Saldiva, P. (2013). Air pollution: a potentially modifiable risk factor for lung cancer. *Nature Reviews Cancer*, *13*(9), 674-678.

Faling, W., Tempelhoff, J. W., and Van Niekerk, D. (2012). Rhetoric or action: Are South African municipalities planning for climate change? *Development Southern Africa*, *29*(2), 241-257.

Formenti, P., Winkler, H., Fourie, P., Piketh, S., Makgopa, B., Helas, G., and Andreae, M. O. (2002). Aerosol optical depth over a remote semi-arid region of South Africa from spectral measurements of the daytime solar extinction and the nighttime stellar extinction. *Atmospheric Research*, *62*(1), 11-32.

Forster, P., Ramaswamy, V., Artaxo, P., Berntsen, T., Betts, R., Fahey, D. W., ... and Van Dorland, R. (2007). Changes in Atmospheric Constituents and in Radiative Forcing. *In: Climate Change 2007:The Physical Science Basis. Contribution of Working Group I to the Fourth Assessment Report of the Intergovernmental Panel on Climate Change* [Solomon, S., D. Qin, M. Manning, Z. Chen, M. Marquis, K.B. Averyt, M.Tignor and H.L. Miller (eds.)]. Cambridge University Press, Cambridge, United Kingdom and New York, NY, USA.

Fouche, I. (2007). *Assessing the use of GIS in the poverty alleviation strategy of the West Coast District Municipality* (Doctoral dissertation, Stellenbosch: Stellenbosch University).

Freiman, M. T., and Piketh, S. J. (2003). Air transport into and out of the industrial Highveld region of South Africa. *Journal of Applied Meteorology*, *42*(7), 994-1002.

Galindo, N., Varea, M., Gil-Moltó, J., Yubero, E., and Nicolás, J. (2011). The influence of meteorology on particulate matter concentrations at an urban Mediterranean location. *Water, Air, and Soil Pollution*, *215*(1-4), 365-372.

Garland, RM and Sivakumar, V. 2012. Exploring the relationship between monitored ground-based and satellite aerosol measurements over the City of Johannesburg. South African Society for Atmospheric Sciences Annual Conference, Cape Town, 26-27 September 2012.

Garratt, J. R. (1992). The atmospheric boundary layer, Cambridge atmospheric and space science series. *Cambridge University Press, Cambridge*, *416*, 444.

Giorio, C., Tapparo, A., Scapellato, M. L., Carrieri, M., Apostoli, P., and Bartolucci, G. B. (2013). Field comparison of a personal cascade impactor sampler, an optical particle counter and CEN-EU standard methods for PM_{10}, $PM_{2.5}$ and PM_1 measurement in urban environment. *Journal of Aerosol Science*, *65*, 111-120.

Gogoi, M. M., Bhuyan, P. K., and Krishna Moorthy, K. (2008, June). Estimation of the effect of long-range transport on seasonal variation of aerosols over northeastern India. In *Annales Geophysicae* (Vol. 26, No. 6, pp. 1365-1377). European Geosciences Union.

Gounden, Y. (2010). *Ambient sulphur dioxide (SO_2) and particulate matter (PM_{10}) concentrations measured in selected communities of north and south Durban* (Doctoral dissertation, Durban: University of KwaZulu-Natal).

Gramsch, E., Cereceda-Balic, F., Oyola, P., and Von Baer, D. (2006). Examination of pollution trends in Santiago de Chile with cluster analysis of PM_{10} and Ozone data. *Atmospheric Environment*, *40*(28), 5464-5475.

Grgurić, S., Križan, J., Gašparac, G., Antonić, O., Špirić, Z., Mamouri, R., ... and Fedra, K. (2014). Relationship between MODIS based aerosol optical depth and PM_{10} over Croatia. *Open Geosciences*, *6*(1), 2-16.

Grivas, G., Chaloulakou, A., Samara, C., and Spyrellis, N. (2004). Spatial and temporal variation of PM_{10} mass concentrations within the greater area of Athens, Greece. *Water, Air, and Soil Pollution*, *158*(1), 357-371.

Grivas, G., and Chaloulakou, A. (2006). Artificial neural network models for prediction of PM_{10} hourly concentrations, in the Greater Area of Athens, Greece. *Atmospheric Environment*, *40*(7), 1216-1229.

Grivas, G., Chaloulakou, A., and Kassomenos, P. (2008). An overview of the PM_{10} pollution problem, in the metropolitan area of Athens, Greece. Assessment of controlling factors and potential impact of long range transport. *Science of the Total Environment*, *389*(1), 165-177.

Grythe, H., Ström, J., Krejci, R., Quinn, P., and Stohl, A. (2014). A review of sea-spray aerosol source functions using a large global set of sea salt aerosol concentration measurements. *Atmospheric Chemistry and Physics*, *14*(3), 1277-1297.

Guenther, A., Hewitt, C. N., Erickson, D., Fall, R., Geron, C., Graedel, T., ... and Pierce, T. (1995). A global model of natural volatile organic compound emissions. *Journal of Geophysical Research: Atmospheres (1984–2012)*, *100*(D5), 8873-8892.

Guo, J. P., Zhang, X. Y., Che, H. Z., Gong, S. L., An, X., Cao, C. X., ... and Xue, M. (2009). Correlation between PM concentrations and aerosol optical depth in eastern China. *Atmospheric Environment*, *43*(37), 5876-5886.

Gupta, P., and Christopher, S. A. (2008). Seven year particulate matter air quality assessment from surface and satellite measurements. *Atmospheric Chemistry and Physics*, *8*(12), 3311-3324.

Gupta, P., and Christopher, S. A. (2009). Particulate matter air quality assessment using integrated surface, satellite, and meteorological products: Multiple regression approach. *Journal of Geophysical Research: Atmospheres (1984–2012)*, *114*(D14).

Gwaze, P., Helas, G., Annegarn, H. J., Huth, J., and Piketh, S. J. (2007). Physical, chemical and optical properties of aerosol particles collected over Cape Town during winter haze episodes. *South African Journal of Science*, *103*(1/2), 35.

Hadjimitsis, D. G. (2009). Aerosol optical thickness (AOT) retrieval over land using satellite image-based algorithm. *Air Quality, Atmosphere and Health*, *2*(2), 89-97.

Hadjimitsis, D. G., and Clayton, C. (2009). Determination of aerosol optical thickness through the derivation of an atmospheric correction for short-wavelength Landsat TM

and ASTER image data: an application to areas located in the vicinity of airports at UK and Cyprus. *Applied Geomatics*, *1*(1-2), 31-40.

Halpern, A. B. W., and Meadows, M. E. (2013). Fifty years of land use change in the Swartland, Western Cape, South Africa: characteristics, causes and consequences. *South African Geographical Journal*, *95*(1), 38-49.

Hamilton, J. F., Webb, P. J., Lewis, A. C., Hopkins, J. R., Smith, S., and Davy, P. (2004). Partially oxidised organic components in urban aerosol using GCXGC-TOF/MS. *Atmospheric Chemistry and Physics*, *4*(5), 1279-1290.

Han, Q., and Zender, C. S. (2010). Desert dust aerosol age characterized by mass-age tracking of tracers. *Journal of Geophysical Research: Atmospheres (1984–2012)*, *115*(D22).

Harbula, J., Tuček, P., and Pechanec, V. (2010). Dependence of PM_{10} particles concentration on aerosol optical thickness value from the MODIS data. *Proc. Sympozium GIS Ostrava*.

Harrison, R. M., Yin, J., Mark, D., Stedman, J., Appleby, R. S., Booker, J., and Moorcroft, S. (2001). Studies of the coarse particle (2.5–10μm) component in UK urban atmospheres. *Atmospheric Environment*, *35*(21), 3667-3679.

Haywood, J., and Boucher, O. (2000). Estimates of the direct and indirect radiative forcing due to tropospheric aerosols: A review. *Reviews of Geophysics*, *38*(4), 513-543.

Haywood, J. M., and Shine, K. P. (1995). The effect of anthropogenic sulfate and soot aerosol on the clear sky planetary radiation budget. *Geophysical Research Letters*, *22*(5), 603-606.

Heal, M. R., Beverland, I. J., McCabe, M., Hepburn, W., and Agius, R. M. (2000). Intercomparison of five PM_{10} monitoring devices and the implications for exposure measurement in epidemiological research. *Journal of Environmental Monitoring*, *2*(5), 455-461.

Hersey, S. P., Garland, R. M., Crosbie, E., Shingler, T., Sorooshian, A., Piketh, S., and Burger, R. (2015). An overview of regional and local characteristics of aerosols in South Africa using satellite, ground, and modeling data. *Atmospheric Chemistry and Physics*, *15*(8), 4259-4278.

Hien, P. D., Bac, V. T., Tham, H. C., Nhan, D. D., and Vinh, L. D. (2002). Influence of meteorological conditions on $PM_{2.5}$ and $PM_{2.5-10}$ concentrations during the monsoon season in Hanoi, Vietnam. *Atmospheric Environment*, *36*(21), 3473-3484.

Higgs, G., Sterling, D. A., Aryal, S., Vemulapalli, A., Priftis, K. N., and Sifakis, N. I. (2015). Aerosol optical depth as a measure of particulate exposure using imputed censored data, and relationship with childhood asthma hospital admissions for 2004 in Athens, Greece. *Environmental Health Insights*, *9*(Suppl 1), 27.

Hirsikko, A., Vakkari, V., Tiitta, P., Manninen, H. E., Gagné, S., Laakso, H., ... and Laakso, L. (2012). Characterisation of sub-micron particle number concentrations and formation events in the western Bushveld Igneous Complex, South Africa. *Atmospheric Chemistry and Physics*, *12*(9), 3951-3967.

Hoff, R. M., & Christopher, S. A. (2009). Remote sensing of particulate pollution from space: have we reached the promised land?. Journal of the Air & Waste Management Association, 59(6), 645-675.

Holben, B. N., Eck, T. F., Slutsker, I., Tanre, D., Buis, J. P., Setzer, A., ... and Lavenu, F. (1998). AERONET—A federated instrument network and data archive for aerosol characterization. *Remote sensing of Environment*, *66*(1), 1-16.

Holmes, N. S., and Morawska, L. (2006). A review of dispersion modelling and its application to the dispersion of particles: an overview of different dispersion models available. *Atmospheric Environment*, *40*(30), 5902-5928.

Hsu, N. C., Gautam, R., Sayer, A. M., Bettenhausen, C., Li, C., Jeong, M. J., ... and Holben, B. N. (2012). Global and regional trends of aerosol optical depth over land and ocean using SeaWiFS measurements from 1997 to 2010. *Atmospheric Chemistry and Physics*, *12*(17), 8037-8053.

Hu, H., Li, X., Zhang, Y., and Li, T. (2006). Determination of the refractive index and size distribution of aerosol from dual-scattering-angle optical particle counter measurements. *Applied Optics*, *45*(16), 3864-3870.

Huang, X. F., Yu, J. Z., Yuan, Z., Lau, A. K., and Louie, P. K. (2009). Source analysis of high particulate matter days in Hong Kong. *Atmospheric Environment*, *43*(6), 1196-1203.

Huang, X., Yang, P., Kattawar, G., and Liou, K. N. (2015). Effect of mineral dust aerosol aspect ratio on polarized reflectance. *Journal of Quantitative Spectroscopy and Radiative Transfer*, *151*, 97-109.

Hutchison, K. D., Smith, S., & Faruqui, S. J. (2005). Correlating MODIS aerosol optical thickness data with ground-based PM 2.5 observations across Texas for use in a real-time air quality prediction system. Atmospheric Environment, 39(37), 7190-7203.

Hyvärinen, A. P., Raatikainen, T., Brus, D., Komppula, M., Panwar, T. S., Hooda, R. K., ... and Lihavainen, H. (2011). Effect of the summer monsoon on aerosols at two measurement stations in Northern India- Part 1: PM and BC concentrations. *Atmospheric Chemistry and Physics*, *11*(16), 8271-8282

Ichoku, C., Chu, D. A., Mattoo, S., Kaufman, Y. J., Remer, L. A., Tanré, D., ... and Holben, B. N. (2002). A spatio-temporal approach for global validation and analysis of MODIS aerosol products. *Geophysical Research Letters*, *29*(12), MOD1-1.

Ichoku, C., Remer, L. A., Kaufman, Y. J., Levy, R., Chu, D. A., Tanré, D., and Holben, B. N. (2003). MODIS observation of aerosols and estimation of aerosol radiative forcing over southern Africa during SAFARI 2000. *Journal of Geophysical Research: Atmospheres (1984–2012)*, *108*(D13).

Ichoku, C., Remer, L. A., and Eck, T. F. (2005). Quantitative evaluation and intercomparison of morning and afternoon Moderate Resolution Imaging Spectroradiometer (MODIS) aerosol measurements from Terra and Aqua. *Journal of Geophysical Research: Atmospheres (1984–2012)*, *110*(D10).

Im, U., Markakis, K., Koçak, M., Gerasopoulos, E., Daskalakis, N., Mihalopoulos, N., ... and Kanakidou, M. (2012). Summertime aerosol chemical composition in the Eastern Mediterranean and its sensitivity to temperature. *Atmospheric Environment*, *50*, 164-173.

Jacob, D. J. (2000). Heterogeneous chemistry and tropospheric ozone. *Atmospheric Environment*, *34*(12), 2131-2159.

Jennings, C. A. (2013). *Estimating PM$_{2.5}$ concentrations using MODIS and meteorological measurements for the San Francisco bay area* (Doctoral dissertation, San Francisco, San Francisco State University).

Jerez, S. B., Zhang, Y., McClure, J. W., Jacobson, L., Heber, A., Hoff, S., ... and Beasley, D. (2006). Comparison of measured total suspended particulate matter concentrations using tapered element oscillating microbalance and a total suspended particulate sampler. *Journal of the Air and Waste Management Association*, *56*(3), 261-270.

Jerrett, M., Arain, A., Kanaroglou, P., Beckerman, B., Potoglou, D., Sahsuvaroglu, T., ... and Giovis, C. (2005). A review and evaluation of intraurban air pollution exposure models. *Journal of Exposure Science and Environmental Epidemiology*, *15*(2), 185-204.

Jiang, X., Liu, Y., Yu, B., and Jiang, M. (2007). Comparison of MISR aerosol optical thickness with AERONET measurements in Beijing metropolitan area. *Remote Sensing of Environment*, *107*(1), 45-53.

Jickells, T. D., An, Z. S., Andersen, K. K., Baker, A. R., Bergametti, G., Brooks, N., ... and Kawahata, H. (2005). Global iron connections between desert dust, ocean biogeochemistry, and climate. *Science*, *308*(5718), 67-71.

Jones, C., Mahowald, N., and Luo, C. (2004). Observational evidence of African desert dust intensification of easterly waves. *Geophysical Research Letters*, *31*(17).

Juneng, L., Latif, M. T., and Tangang, F. (2011). Factors influencing the variations of PM$_{10}$ aerosol dust in Klang Valley, Malaysia during the summer. *Atmospheric Environment*, *45*(26), 4370-4378.

Jury, M., Tegen, A., Ngeleza, E., and Dutoit, M. (1990). Winter air pollution episodes over Cape Town. *Boundary-Layer Meteorology*, *53*(1-2), 1-20.

Justice, E., Huston, L., Krauth, D., Mack, J., Oza, S., Strawa, A. W., ... and Schmidt, C. (2009, October). Investigating correlations between satellite-derived aerosol optical depth and ground PM$_{2.5}$ measurements in California's San Joaquin valley with modis deep blue. In *American Society of Photogrammetry and Remote Sensing Annual Conference* (pp. 9-13).

Kahn, R., Nelson, D. L., Garay, M. J., Levy, R. C., Bull, M., Diner, D. J., ... and Remer, L. (2009). MISR aerosol product attributes and statistical comparisons with MODIS. *Geoscience and Remote Sensing, IEEE Transactions on*, *47*(12), 4095-4114.

Kanakidou, M., Seinfeld, J. H., Pandis, S. N., Barnes, I., Dentener, F. J., Facchini, M. C., ... and Swietlicki, E. (2005). Organic aerosol and global climate modelling: a review. *Atmospheric Chemistry and Physics*, *5*(4), 1053-1123.

Kanitz, T., Ansmann, A., Seifert, P., Engelmann, R., Kalisch, J., and Althausen, D. (2013). Radiative effect of aerosols above the northern and southern Atlantic Ocean as determined from shipborne lidar observations. *Journal of Geophysical Research: Atmospheres*, *118*(22), 12-556.

Kaonga, B., and Kgabi, N. A. (2011). Investigation into presence of atmospheric particulate matter in Marikana, mining area in Rustenburg Town, South Africa. *Environmental Monitoring and Assessment*, *178*(1-4), 213-220.

Kaskaoutis, D. G., Kosmopoulos, P., Kambezidis, H. D., and Nastos, P. T. (2007). Aerosol climatology and discrimination of different types over Athens, Greece, based on MODIS data. *Atmospheric Environment*, *41*(34), 7315-7329.

Kaskaoutis, D.G., Kambezidis, H.D., Nastos, P.T. and Kosmopoulos, P.G., 2008. Study on an intense dust storm over Greece. *Atmospheric Environment*, *42*(29), pp.6884-6896.

Kaskaoutis, D. G., Sifakis, N., Retalis, A., and Kambezidis, H. D. (2010). Aerosol monitoring over Athens using satellite and ground-based measurements. *Advances in Meteorology*, *2010*.

Kassomenos, P. A., Kelessis, A., Paschalidou, A. K., and Petrakakis, M. (2011). Identification of sources and processes affecting particulate pollution in Thessaloniki, Greece. *Atmospheric Environment*, *45*(39), 7293-7300.

Kassomenos, P., Vardoulakis, S., Chaloulakou, A., Grivas, G., Borge, R., and Lumbreras, J. (2012). Levels, sources and seasonality of coarse particles ($PM_{10} - PM_{2.5}$) in three European capitals–Implications for particulate pollution control. *Atmospheric Environment*, *54*, 337-347.

Kaufman, Y. J., Tanré, D., and Boucher, O. (2002). A satellite view of aerosols in the climate system. *Nature*, *419*(6903), 215-223.

Kgabi, N. A., Pienaar, J. J., and Kulmala, M. (2006). Sources of atmospheric pollutants in the North West province of South Africa: a case of the Rustenburg municipality. *Management of Natural Resources, Sustainable Development and Ecological Hazards, Brebbia CA, Conti ME &Tiezzi E (Eds.), WIT Transactions on Ecology and the Environment, Southampton*, 599-608.

Kim, H. S., Chung, Y. S., and Lee, S. G. (2013). Analysis of spatial and seasonal distributions of MODIS aerosol optical properties and ground-based measurements of mass concentrations in the Yellow Sea region in 2009. *Environmental Monitoring and Assessment*, *185*(1), 369-382.

Kim, S. W., Yoon, S. C., Dutton, E. G., Kim, J., Wehrli, C., and Holben, B. N. (2008). Global surface-based sun photometer network for long-term observations of column aerosol optical properties: intercomparison of aerosol optical depth. *Aerosol Science and Technology*, *42*(1), 1-9.

Kittaka, C., Winker, D. M., Vaughan, M. A., Omar, A., and Remer, L. A. (2011). Intercomparison of column aerosol optical depths from CALIPSO and MODIS-Aqua. *Atmospheric Measurement Techniques*, *4*(2), 131-141.

Klimont, Z., Smith, S. J., and Cofala, J. (2013). The last decade of global anthropogenic sulfur dioxide: 2000–2011 emissions. *Environmental Research Letters*, *8*(1), 014003.

Koçak, M., Theodosi, C., Zarmpas, P., Im, U., Bougiatioti, A., Yenigun, O., and Mihalopoulos, N. (2011). Particulate matter (PM_{10}) in Istanbul: origin, source areas and potential impact on surrounding regions. *Atmospheric Environment*, *45*(38), 6891-6900.

Koelemeijer, R. B. A., Homan, C. D., and Matthijsen, J. (2006). Comparison of spatial and temporal variations of aerosol optical thickness and particulate matter over Europe. *Atmospheric Environment*, *40*(27), 5304-5315.

Kokhanovsky, A. A., Breon, F. M., Cacciari, A., Carboni, E., Diner, D., Di Nicolantonio, W., ... and Li, Z. (2007). Aerosol remote sensing over land: A comparison of satellite retrievals using different algorithms and instruments. *Atmospheric Research*, *85*(3), 372-394.

Kokhanovsky, A. A., Curier, R. L., De Leeuw, G., Grey, W. M. F., Lee, K. H., Bennouna, Y., ... and North, P. R. J. (2009). The inter-comparison of AATSR dual-view aerosol

optical thickness retrievals with results from various algorithms and instruments. *International Journal of Remote Sensing*, *30*(17), 4525-4537.

Kolmonen, P., Sundström, A. M., Sogacheva, L., Rodriguez, E., Virtanen, T., and Leeuw, G. D. (2013). Uncertainty characterization of AOD for the AATSR dual and single view retrieval algorithms. *Atmospheric Measurement Techniques Discussions*, *6*(2), 4039-4075.

Krieger, U. K., Rupp, S., Hausammann, E., and Peter, T. (2007). Simultaneous Measurements of PM_{10} and PM_1 using a single TEOM#. *Aerosol Science and Technology*, *41*(11), 975-980.

Ku, B., and Park, R. J. (2013). Comparative inverse analysis of satellite (MODIS) and ground (PM_{10}) observations to estimate dust emissions in East Asia. *Asia-Pacific Journal of Atmospheric Sciences*, *49*(1), 3-17.

Kumar, K. R., Sivakumar, V., Reddy, R. R., Gopal, K. R., and Adesina, A. J. (2014). Identification and classification of different aerosol types over a subtropical rural site in Mpumalanga, South Africa: seasonal variations as retrieved from the AERONET Sunphotometer. *Aerosol and Air Quality Research*, *14*(1), 108-123.

Kumar, N., Chu, A., and Foster, A. (2007). An empirical relationship between $PM_{2.5}$ and aerosol optical depth in Delhi Metropolitan. *Atmospheric Environment*, *41*(21), 4492-4503.

Kumar, N., Chu, A., and Foster, A. (2008). Remote sensing of ambient particles in Delhi and its environs: estimation and validation. *International Journal of Remote Sensing*, *29*(12), 3383-3405.

Kuppen, M. (1996). *On the interaction of laser beams with air: With specific reference to refraction and scattering* (Doctoral dissertation, Durban, University of Natal).

Laakso, L., Vakkari, V., Virkkula, A., Laakso, H., Backman, J., Kulmala, M., ... and Kerminen, V. M. (2012). South African EUCAARI measurements: seasonal variation of trace gases and aerosol optical properties. *Atmospheric Chemistry and Physics*, *12*(4), 1847-1864.

Lammel, G., Heil, A., Stemmler, I., Dvorská, A., and Klánová, J. (2013). On the contribution of biomass burning to POPs (PAHs and PCDDs) in air in Africa. *Environmental Science and Technology*, *47*(20), 11616-11624.

Li, H., Faruque, F., Williams, W., Al-Hamdan, M., Luvall, J., Crosson, W., ... & Limaye, A. (2009). Optimal temporal scale for the correlation of AOD and ground measurements of PM 2.5 in a real-time air quality estimation system. Atmospheric Environment, 43(28), 4303-4310.

Levy, R. C., Remer, L. A., Mattoo, S., Vermote, E. F., and Kaufman, Y. J. (2007). Second-generation operational algorithm: Retrieval of aerosol properties over land from inversion of Moderate Resolution Imaging Spectroradiometer spectral reflectance. *Journal of Geophysical Research: Atmospheres (1984–2012)*, *112*(D13).

Levy, R. C., Remer, L. A., Tanré, D., Mattoo, S., and Kaufman, Y. J. (2009). Algorithm for remote sensing of tropospheric aerosol over dark targets from MODIS: Collections 005 and 051: Revision 2; Feb 2009. Retrieved from http://modis-atmos.gsfc.nasa.gov/_docs/ATBD_MOD04_C005_rev2.pdf. Accessed 15 May 2013.

Levy, R. C., Remer, L. A., Kleidman, R. G., Mattoo, S., Ichoku, C., Kahn, R., and Eck, T. F. (2010). Global evaluation of the Collection 5 MODIS dark-target aerosol products over land. *Atmospheric Chemistry and Physics*, *10*(21), 10399-10420.

Lewis, J., De Young, R., and Chu, D. A. (2010). A Study of air quality in the Southeastern Hampton-Norfolk-Virginia Beach region with airborne lidar measurements and MODIS aerosol optical depth retrievals. *Journal of Applied Meteorology and Climatology*, *49*(1), 3-19.

Lim, S. S., Vos, T., Flaxman, A. D., Danaei, G., Shibuya, K., Adair-Rohani, H., ... and Davis, A. (2013). A comparative risk assessment of burden of disease and injury attributable to 67 risk factors and risk factor clusters in 21 regions, 1990–2010: a systematic analysis for the Global Burden of Disease Study 2010. *The Lancet*, *380*(9859), 2224-2260.

Lindesay, J. A., Andreae, M. O., Goldammer, J. G., Harris, G., Annegarn, H. J., Garstang, M., ... and Wilgen, B. V. (1996). International geosphere-biosphere programme/international global atmospheric chemistry SAFARI-92 field experiment: Background and overview. *Journal of Geophysical Research: Atmospheres (1984–2012)*, *101*(D19), 23521-23530.

Liu, G. R., Chen, A. J., Lin, T. H., and Kuo, T. H. (2002). Applying SPOT data to estimate the aerosol optical depth and air quality. *Environmental Modelling and Software*, *17*(1), 3-9.

Liu, Y., Koutrakis, P., Kahn, R., Turquety, S., and Yantosca, R. M. (2007). Estimating fine particulate matter component concentrations and size distributions using satellite-retrieved fractional aerosol optical depth: part 2—a case study. *Journal of the Air and Waste Management Association*, *57*(11), 1360-1369.

Liu, Y., Kahn, R. A., Chaloulakou, A., and Koutrakis, P. (2009). Analysis of the impact of the forest fires in August 2007 on air quality of Athens using multi-sensor aerosol remote sensing data, meteorology and surface observations. *Atmospheric Environment*, *43*(21), 3310-3318.

Llamas, R. M., Bonifaz, R., Valdés, M., Riveros-Rosas, D., and LeyvaContreras, A. (2013). Spatial and temporal variations of atmospheric aerosol optical thickness in northwestern Mexico. *Geofísica internacional*, *52*(4), 321-341.

Lohmann, U., Stier, P., Hoose, C., Ferrachat, S., Kloster, S., Roeckner, E., and Zhang, J. (2007). Cloud microphysics and aerosol indirect effects in the global climate model ECHAM5-HAM. *Atmospheric Chemistry and Physics*, *7*(13), 3425-3446.

Lonati, G., Giugliano, M., and Cernuschi, S. (2006). The role of traffic emissions from weekends' and weekdays' fine PM data in Milan. *Atmospheric Environment*, *40*(31), 5998-6011.

Löndahl, J. (2014). Physical and biological properties of bioaerosols. In *Bioaerosol Detection Technologies* (pp. 33-48). Springer New York.

Lowry, W. P., & Lowry, P. P. (1989). Fundamentals of biometeorology: interactions of organisms and the atmosphere (No. 04; QC981. 7. M5, L6.). Peavine Publications.

Ma, X., Bartlett, K., Harmon, K., and Yu, F. (2013). Comparison of AOD between CALIPSO and MODIS: significant differences over major dust and biomass burning regions. *Atmospheric Measurement Techniques*, *6*(9), 2391-2401.

Maenhaut, W., Salma, I., Cafmeyer, J., Annegarn, H. J., and Andreae, M. O. (1996). Regional atmospheric aerosol composition and sources in the eastern Transvaal, South Africa, and impact of biomass burning. *Journal of Geophysical Research: Atmospheres*, *101*(D19), 23631-23650.

Maenhaut, W., Vermeylen, R., Claeys, M., Vercauteren, J., Matheeussen, C., and Roekens, E. (2012). Assessment of the contribution from wood burning to the PM_{10} aerosol in Flanders, Belgium. *Science of the Total Environment*, *437*, 226-236.

Mahmud, M. (2013). Assessment of atmospheric impacts of biomass open burning in Kalimantan, Borneo during 2004. *Atmospheric Environment*, *78*, 242-249.

Mahowald, N. (2011). Aerosol indirect effect on biogeochemical cycles and climate. *Science*, *334*(6057), 794-796.

Marcazzan, G. M., Vaccaro, S., Valli, G., and Vecchi, R. (2001). Characterisation of PM_{10} and $PM_{2.5}$ particulate matter in the ambient air of Milan (Italy). *Atmospheric Environment*, *35*(27), 4639-4650.

Matsui, H., Koike, M., Kondo, Y., Takegawa, N., Kita, K., Miyazaki, Y., ... and Zaveri, R. A. (2009). Spatial and temporal variations of aerosols around Beijing in summer 2006: Model evaluation and source apportionment. *Journal of Geophysical Research: Atmospheres (1984–2012)*, *114*(D2).

Mauderly, J. L., and Chow, J. C. (2008). Health effects of organic aerosols. *Inhalation Toxicology*, *20*(3), 257-288.

McKendry, I. G. (2000). PM_{10} levels in the Lower Fraser Valley, British Columbia, Canada: an overview of spatiotemporal variations and meteorological controls. *Journal of the Air and Waste Management Association*, *50*(3), 443-452.

Miller, R. L., Perlwitz, J., and Tegen, I. (2004). Feedback upon dust emission by dust radiative forcing through the planetary boundary layer. *Journal of Geophysical Research: Atmospheres*, *109*(D24).

Moodley, G. (2008). *A comparison of Particulate Matter (PM_{10}) in industrially exposed and non-exposed communities* (Masters of Public Health Thesis, Durban, University of KwaZulu-Natal).

Moorgawa, A., Bencherif, H., Michaelis, M. M., Porteneuve, J., and Malinga, S. (2007). The Durban atmospheric LIDAR. *Optics and Laser Technology*, *39*(2), 306-312.

Motallebi, N., Tran, H., Croes, B. E., and Larsen, L. C. (2003). Day-of-week patterns of particulate matter and its chemical components at selected sites in California. *Journal of the Air and Waste Management Association*, *53*(7), 876-888

Moulin, C., and Chiapello, I. (2004). Evidence of the control of summer atmospheric transport of African dust over the Atlantic by Sahel sources from TOMS satellites (1979–2000). *Geophysical research letters*, *31*(2).

Mendez, D., Perez, A. J., Labrador, M., and Marron, J. J. (2011, March). P-sense: A participatory sensing system for air pollution monitoring and control. In *Pervasive Computing and Communications Workshops (PERCOM Workshops), 2011 IEEE International Conference on* (pp. 344-347). IEEE.

Moja, S. J., Mnisi, J. S., Nindi, M. M., and Okonkwo, J. O. (2013). Characterization of PM_{10} samples from Vanderbijlpark in South Africa. *Journal of Environmental Science and Health, Part A*, *48*(1), 99-107.

Molekwa, S. Cutt-off lows over South Africa and their contribution to total rainfall of the Eastern Cape Province. *(Master of Science thesis, Pretoria, University of Pretoria).*

Moreno, T., Querol, X., Alastuey, A., Dos Santos, S. G., and Gibbons, W. (2006). Controlling influences on daily fluctuations of inhalable particles and gas concentrations: local versus regional and exotic atmospheric pollutants at Puertollano, Spain. *Atmospheric Environment*, *40*(17), 3207-3218.

Mugabo, C. (2011). *Ambient air quality in a low income urban area on the South African highveld: a case study of Leandra Township.* (Master of Science in Environmental Sciences thesis, Johannesburg, University of Witwatersrand).

Myhre, G., Shindell, D., Bréon, F. M., Collins, W., Fuglestvedt, J., Huang, J., ... and Zhang, H. (2013). Anthropogenic and Natural Radiative Forcing. In: *Climate Change 2013: The Physical Science Basis. Contribution of Working Group I to the Fifth Assessment Report of the Intergovernmental Panel on Climate Change* [Stocker, T.F., D. Qin, G.-K. Plattner, M. Tignor, S.K. Allen, J. Boschung, A. Nauels, Y. Xia, V. Bex

and P.M. Midgley (eds.)]. Cambridge University Press, Cambridge, United Kingdom and New York, NY, USA.

Naidoo, R. N., Robins, T. G., Batterman, S., Mentz, G., and Jack, C. (2013). Ambient pollution and respiratory outcomes among schoolchildren in Durban, South Africa. *South African Journal of Child Health*, *7*(4), 127-134.

Ningwei, L., Yanjun, M., and Yangfeng, W. (2012, June). Research on the correlations of inhalable particulate matter and atmospheric variables in multi-cities. In *Remote Sensing, Environment and Transportation Engineering (RSETE), 2012 2nd International Conference on* (pp. 1-8). IEEE.

Niyobuhungiro, R. V., and von Blottnitz, H. (2013). Investigation of arsenic airborne in particulate matter around caterers' wood fires in the Cape Town region. *Aerosol and Air Quality Research*, *13*(1), 219-224.

Nordio, F., Kloog, I., Coull, B. A., Chudnovsky, A., Grillo, P., Bertazzi, P. A., ... and Schwartz, J. (2013). Estimating spatio-temporal resolved PM_{10} aerosol mass concentrations using MODIS satellite data and land use regression over Lombardy, Italy. *Atmospheric Environment*, *74*, 227-236.

Oke, T. R. (1982). The energetic basis of the urban heat island. Quarterly Journal of the Royal Meteorological Society, 108(455), 1-24.

Oke, T. R. (1987). *Boundary layer climates*. Routledge.

Onishi, K., Kurosaki, Y., Otani, S., Yoshida, A., Sugimoto, N., and Kurozawa, Y. (2012). Atmospheric transport route determines components of Asian dust and health effects in Japan. *Atmospheric Environment*, *49*, 94-102.

Parkinson, C. L. (2003). Aqua: An Earth-observing satellite mission to examine water and other climate variables. IEEE Transactions on Geoscience and Remote Sensing, 41(2), 173-183.

Penner, J. E., Andreae, M., Annegarn, H., Barrie, L., Feichter, J., Hegg, D., ... Nganga, J., and Pitari, G (2001). Aerosols, their direct and indirect effects. In: *Climate Change 2001: The Scientific Basis. Contribution of Working Group I to the Third Assessment Report of the Intergovernmental Panel on Climate Change* [Houghton, J. T., Ding, Y., Griggs, D. J., Noguer, M., van der Linden, P. J., Dai, X., Maskell, K., and Johnson, C.

A. (eds.)]. Cambridge University Press, Cambridge, United Kingdom and New York, NY, USA.

Piketh, S. J., Annegarn, H. J., and Tyson, P. D. (1999a). Lower tropospheric aerosol loadings over South Africa: The relative contribution of aeolian dust, industrial emissions, and biomass burning. *Journal of Geophysical Research: Atmospheres (1984–2012)*, *104*(D1), 1597-1607.

Piketh, S. J., Swap, R. J., Anderson, C. A., Freiman, M. T., Zunckel, M., and Held, G. (1999b). The Ben Macdhui high altitude trace gas and aerosol transport experiment. *South African Journal of Science*, *95*(1), 35-43.

Poggi, J. M., and Portier, B. (2011). PM_{10} forecasting using clusterwise regression. *Atmospheric Environment*, *45*(38), 7005-7014.

Pool, C. F., and de Ronde, C. (2002). Integration of fire management systems in the Southern Cape region of South Africa. In *Forest fire research and wildland fire safety: proceedings of IV International Conference on Forest Fire Research* (pp. 1-9).

Pope, R., and Wu, J. (2014). Characterizing air pollution patterns on multiple time scales in urban areas: a landscape ecological approach. *Urban Ecosystems*, *17*(3), 855-874.

Popp, C., Hauser, A., Foppa, N., and Wunderle, S. (2007). Remote sensing of aerosol optical depth over central Europe from MSG-SEVIRI data and accuracy assessment with ground-based AERONET measurements. *Journal of Geophysical Research: Atmospheres (1984–2012)*, *112*(D24).

Potts, D. (2009). The slowing of sub-Saharan Africa's urbanization: evidence and implications for urban livelihoods. *Environment and Urbanization*, *21*(1), 253-259.

Prasad, A. K., and Singh, R. P. (2007). Comparison of MISR-MODIS aerosol optical depth over the Indo-Gangetic basin during the winter and summer seasons (2000–2005). *Remote Sensing of Environment*, *107*(1), 109-119.

Preston-Whyte, R. A., and Tyson, P. D. (2004). The weather and climate of Southern Africa. Oxford University Press.

Queface, A. J., Piketh, S. J., Eck, T. F., Tsay, S. C., and Mavume, A. F. (2011). Climatology of aerosol optical properties in Southern Africa. *Atmospheric Environment*, *45*(17), 2910-2921.

Querol, X., Alastuey, A., Rodriguez, S., Plana, F., Ruiz, C. R., Cots, N., ... and Puig, O. (2001). PM_{10} and $PM_{2.5}$ source apportionment in the Barcelona Metropolitan area, Catalonia, Spain. *Atmospheric Environment*, *35*(36), 6407-6419.

Querol, X., Alastuey, A., Rodrıguez, S., Viana, M. M., Artınano, B., Salvador, P., ... and De La Campa, A. S. (2004). Levels of particulate matter in rural, urban and industrial sites in Spain. *Science of the Total Environment*, *334*, 359-376.

Qin, Y., Tonnesen, G. S., & Wang, Z. (2004). Weekend/weekday differences of ozone, NO x, CO, VOCs, PM 10 and the light scatter during ozone season in southern California. *Atmospheric Environment*, *38*(19), 3069-3087.

Ragosta, M., Caggiano, R., Macchiato, M., Sabia, S., and Trippetta, S. (2008). Trace elements in daily collected aerosol: Level characterization and source identification in a four-year study. *Atmospheric Research*, *89*(1), 206-217.

Rajšić, S. F., Tasić, M. D., Novaković, V. T., and Tomašević, M. N. (2004). First assessment of the PM_{10} and $PM_{2.5}$ particulate level in the ambient air of Belgrade city. *Environmental Science and Pollution Research*, *11*(3), 158-164.

Reason, C. J. C., & Jury, M. R. (1990). On the generation and propagation of the Southern African coastal low. *Quarterly Journal of the Royal Meteorological Society*, *116*(495), 1133-1151

Reddy, P., Naidoo, R. N., Robins, T. G., Mentz, G., Li, H., London, S. J., and Batterman, S. (2012). GSTM1 and GSTP1 gene variants and the effect of air pollutants on lung function measures in South African children. *American Journal of Industrial Medicine*, *55*(12), 1078-1086.

Remer, L. A., Kaufman, Y. J., Tanré, D., Mattoo, S., Chu, D. A., Martins, J. V., ... and Eck, T. F. (2005). The MODIS aerosol algorithm, products, and validation. *Journal of the atmospheric sciences*, *62*(4), 947-973.

Remer, L. A., Kleidman, R. G., Levy, R. C., Kaufman, Y. J., Tanré, D., Mattoo, S., ... and Holben, B. N. (2008). Global aerosol climatology from the MODIS satellite sensors. *Journal of Geophysical Research: Atmospheres (1984–2012)*, *113*(D14).

Roberts, G., Wooster, M. J., and Lagoudakis, E. (2009). Annual and diurnal African biomass burning temporal dynamics. *Biogeosciences*, *6*, 849-866.

Rodrıguez, S., Querol, X., Alastuey, A., Kallos, G., and Kakaliagou, O. (2001). Saharan dust contributions to PM_{10} and TSP levels in Southern and Eastern Spain. *Atmospheric Environment*, *35*(14), 2433-2447.

Rohen, G. J., Hoyningen-Huene, W. V., Kokhanovsky, A., Dinter, T., Vountas, M., and Burrows, J. P. (2011). Retrieval of aerosol mass load (PM_{10}) from MERIS/Envisat top of atmosphere spectral reflectance measurements over Germany. *Atmospheric Measurement Techniques*, *4*(3), 523-534.

Rubel, F., and Kottek, M. (2010). Observed and projected climate shifts 1901–2100 depicted by world maps of the Köppen-Geiger climate classification. *Meteorologische Zeitschrift*, *19*(2), 135-141.

Sahan, E., Brink, H. M., and Weijers, E. P. (2008). *Carbon in atmospheric particulate matter*. Energy Research Centre of the Netherlands.

Şahin, Ü. A., Ucan, O. N., Bayat, C., and Tolluoglu, O. (2011). A new approach to prediction of SO_2 and PM_{10} concentrations in Istanbul, Turkey: Cellular Neural Network (CNN). *Environmental Forensics*, *12*(3), 253-269.

Saide, P. E., Carmichael, G. R., Liu, Z., Schwartz, C. S., Lin, H. C., da Silva, A. M., and Hyer, E. (2013). Aerosol optical depth assimilation for a size-resolved sectional model: impacts of observationally constrained, multi-wavelength and fine mode retrievals on regional scale analyses and forecasts. *Atmospheric Chemistry and Physics*, *13*(20), 10425-10444.

Saide, P. E., Kim, J., Song, C. H., Choi, M., Cheng, Y., and Carmichael, G. R. (2014). Assimilation of next generation geostationary aerosol optical depth retrievals to improve air quality simulations. *Geophysical Research Letters*, *41*(24), 9188-9196.

Saliba, N. A., Moussa, S., Salame, H., and El-Fadel, M. (2006). Variation of selected air quality indicators over the city of Beirut, Lebanon: Assessment of emission sources. Atmospheric Environment, 40(18), 3263-3268.

Santer, R. and Ramon, D. (2011). MERIS aerosol remote sensing over land. Retrieved from https://earth.esa.int/documents/700255/2042855/MERIS_ATBD_2.15_v5.0+-+2011.pdf. Accessed online 31 March 2014.

Santer, R., Carrere, V., Dubuisson, P., and Roger, J. C. (1999). Atmospheric correction over land for MERIS. *International Journal of Remote Sensing*, *20*(9), 1819-1840.

Sayer, A. M., Hsu, N. C., Bettenhausen, C., Jeong, M. J., Holben, B. N., and Zhang, J. (2012). Global and regional evaluation of over-land spectral aerosol optical depth retrievals from SeaWiFS. *Atmospheric Measurement Techniques*, *5*(7), 1761-1778.

Schaap, M., Apituley, A., Timmermans, R. M. A., Koelemeijer, R. B. A., and Leeuw, G. D. (2009). Exploring the relation between aerosol optical depth and $PM_{2.5}$ at Cabauw, the Netherlands. *Atmospheric Chemistry and Physics*, *9*(3), 909-925.

Schuster, G. L., Vaughan, M., MacDonnell, D., Su, W., Winker, D., Dubovik, O., ... and Trepte, C. (2012). Comparison of CALIPSO aerosol optical depth retrievals to AERONET measurements, and climatology for the lidar ratio of dust. *Atmospheric Chemistry and Physics*, *12*(16), 7431-7452.

Schwela, D. (2012). Review of Urban Air Quality in Sub-Saharan Africa Region - Air Quality profile of SSA countries. Retrieved from http://www-wds.worldbank.org/external/default/WDSContentServer/WDSP/IB/2012/04/02/000386194_20120402015455/Rendered/PDF/677940WP0P07690020120Box367897B0ACS.pdf. Accessed 6 May 2015.

Seaman, N. L. (2000). Meteorological modeling for air-quality assessments. *Atmospheric Environment*, *34*(12), 2231-2259.

Sgrigna, G., Sæbø, A., Gawronski, S., Popek, R., and Calfapietra, C. (2015). Particulate Matter deposition on Quercus ilex leaves in an industrial city of central Italy. *Environmental Pollution*, *197*, 187-194.

Sharon, T. M., Albrecht, B. A., Jonsson, H. H., Minnis, P., Khaiyer, M. M., van Reken, T. M., ... and Flagan, R. (2006). Aerosol and cloud microphysical characteristics of rifts

and gradients in maritime stratocumulus clouds. *Journal of the Atmospheric Sciences*, *63*(3), 983-997.

Sivakumar, V., Tesfaye, M., Alemu, W., Moema, D., Sharma, A., Bollig, C., and Mengistu, G. (2009). CSIR South Africa mobile LIDAR-First scientific results: comparison with satellite, sun photometer and model simulations. *South African Journal of Science*, *105*(11-12), 449-455.

Sivakumar, V., Tesfaye, M., Alemu, W., Sharma, A., Bollig, C., & Mengistu, G. (2010). Aerosol measurements over South Africa using satellite, sun-photometer and LIDAR. Advances in Geosciences, 16, 253-262.

Smith, K. R., Jerrett, M., Anderson, H. R., Burnett, R. T., Stone, V., Derwent, R., ... and Thurston, G. (2010). Public health benefits of strategies to reduce greenhouse-gas emissions: health implications of short-lived greenhouse pollutants. *The Lancet*, *374*(9707), 2091-2103.

Sogacheva, L., de Leeuw, G., Kolmonen, P., Sundström, A. M., and Rodriques, E. (2010, May). Aerosol Optical Depth over Africa retrieved from AATSR. In *EGU General Assembly Conference Abstracts* (Vol. 12, p. 4825).

Soulakellis, N. A., Sifakis, N. I., Tombrou, M., Sarigiannis, D., and Schaefer, K. (2004). Estimation and mapping of aerosol optical thickness over the city of Brescia-Italy using diachronic and multiangle SPOT-1, SPOT-2 and SPOT-4 Imagery. *Geocarto International*, *19*(4), 57-65.

Spada, M., Jorba, O., Pérez García-Pando, C., Janjic, Z., and Baldasano, J. M. (2013). Modeling and evaluation of the global sea-salt aerosol distribution: sensitivity to size-resolved and sea-surface temperature dependent emission schemes. *Atmospheric Chemistry and Physics*, *13*(23), 11735-11755.

Stein-Zweers, D. Sneep, M. and Veefkind, J.P. (2011). OMAERO README File. Retrieved from http://disc.sci.gsfc.nasa.gov/Aura/data-holdings/OMI/documents/v003/OMAERO_README_V003.doc. . Accessed online 31 March 2014.

Stevens, B. (2013). Aerosols: Uncertain then, irrelevant now. *Nature*, *503*(7474), 47-48.

Stewart, I. D., & Oke, T. R. (2012). Local climate zones for urban temperature studies. Bulletin of the American Meteorological Society, 93(12), 1879-1900.

Stull, R. (2005). The Atmospheric Boundary Layer. Retrieved from ftp://ftp.atmos.washington.edu/debbie/Wallace_Hobbs_Dec19_05_proofs/P732951-Ch09.pdf. Accessed 15 February 2012.

Sorek-Hamer, M., Cohen, A., Levy, R. C., Ziv, B., and Broday, D. M. (2013). Classification of dust days by satellite remotely sensed aerosol products. *International Journal of Remote Sensing*, *34*(8), 2672-2688.

Stocker, T. F., Clarke, G. K. C., LeTreut, H., Lindzen, R. S., Meleshko, V. P., Mugara, R. K., Palmer, T. N., Pierrehumbert, R. T., Sellers, P. J., Trenberth, K. E., and Willebrand, J. (2001): Physical climate processes and feedbacks, *in: Climate Change 2001: The Scientific Basis. Contribution of working group I to the Third Assessment Report of the Intergovernmental Panel on Climate Change* [Houghton, J. T., Ding, Y., Griggs, D. J., Noguer,M., van der Linden, P. J., Dai, X., Maskell, K., and Johnson, C. A. (eds.)]. Cambridge University Press, Cambridge, United Kingdom and New York, NY, USA.

Storelvmo, T., Kristjánsson, J. E., Lohmann, U., Iversen, T., Kirkevåg, A., and Seland, Ø. (2008). Modeling of the Wegener–Bergeron–Findeisen process—implications for aerosol indirect effects. *Environmental Research Letters*, *3*(4), 045001.

Strawa, A. W., Chatfield, R. B., Legg, M., Scarnato, B., and Esswein, R. (2011). Improving $PM_{2.5}$ retrievals in the San Joaquin Valley using A-Train Multi-Satellite Observations. *Atmospheric Chemistry and Physics Discussions*, *11*(11), 30563-30598.

Sukitpaneenit, M., and Oanh, N. T. K. (2014). Satellite monitoring for carbon monoxide and particulate matter during forest fire episodes in Northern Thailand. *Environmental Monitoring and Assessment*, *186*(4), 2495-2504.

Tang, J., Xue, Y., Yu, T., & Guan, Y. (2005). Aerosol optical thickness determination by exploiting the synergy of TERRA and AQUA MODIS. Remote Sensing of Environment, 94(3), 327-334.

Tanimowo, M. O. (2000). Air pollution and respiratory health in Africa: A Review. *East African Medical Journal, 77*(2), 71-75.

Terblanche, D. E., Mittermaier, M. P., Burger, R. P., Piketh, S. J., and Bruintjes, R. T. (2000). The Aerosol Recirculation and Rainfall Experiment (ARREX): an initial study on aerosol-cloud over South Africa. *South African Journal of Science*, *96*(1).

Tesfaye, M., Sivakumar, V., Botai, J., and Mengistu Tsidu, G. (2011). Aerosol climatology over South Africa based on 10 years of Multiangle Imaging Spectroradiometer (MISR) data. *Journal of Geophysical Research: Atmospheres (1984–2012)*, *116*(D20).

Tesfaye, M., Botai, J., Sivakumar, V., and Tsidu, G. M. (2014). Simulation of biomass burning aerosols mass distributions and their direct and semi-direct effects over South Africa using a regional climate model. *Meteorology and Atmospheric Physics*, *125*(3-4), 177-195.

Tesfaye, M., Tsidu, G. M., Botai, J., and Sivakumar, V. (2015). Mineral dust aerosol distributions, its direct and semi-direct effects over South Africa based on regional climate model simulation. *Journal of Arid Environments*, *114*, 22-40.

Tessema, M. A. (2011). *Particulate matter (PM$_{10}$) pollution in Khayelitsha, Cape Town*. (mini thesis, Cape Town, African Institute for Mathematical Sciences).

Thishan Dharshana, K. G., Kravtsov, S., and Kahl, J. D. (2010). Relationship between synoptic weather disturbances and particulate matter air pollution over the United States. *Journal of Geophysical Research: Atmospheres (1984–2012)*, *115*(D24).

Tian, J., and Chen, D. (2010). A semi-empirical model for predicting hourly ground-level fine particulate matter (PM$_{2.5}$) concentration in southern Ontario from satellite remote sensing and ground-based meteorological measurements. *Remote Sensing of Environment*, *114*(2), 221-229.

Toro, R., Canales, M., and Gonzalez-Rojas, C. (2014). Inhaled and inspired particulates in Metropolitan Santiago Chile exceed air quality standards. *Building and Environment*, *79*, 115-123.

Tosca, M. G., Randerson, J. T., and Zender, C. S. (2013). Global impact of smoke aerosols from landscape fires on climate and the Hadley circulation. *Atmospheric Chemistry and Physics*, *13*(10), 5227-5241

Toth, T. D., Zhang, J., Campbell, J. R., Hyer, E. J., Reid, J. S., Shi, Y., and Westphal, D. L. (2014). Impact of data quality and surface-to-column representativeness on the $PM_{2.5}$/satellite AOD relationship for the contiguous United States. *Atmospheric Chemistry and Physics*, *14*(12), 6049-6062.

Triantafyllou, E., and Biskos, G. (2012). Overview of the temporal variation of PM_{10} mass concentrations in the two major cities in Greece: Athens and Thessaloniki. *Global NEST Journal*, *14*(4), 431-441.

Trivedi, D. K., Ali, K., and Beig, G. (2014). Impact of meteorological parameters on the development of fine and coarse particles over Delhi. *Science of the Total Environment*, *478*, 175-183.

Tsay, S. C., Stephens, G. L., and Greenwald, T. J. (1991). An investigation of aerosol microstructure on visual air quality. *Atmospheric Environment. Part A. General Topics*, *25*(5), 1039-1053.

Turns, S. (2006). *Thermal-fluid sciences: an integrated approach* (Vol. 1). Cambridge University Press.

United Nations, Department of Economic and Social Affairs, Population Division (2014). World Urbanization Prospects: The 2014 Revision, Highlights (ST/ESA/SER.A/352).

Vahlsing, C., and Smith, K. R. (2012). Global review of national ambient air quality standards for PM_{10} and SO_2 (24 h). *Air Quality, Atmosphere and Health*, *5*(4), 393-399.

Vakkari, V., Beukes, J. P., Laakso, H., Mabaso, D., Pienaar, J. J., Kulmala, M., and Laakso, L. (2013). Long-term observations of aerosol size distributions in semi-clean and polluted savannah in South Africa. *Atmospheric Chemistry and Physics*, *13*(4), 1751-1770.

van Wilgen, B. W., Forsyth, G. G., and Prins, P. (2012). The management of fire-adapted ecosystems in an urban setting: the case of Table Mountain National Park, South Africa. *Ecology and Society*, *17*(1), 8.

van Zyl, P. G., Beukes, J. P., Du Toit, G., Mabaso, D., Hendriks, J., Vakkari, V., ... and Laakso, L. (2014). Assessment of atmospheric trace metals in the western Bushveld Igneous Complex, South Africa. *South African Journal of Science*, *110*(3-4), 01-10.

Vardoulakis, S., and Kassomenos, P. (2008). Sources and factors affecting PM_{10} levels in two European cities: implications for local air quality management. *Atmospheric Environment*, *42*(17), 3949-3963.

Veefkind, J. P., and de Leeuw, G. (1998). A new algorithm to determine the spectral aerosol optical depth from satellite radiometer measurements. *Journal of Aerosol Science*, *29*(10), 1237-1248.

Venter, A.D. (2011). *Air quality assessment of the industrialized western Bushveld Igneous Complex*. (Master of Science in Chemistry, Potchefstroom, North West University).

Venter, A. D., Vakkari, V., Beukes, J. P., Van Zyl, P. G., Laakso, H., Mabaso, D., ... and Laakso, L. (2012). An air quality assessment in the industrialised western Bushveld Igneous Complex, South Africa. *South African Journal of Science*, *108*(9-10), 1-10.

Vidot, J., Santer, R., and Ramon, D. (2007). Atmospheric particulate matter (PM) estimation from SeaWiFS imagery. *Remote Sensing of Environment*, *111*(1), 1-10.

Wang, J., and Christopher, S. A. (2003). Intercomparison between satellite-derived aerosol optical thickness and $PM_{2.5}$ mass: implications for air quality studies. *Geophysical Research Letters*, *30*(21).

Wang, L., Xin, J., Wang, Y., Li, Z., Wang, P., Liu, G., and Wen, T. (2007). Validation of MODIS aerosol products by CSHNET over China. *Chinese Science Bulletin*, *52*(12), 1708-1718.

Wang, T., Li, S., Shen, Y., Deng, J., and Xie, M. (2010a). Investigations on direct and indirect effect of nitrate on temperature and precipitation in China using a regional climate chemistry modeling system. *Journal of Geophysical Research: Atmospheres (1984–2012)*, *115*(D7).

Wang, Z., Chen, L., Tao, J., Zhang, Y., and Su, L. (2010b). Satellite-based estimation of regional particulate matter (PM) in Beijing using vertical-and-RH correcting method. *Remote Sensing of Environment*, *114*(1), 50-63.

Wang, Z., Liu, Y., Hu, M., Pan, X., Shi, J., Chen, F., ... and Christiani, D. C. (2013). Acute health impacts of airborne particles estimated from satellite remote sensing. *Environment International*, *51*, 150-159.

Wang, C., Zhang, Z., and Yue, S. (2011, November). Correlating aerosol optical thickness measurement with PM$_{10}$ mass concentration in Wuhan area. In *International Conference on Optical Instruments and Technology (OIT2011)* (pp. 82010D-82010D). International Society for Optics and Photonics.

Watson, T. (2014). Environment: breathing trouble. *Nature*, *513*(7517), S14-S15.

Welton, E. J., Voss, K. J., Quinn, P. K., Flatau, P. J., Markowicz, K., Campbell, J. R., ... and Johnson, J. E. (2002). Measurements of aerosol vertical profiles and optical properties during INDOEX 1999 using micropulse lidars. *Journal of Geophysical Research: Atmospheres (1984–2012)*, *107*(D19), INX2-18.

White, N., teWaterNaude, J., van der Walt, A., Ravenscroft, G., Roberts, W., and Ehrlich, R. (2008). Meteorologically estimated exposure but not distance predicts asthma symptoms in schoolchildren in the environs of a petrochemical refinery: a cross-sectional study. *Environmental Health*, *8*, 45-45.

Wichmann, J. (2006). *Probing secondary exposure and health data as a tool to improve public health in South Africa* (Doctoral dissertation, Pretoria, University of Pretoria).

Wichmann, J., and Voyi, K. (2012). Ambient Air Pollution Exposure and Respiratory, Cardiovascular and Cerebrovascular Mortality in Cape Town, South Africa: 2001–2006. *International Journal of Environmental Research and Public Health*, *9*(11), 3978-4016.

Wichmann, J., Wolvaardt, J. E., Maritz, C., and Voyi, K. V. (2009). Household conditions, eczema symptoms and rhinitis symptoms: relationship with wheeze and severe wheeze in children living in the Polokwane area, South Africa. *Maternal and Child Health Journal*, *13*(1), 107-118.

Winker, D. M., Vaughan, M. A., Omar, A., Hu, Y., Powell, K. A., Liu, Z., ... and Young, S. A. (2009). Overview of the CALIPSO mission and CALIOP data processing algorithms. *Journal of Atmospheric and Oceanic Technology*, *26*(11), 2310-2323.

Winkler, H., Formenti, P., Esterhuyse, D. J., Swap, R. J., Helas, G., Annegarn, H. J., and Andreae, M. O. (2008). Evidence for large-scale transport of biomass burning aerosols from sunphotometry at a remote South African site. *Atmospheric Environment*, *42*(22), 5569-5578.

Wong, M. S., Shahzad, M. I., Nichol, J. E., Lee, K. H., and Chan, P. W. (2013). Validation of MODIS, MISR, OMI, and CALIPSO aerosol optical thickness using ground-based sunphotometers in Hong Kong. *International Journal of Remote Sensing*, *34*(3), 897-918.

World Health Organization (2006). World Health Guidelines Global Update 2005. Retrieved from http://www.euro.who.int/__data/assets/pdf_file/0005/78638/E90038.pdf?ua=1. Accessed 26 December 2015.

Worobiec, A., Potgieter-Vermaak, S. S., Berghmans, P., Winkler, H., Burger, R., and Van Grieken, R. (2011). Air particulate emissions in developing countries: a case study in South Africa. *Analytical Letters*, *44*(11), 1907-1924.

Wright, C., Oosthuizen, M. A., Mostert, J., and Van Niekerk, L. (2011a). Investigating air quality and air-related complaints in the City of Tshwane, South Africa. *Clean Air Journal= Tydskrif vir Skoon Lug*, *20*(2), 3-12.

Wright, C. Y., Oosthuizen, R., John, J., Garland, R. M., Albers, P., and Pauw, C. (2011b). Air quality and human health among a low income community in the highveld priority area. *Clean Air Journal= Tydskrif vir Skoon Lug*, *20*(1), 12-20.

Wu, Y., Hao, J., Fu, L., Hu, J., Wang, Z., and Tang, U. (2003). Chemical characteristics of airborne particulate matter near major roads and at background locations in Macao, China. *Science of the Total Environment*, *317*(1), 159-172.

Wu, Y., Guo, J., Zhang, X., Tian, X., Zhang, J., Wang, Y., ... and Li, X. (2012). Synergy of satellite and ground based observations in estimation of particulate matter in eastern China. *Science of the Total Environment*, *433*, 20-30.

Xia, X., Eck, T. F., Holben, B. N., Phillippe, G., & Chen, H. (2008). Analysis of the weekly cycle of aerosol optical depth using AERONET and MODIS data. *Journal of Geophysical Research: Atmospheres*, *113*(D14).

Yap, X. Q., Hashim, M., and Marghany, M. (2011, July). Retrieval of PM_{10} concentration from Moderate Resolution Imaging Spectroradiometer (MODIS) derived AOD in Peninsular Malaysia. In *Geoscience and Remote Sensing Symposium (IGARSS), 2011 IEEE International* (pp. 4022-4025). IEEE.

Yoon, J., Vountas, M., von Hoyningen-Huene, W., Chang, D. Y., and Burrows, J. P. (2012, April). Trend Analysis of global AOT based on various Polar Orbiting Satellite Observations: MODIS (Terra), MISR (Terra), SeaWiFS (OrbView-2), and MODIS (Aqua). In *EGU General Assembly Conference Abstracts* (Vol. 14, p. 8912).

Young, S. A., and Vaughan, M. A. (2009). The retrieval of profiles of particulate extinction from Cloud-Aerosol Lidar Infrared Pathfinder Satellite Observations (CALIPSO) data: Algorithm description. *Journal of Atmospheric and Oceanic Technology*, *26*(6), 1105-1119.

Yu, H., Chin, M., Yuan, T., Bian, H., Remer, L. A., Prospero, J. M., ... & Zhang, Z. (2015). The fertilizing role of African dust in the Amazon rainforest: A first multiyear assessment based on data from Cloud-Aerosol Lidar and Infrared Pathfinder Satellite Observations. Geophysical Research Letters, 42(6), 1984-1991.

Zha, Y., Gao, J., Jiang, J., Lu, H., and Huang, J. (2010). Monitoring of urban air pollution from MODIS aerosol data: effect of meteorological parameters. *Tellus B*, *62*(2), 109-116.

Zhang, J., and Christopher, S. A. (2003). Longwave radiative forcing of Saharan dust aerosols estimated from MODIS, MISR, and CERES observations on Terra. *Geophysical Research Letters*, *30*(23).

Zhang, X. Y., Lu, H. Y., Arimoto, R., and Gong, S. L. (2002). Atmospheric dust loadings and their relationship to rapid oscillations of the Asian winter monsoon climate: two 250-kyr loess records. *Earth and Planetary Science Letters*, *202*(3), 637-643.

Zhang, J. P., Zhu, T., Zhang, Q. H., Li, C. C., Shu, H. L., Ying, Y., ... and Shen, H. X. (2012). The impact of circulation patterns on regional transport pathways and air quality over Beijing and its surroundings. *Atmospheric Chemistry and Physics*, *12*(11), 5031-5053.

Zeeshan, M., and Oanh, N. K. (2014). Assessment of the relationship between satellite AOD and ground PM_{10} measurement data considering synoptic meteorological patterns and lidar data. *Science of the Total Environment*, *473*, 609-618.

Zeeshan, M., and Oanh, N. K. (2015). Relationship of MISR component AODs with black carbon and other ground monitored particulate matter composition. *Atmospheric Pollution Research, 6*.

APPENDICES

Appendix A: Studies which have investigated the AOD-PM$_{10}$ relationship.

Reference	Time period	Location	Number of AQM stations	AOD measurement	Correlation coefficients	Meteorological parameters	Reason for correlation differences
Koelemeijer *et al.* (2006)	2003	Europe	> 100 AQM stations	MODIS AOD at 550nm	$R^2 = 0.17$-0.54	MLH and RH	Different AQM stations; correction for RH and MLH effects
An *et al.* (2007)	3-7 April 2005	Beijing, China	PM modelled	MODIS AOD at 550nm	$R^2 = 0.84$	temperature, pressure, RH, wind speed and wind direction	
Vidot *et al.* (2007)	1999-2004	Europe (England, France and Belgium)	80 AQM stations	SeaWiFS AOD at 550nm	$R^2 = 0.43$	zonal and meridional wind speed , the surface pressure (hPa), the RH (%) and the precipitable water	
Kumar *et al.* (2008)	Passive sampling campaign July –December 2003; Continuous sampling 2000-2005	New Delhi, India	113 passive AQM sites, 1 AQM station	5 km MODIS AOD and Level 2 MODIS 10km AOD	$R = 0.61$-0.64	sea-level pressure and RH, atmospheric pressure, wind velocity, wind direction and rainfall	Pixel to pixel comparison of AOD-PM$_{10}$, Pixel to station comparison of AOD-PM$_{10}$
Guo *et al.* (2009)	2007	China	11 AQM stations	Level 2 MODIS AOD at 550nm,	$R = 0.35$-0.62	RH	AOD corrected effects of RH
Emili *et al.* (2010)	2008	Switzerland	13 AQM stations	SEVIRI sat AOD at 600 nm and MODIS AOD at 550nm	$R = 0.46$-0.72	MLH and RH	Temporal averaging (1 hour and 24 hours); AOD products from different satellite sensors
Zha *et al.* (2010)	2004-2006	Nanjing, China	6 AQM stations	MODIS AOD at 550nm	$R^2 = 0.19$-0.75	air pressure, air temperature, RH, and wind velocity	Use of k-means clustering

Emili *et al* (2011)	2008-2009	Italy and Switzerland	27 AQM stations	SEVIRI sat AOD at 600 nm and MODIS AOD at 550nm	R = 0.50-0.51	MLH	Use of AOD from different satellites
Mahmud *et al.* (2012)	1 August 2004	Bornei, Indonesia	7 AQM stations	Level 3 MODIS AOD	R = 0.17-0.36	rainfall, wind speed, visibility, mean temperature, RH, Active fire counts	Correlations for different AQM stations.
Wu *et al.* (2012)	2007-2008	China	7 AQM stations	Level 2 MODIS AOD	R = 0.12-0.66	MLH , RH, temp, wind speed, wind direction	Different cities
Grguric *et al.* (2013)	2008-2012	Croatia	12 AQM stations	MODIS AOD at 550nm	R = 0.28-0.6	temperature, air pressure, RH, wind speed, wind direction, and MLH	Different statistical models used.
Kim *et al.* (2013)	2009	Anmyon,Cheong won, and Ulleung, South Korea	3 AQM stations	MODIS AOD at 550nm	R = 0.43-0.55	RH	Different AQM stations
Nordio *et al.* (2013)	2000-2009	Lombardy, Italy		MODIS AOD at 550nm	R = 0.787	temperature, wind speed, RH, visibility and sea level pressure	
Wang *et al.* (2013)	2006	Beijing, China	35 AQM stations	MODIS daily 550nm	R = 0.22	Absolute humidity	
Zeeshan and Oanh (2014)	Dry season 2000-2010		; Thailand; 22 AQM stations	MODIS AOD at 550nm	R = 0.27-0.58	dry bulb, temperature, dew point, wind speed, total cloud cover, sea level, pressure, visibility and wind direction index	Ordering of meteorological parameters used in statistical analysis and correlations at different stations